GEOCHRONOLOGICAL AND GEOCHEMICAL ASSESSMENT OF
CENOZOIC VOLCANISM FROM THE TERROR RIFT REGION
OF THE WEST ANTARCTIC RIFT SYSTEM

by

Sarah E. Rilling

A dissertation submitted in partial fulfillment
of the requirements for the degree of
Doctor of Philosophy
(Geology)
in The University of Michigan
2009

Doctoral Committee:
　　　Professor Samuel B. Mukasa, Chair
　　　Professor Rebecca A. Lange
　　　Professor Peter E. van Keken
　　　Professor Youxue Zhang
　　　Associate Professor Anna M. Michalak
　　　Assistant Professor Nathan A. Niemi

ACKNOWLEDGEMENTS

I would like to first thank my advisor, Sam Mukasa, for all of the guidance he has provided me both during my graduate research and while I was debating career options. I would also like to thank my dissertation committee for all of their thoughtful advice and discussion during our lengthy meetings over the past few years.

Many people have helped me along the way, and I could not have completed this work without the help of Alex Andronikov, Jaime Gleason, Chris Hall, Carl Henderson, Anne Hudon, Ted Huston, Marcus Johnson, and many others. I also received a great deal of assistance from the scientists at the Carnegie Institution, Department of Terrestrial Magnetism, and am greatly indebted to Rick Carlson, Mary Horan, Tim Mock, and Steve Shirey for providing everything from isotopic spikes to encouragement to keep trying when things were not working as planned. Thank you to Terry Wilson, for being such a positive role model during both my undergraduate and graduate career. My friends and officemates at Michigan have helped make Ann Arbor a great place to be during the last four years. I could not have done this without all of them.

Finally, I would like to thank my family for their constant support and for encouraging me to do what makes me happy. And also for putting up with me in general over the last few months. To Jerome, thank you for reading more than you could ever have really wanted to, for listening to me talk through all the details that I was trying to put together, and most importantly, for your patience and understanding.

TABLE OF CONTENTS

CHAPTER 1

INTRODUCTION

While most sources of volcanism located along major plate boundaries have been explained easily in the context of plate tectonic theory, intra-plate volcanism remains controversial and poorly understood. Morgan [1971] developed the concept of relatively stable areas of mantle upwelling, or mantle plumes, as the source for hotspots or intra-plate magmatism. This model continues to be supported by studies of linear volcanic chains, such as the Hawaiian Islands, and areas of crustal doming and rifting, such as the Afar province of the East African Rift. Tomographic imaging has even captured features interpreted as mantle plumes below these and many other locations [*Zhao*, 2007].

Although the mantle plume model works well for some hotspots, other locations of intra-plate alkaline magmatism remain enigmatic. Some geoscientists, led by Don Anderson and Gillian Foulger, have used these ambiguous sites to argue against the existence of mantle plumes [*Favela and Anderson*, 2000; *Foulger and Anderson*, 2005]. Much of the debate is focused on discrepancies between interpretations of geochemical and geophysical studies. In actuality, a single explanation for all hotspots and the diverse range of intra-plate magma compositions is unlikely. For example, the presence of alkaline magmatism, common at hotspot and intra-plate locations, is often used in the geochemical debate over mantle plume sources. However, the term "alkaline

magmatism" covers a broad spectrum of compositions that have varying concentrations of Na_2O, K_2O, and CaO (among other chemical variations). These magmas have been shown experimentally to result from melting of fertile peridotite, carbonated peridotite, hydrated peridotite, Si-rich pyroxenite, and Si-deficient pyroxenite (also used as an analogue for melting of eclogite) [*Hirschmann, et al.*, 2003; *Dasgupta and Hirschmann*, 2007]. Mantle plumes may be responsible for some ocean island basalts (as in the case of Hawaii), but not all, and may lead to some areas of active continental rifting (as in the case of the Afar region of the East African Rift), but not all. One alternative explanation for hotspot volcanism, which has recently gained favor, is decompressional melting of metasomatized mantle sources [*Halliday, et al.*, 1995; *Pilet, et al.*, 2002; *Panter, et al.*, 2006; *Pilet, et al.*, 2008]. The role of volatiles in the generation of intra-plate volcanism is not only important in understanding the geology of a particular region, but also affects assumptions of water and carbon dioxide development in the atmosphere due to volcanic degassing.

The source of magmatism in the West Antarctic Rift System (WARS) is still in question, not yet adequately explained by either active or passive models, and it invites a fresh test of these competing models of intra-plate alkaline magmatism. Initial studies in the area attributed Cenozoic alkaline magmatism to a mantle plume [*Behrendt, et al.*, 1994; *Behrendt, et al.*, 1996; *LeMasurier and Landis*, 1996] which then led to rifting; however, more recent studies have begun proposing that extensional faulting began first and led to passive generation of alkaline magmatism [*Rocchi, et al.*, 2002; *Di Vincenzo, et al.*, 2004; *Cande and Stock*, 2006; *Davey and De Santis*, 2006; *Fielding, et al.*, 2006; *Rossetti, et al.*, 2006]. Mantle plumes have been proposed beneath Mt. Erebus [*Zhao*,

2007] and the West Antarctica portion of the WARS [*LeMasurier and Landis*, 1996], but the remaining extensive areas of magmatism do not fit this model. Alternatively, a broad seismic anomaly has been observed in the upper mantle beneath the entire WARS and the Southern Ocean and has been attributed to interstitial melt due to the lower melting temperatures of an anomalously volatile-rich mantle [*Finn, et al.*, 2005]. During the Paleozoic and Mesozoic, Antarctica comprised the central portion of the subduction margin – with Australia and South America at either end – along the edge of the long-lived supercontinent Gondwana. This history provides a plausible source of additional volatiles in the mantle lithosphere, and potentially the entire upper mantle, beneath Antarctica. Cenozoic WARS magmatism is likely to be the result of extension-induced decompressional melting and thermal erosion of these metasomatized materials -- if magmatism post-dates the main phases of rifting. The geochemical signatures of these lavas must also support decompressional melting in order to conclusively determine the source of WARS magmatism.

This dissertation provides new geochronological and geochemical data for submarine volcanism developed within the Terror Rift region of the Ross Sea, Antarctica, and subaerial samples from Franklin and Beaufort Islands (Fig. 1-1). This area is regarded as the youngest segment of the WARS. These samples are compared to new data from within the nearby, previously defined Melbourne Volcanic Province to the north and Erebus Volcanic Province to the south.

Chapter 2 provides new determinations of $^{40}Ar/^{39}Ar$ isotopic ages along with flow volumes for both submarine and subaerial Neogene volcanism. These ages significantly expand the documented area of Neogene magmatism in Victoria Land and support a lack
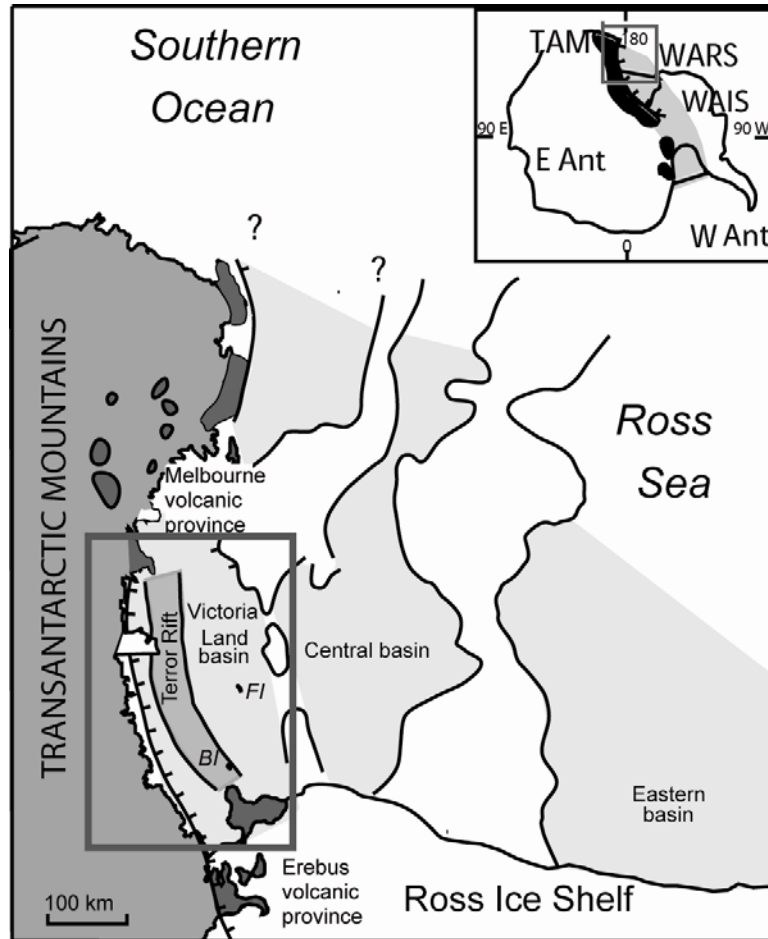
Figure 1-1. Location of study area in the West Antarctic Rift System (WARS). WAIS-West Antarctic Ice Sheet. FI – Franklin Island. BI – Beaufort Island. Lightest grey outlines rift basin locations within the Ross Sea. Dark grey areas outline areas of previously studies Cenozoic age magmatism in Victoria Land, Antarctica.

of geographic propagation of volcanism through time. Instead, voluminous volcanism became prominent by the Pliocene, and particularly widespread during the Pleistocene, post-dating the main phases of Miocene rifting in the region. The degree of decompression from Terror Rift extension is calculated to be minor and requires a metasomatized mantle source which would have a solidus close to the regional geotherm. This study has been submitted and reviewed for publication in the Journal of Geophysical Research.

Chapter 3 provides new elemental concentration and radiogenic isotope data for the samples dated in chapter 2. This study illustrates that major element compositions of the Ross Sea lavas more closely match experimental melts of carbonated peridotite than fertile peridotite. This information, along with new interpretations of the enriched trace element signatures, supports a hypothesis that melts are the result of both a metasomatized, lithospheric mantle source and asthenospheric mantle source. This model explains the minor isotopic variations in the WARS lavas as a result of variations in the mantle lithosphere along the ancient subduction margin, and eliminates the need for a complex mantle source stratified with numerous endmember compositions. This chapter is formatted for submission to Earth and Planetary Science Letters.

Chapter 4 provides the first Os isotopic ratios and platinum-group-element (PGE) concentrations for WARS-related magmatism in the Antarctic continent. This study shows that the Ross Sea lavas have lower PGE concentrations than other previously studied areas of intra-plate volcanism, and components with extremely unradiogenic $^{187}Os/^{188}Os$ values in the source. The PGE distribution patterns support a model of a residual lithospheric magma source that has undergone previous melting and removal of sulfides. Although most samples overlap values for asthenospheric melts, the most unradiogenic Os isotopic compositions convincingly support contributions of a lithospheric mantle source, with a time-integrated record of low Re/Os values, rather than a mantle plume source, which would likely have more radiogenic Os isotopic signatures. This chapter is formatted for submission to Geochimica et Cosmochimica Acta.

References

Behrendt, J. C., D. D. Blankenship, C. A. Finn, R. E. Bell, R. E. Sweeney, S. M. Hodge, and J. M. Brozena (1994), CASERTZ aeromagnetic data reveal late Cenozoic flood basalts in the West Antarctic rift system, *Geology*, *22*, 527-530.

Behrendt, J. C., R. Saltus, D. Damaske, A. McCafferty, C. A. Finn, D. Blankenship, and R. E. Bell (1996), Patterns of late Cenozoic volcanic and tectonic activity in the West Antarctic rift system revealed by aeromagnetic surveys, *Tectonics*, *15*, 660-676.

Cande, S. C., and J. M. Stock (2006), Antarctica: Contributions to global earth sciences. "Constraints on the Timing of Extension in the Northern Basin, Ross Sea, 319-326.

Dasgupta, R., and M. M. Hirschmann (2007), Effect of variable carbonate concentration on the solidus of mantle peridotite, *American Mineralogist*, *92*, 370-379.

Davey, F. J., and L. De Santis (2006), A multi-phase rifting model for the Victoria Land Basin, western Ross Sea, *Antarctica: Contributions to Global Earth Sciences*, 303-308.

Di Vincenzo, G., S. Rocchi, F. Rossetti, and F. Storti (2004), Ar-40-Ar-39 dating of pseudotachylytes: the effect of clast-hosted extraneous argon in Cenozoic fault-generated friction melts from the West Antarctic Rift System, *Earth And Planetary Science Letters*, *223*, 349-364.

Favela, J., and D. L. Anderson (2000), Extensional tectonics and global volcanism, *Problems In Geophysics For The New Millennium*, 463-498.

Fielding, C. R., S. A. Henrys, and T. J. Wilson (Eds.) (2006), *Rift history of the western Victoria Land Basin: a new perspective based on integration of cores with seismic reflection data*, Springer-Verlag, New York.

Finn, C. A., R. D. Muller, and K. S. Panter (2005), A Cenozoic diffuse alkaline magmatic province (DAMP) in the southwest Pacific without rift or plume origin, *Geochemistry Geophysics Geosystems*, *6*.

Foulger, G. R., and D. L. Anderson (2005), A cool model for the Iceland hotspot, *Journal Of Volcanology And Geothermal Research*, *141*, 1-22.

Halliday, A. N., D. C. Lee, S. Tommasini, G. R. Davies, C. R. Paslick, J. G. Fitton, and D. E. James (1995), Incompatible Trace-Elements In Oib And Morb And Source Enrichment In The Sub-Oceanic Mantle, *Earth And Planetary Science Letters*, *133*, 379-395.

Hirschmann, M. M., T. Kogiso, M. B. Baker, and E. M. Stolper (2003), Alkalic magmas generated by partial melting of garnet pyroxenite, *Geology*, *31(6)*, 481-484.

LeMasurier, W. E., and C. A. Landis (1996), Mantle-plume activity recorded by low-relief erosion surfaces in West Antarctica and New Zealand, *GSA Bulletin*, *108*, 1450-1466.

Morgan, J. P. (1971), Convection plumes in the lower mantle, *Nature*, *230*, 42-43.

Panter, K. S., J. Blusztajn, S. R. Hart, P. R. Kyle, R. Esser, and W. C. McIntosh (2006), The Origin of HIMU in the SW Pacific: Evidence from Intraplate Volcanism in Southern New Zealand and Subantarctic Islands, *Journal of Petrology*, *47(9)*, 1673-1704.

Pilet, S., M. B. Baker, and E. M. Stolper (2008), Metasomatized lithosphere and the origin of alkaline lavas, *Science*, *320*, 916-919.

Pilet, S., J. Hernandez, and B. Villemant (2002), Evidence for high silicic melt circulation and metasomatic events in the mantle beneath alkaline provinces: the Na-Fe-augitic green-core pyroxenes in the tertiary alkali basalts of the Cantal massif (French Massif Central), *Mineralogy And Petrology*, *76*, 39-62.

Rocchi, S., P. Armienti, M. D'Orazio, S. Tonarini, J. R. Wijbrans, and G. DiVincenzo (2002), Cenozoic magmatism in the western Ross Embayment: Role of mantle plume versus plate dynamics in the development of the West Antarctic Rift System, *Journal of Geophysical Research*, *107*.

Rossetti, F., F. Storti, M. Busetti, F. Lisker, G. Di Vincenzo, A. L. Laufer, S. Rocchi, and F. Salvini (2006), Eocene initiation of Ross Sea dextral faulting and implications for East Antarctic neotectonics, *Journal of the Geological Society of London*, *163*, 119-126.

Zhao, D. P. (2007), Seismic images under 60 hotspots: Search for mantle plumes, *Gondwana Research*, *12*, 335-355.

CHAPTER 2

NEW DETERMINATIONS OF ^{40}AR/^{39}AR ISOTOPIC AGES AND FLOW VOLUMES FOR CENOZOIC VOLCANISM IN THE TERROR RIFT, ROSS SEA, ANTARCTICA

ABSTRACT

This study provides new determinations of ^{40}Ar/^{39}Ar isotopic ages and flow volumes for submarine and subaerial Neogene volcanism developed within the Terror Rift, Ross Sea, Antarctica, the youngest segment of the West Antarctic Rift System. The study is based on the first dredged samples from seven seamounts north of Ross Island, as well as new data from Franklin and Beaufort Islands. The sampled foidite and basanitic lavas range in age from Quaternary (90±66 ka) on a small seamount ~10 km north of Franklin Island to 6.80±0.05 Ma on Beaufort Island. These ages are consistent with ages of volcanism in both the Melbourne and Erebus Volcanic Provinces and significantly expand the documented area of Neogene magmatism in Victoria Land. There is no geographic progression of volcanism through time, but volcanism was voluminous in the Pliocene and particularly widespread during the Pleistocene. Two of the dredges sampled edifices comprised of less than 0.2 km3 of volcanic materials. The largest seamount in the study area has 58.8 km3 of volcanic material and represents growth over a period of several thousand years. Estimated minimum eruption rates range from 2E-4 km3/yr to 2E-3 km3/yr, consistent with rates proposed for other rift systems and nearby Mt. Erebus.

Recent estimates of extension magnitude for the Terror Rift correspond to minimal decompression of only 0.10 to 0.22 GPa and therefore limited melt output of a typical peridotite source.

INTRODUCTION

The West Antarctic Rift System (WARS) has been defined as one of Earth's major rift zones based on its size of over 2,000 km^2 in the Ross Sea embayment alone [*Tessensohn and Worner*, 1991; *Worner*, 1999], yet studies of its magmatic history have remained sparse due to difficult field conditions and limited bedrock exposures. Three rift basins, the Eastern Basin, the Central Trough, and the Victoria Land Basin (VLB), were recognized in the Ross Sea by Cooper et al. [1987] on the basis of marine geophysical data, and the Northern Basin was subsequently identified [*Davey and Brancolini*, 1995] (Fig. 2-1). Debate continues over the times and rates of extension in the WARS determined from the age of rift basin strata, ages of subvolcanic intrusions and volcanic eruptions, and movement along faults during the various stages of WARS development [*Cande and Stock*, 2006; *Davey and De Santis*, 2006; *Di Vincenzo, et al.*, 2004; *Fielding, et al.*, 2006; *Rocchi, et al.*, 2002; *Rossetti, et al.*, 2006]. Rift-related magmatism has been studied along the Transantarctic Mountains (TAM), the western rift shoulder, and on a few volcanic islands in the western Ross Sea (LeMasurier and Thomson, 1990). It has long been known that rift-related magmatism was also present in the surrounding, submarine portion of the rift in the western Ross Sea, based on regional aeromagnetic studies and relatively sparse seismic profiling (Cooper et al., 1987; Behrendt et al., 1996). We present new information about seafloor volcanism from

multibeam bathymetry and reflection seismic profiling in the western Ross Sea (Wilson et al., 2004). This study reports the first ages and volume estimates from seamounts along the Terror Rift region of the VLB. Volcanism associated with the Neogene Terror Rift provides the opportunity to date rifting by isotopic methods and allows us to address the question of whether magmatism has a causal or resultant relationship to the extension.
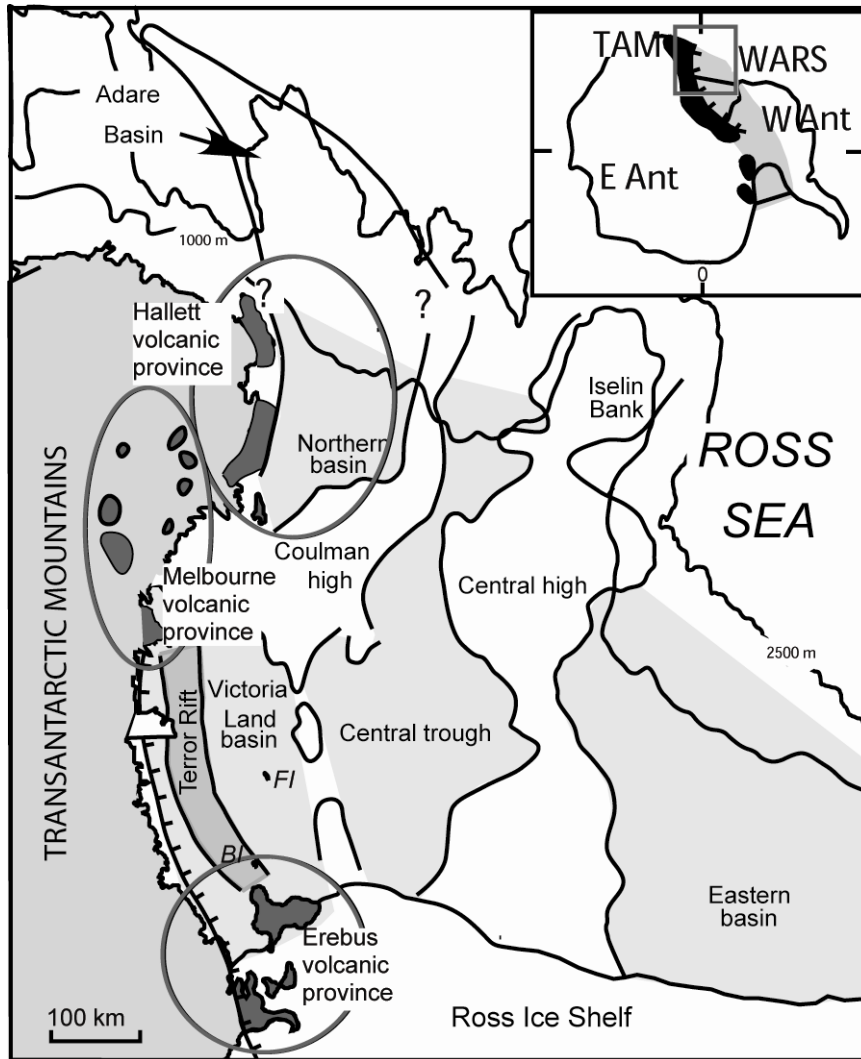
Figure 2-1. Simplified regional map of the study area. The Transantarctic Mountains represent the western rift shoulder of the West Antarctic Rift System (WARS) which extends across the Ross Sea into West Antarctica. The rift detachment runs along the eastern margin of the range. Black areas represent subaerial Cenozoic volcanism and the circles outline the division into three major volcanic provinces. Light grey shading indicates basin fill greater than 3000m. Figure modified from [Hall, et al., 2007].

BACKGROUND

1. Tectonic History

The major phase of extension in the WARS is generally accepted to have begun in the mid-Cretaceous and most, if not all, of the major rift basins in the Ross Sea sector of the rift were formed during this rift phase [*Davey and Brancolini*, 1995; *Lawver and Gahagan*, 2003; *Salvini, et al.*, 1997; *Siddoway*, 2008]. Relatively minor Cenozoic extension may have been ongoing across the Ross Sea Embayment [*Decesari, et al.*, 2007; *LeMasurier*, 2008]; however, there is accumulating evidence for major Cenozoic extension restricted to the western Ross Sea region. Cande et al. [2000] presented marine geophysical data indicating 150-180 km of seafloor spreading in the Adare Basin during the Eocene and Oligocene (43 to 26 Ma), which is likely linked southward into the Antarctic continent with extension in the Northern Basin and the Victoria Land Basin [*Cande and Stock*, 2006; *Davey and De Santis*, 2006]. Superimposed on the central VLB is a younger zone of rifting named the Terror Rift, marked by faults that reach the seafloor and associated active volcanism [*Cooper, et al.*, 1987]. Cape Roberts Project drilling results, integrated with regional seismic data, showed that main-phase orthogonal rifting in the VLB was latest Eocene-Oligocene in age, and suggested that faulting associated with the Terror Rift commenced after 17 Ma, in the Miocene [*Barrett*, 2009; *Fielding, et al.*, 2006; *Henrys, et al.*, 2007].

A multistage rift model for the western Ross Sea was proposed by Salvini et al. [1997], beginning with regional Basin and Range-style faulting and crustal thinning between 105 and 80 Ma, followed by extension associated with Transantarctic Mountains uplift in the Paleogene. Salvini et al. [1997] proposed a fundamental shift to

11

transstensional deformation at ~30 Ma marked by onshore dextral strike-slip faulting in northern Victoria Land linked with extension and transtension in the offshore Terror Rift. Rosetti et al. [2006] and Storti et al. [2008] have reviewed evidence for Eocene onset of transtensional phase of rifting, and DiVincenzo et al. [2004] showed that strike-slip faulting in northern Victoria Land was active at 34 Ma based on pseudotachylite dating. The onset of Paleogene rift-related magmatism at ~48 Ma marked by emplacement of the Meander intrusive suite in northern Victoria Land has been linked to this shift to transtensional tectonism [*Rocchi, et al.*, 2002]. Faulting in the Terror Rift continued through the Neogene, and could have continuing activity based on faults interpreted to cut and possibly displace the modern sea flow [*Hall*, 2006; *Rossetti, et al.*, 2006].

2. Magmatic History

The McMurdo Volcanic Group is recognized to be one of the most extensive alkali volcanic provinces in the world, extending along the entire western margin of the Ross Sea sector of the WARS. It is comprised of basaltic shield volcanoes and dominantly trachytic or phonolitic stratovolcanoes, with widely scattered fields of basaltic cinder cones and lava flows, and domes of evolved lavas such as phonolite, trachyte and peralkaline rhyolite [*Kyle*, 1990]. In general, rocks in the Ross Island region (Erebus Volcanic Province) are more alkaline and more strongly silica undersaturated than those in the Hallett and Melbourne Volcanic Provinces in northern Victoria Land [*Armienti, et al.*, 1991; *Kyle, et al.*, 1992; *LeMasurier and Thomson*, 1990]. Additional petrologic information about the Cenozoic volcanic activity in the Victoria Land region of the WARS is summarized in LeMasurier and Thomson [1990], and also Armienti

et al. [1991], Kyle et al. [1992], Rocholl et al. [1995], Wörner et al. [1999], and Rocchi et al. [2002].

The Cretaceous phase of regional extension in the WARS appears to have been largely amagmatic. Rift-related magmatism of commenced in the Eocene with emplacement of bimodal plutons in northern Victoria Land, dated between 48 and 28 Ma, which are essentially coeval with emplacement of dike swarms between 48 and 35 Ma [*Rocchi, et al.*, 2002]. The origin of this magmatism has been attributed to the transtensional deformation phase [*Rocchi, et al.*, 2002; *Salvini, et al.*, 1997]. Volcanic rocks in northern Victoria Land range in age from the Miocene to the present, including the active Mt Melbourne volcano [*LeMasurier and Thomson*, 1990; *Salvini, et al.*, 1997].

Volcanic rocks from outcrops in southern Victoria Land have been dated from about 19 Ma to the present, thus apparently occurred over a younger time span than magmatism in northern Victoria Land. Kyle and Muncy [1989] reported the oldest exposed volcanic rocks in the Erebus Volcanic Province in southern Victoria Land with ages between 18.73 ± 0.32 and 14.63 ± 0.21 Ma near Lake Morning and on Gandalf Ridge, on the flanks of Mt Morning. Armstrong [1978] completed an extensive geochronologic study of exposed volcanic rocks in southern Victoria Land using the K-Ar method, which produced ages of varied quality. The majority of samples dated in this initial studied were erupted within the last 5 Ma. Samples from Mt Discovery yielded one of the oldest ages in the study at 5.3 ± 0.14 Ma, while nearby Mt Morning yielded an age of only 1.15 ± 0.02 Ma. The only previous age data from the offshore part of the Erebus Volcanic Province investigated in this study was a single sample from Franklin Island

which yielded an imprecise age of 4.8 ± 2 Ma [*Armstrong*, 1978]. Volcanic activity continues at present at Mt Erebus [*Esser, et al.*, 2004; *Harpel, et al.*, 2004]

Eruptive volumes in the WARS have been difficult to determine due to lack of continuity in exposures owing to extensive ice cover. Previous geophysical studies by Behrendt et al. [1994; 1996] and Behrendt [1999] reported more than 10^6 km^3 of volcanic materials in the WARS, but this volume represents mostly unexposed and unstudied inferred flows and subvolcanic intrusions. This means that published estimates are of total Cenozoic WARS volcanism rather than specific episodes of rift-related volcanism from individual edifices. Volumes of magmatism from separate phases of extension are still unknown, providing little information towards questions over geographic evolution of magmatism in Victoria Land. Detailed studies focused on individual events or edifices, or even basin specific studies on temporal or geographic trends of volcanism, provide valuable information for geodynamic models addressing mechanisms of melting in the region. If extensional tectonics was due to active upwelling of magma, the onset of magmatism should pre-date the main phases of extension in the VLB and Terror Rift. An alternative hypothesis could be that a change in fault orientation and/or higher degrees of localized extension during later rift phases initiated decompressional melting.

SAMPLES AND METHODS

1. Sample collection and description

Samples from Franklin Island were collected by members of the 2004 NBP-0401 cruise on the *Nathaniel B. Palmer*. The submarine samples – collected by the same party – were obtained by dredging seven volcanic edifices associated with a variety of seafloor

structures identified by multibeam bathymetry mapping. Tensions were monitored while the dredge was towed behind the ship, with the highest tensions (ranging from 3200 to 9000 lbs) interpreted as breaking "*in situ* outcrops" from the volcanic edifices. A variety of materials were collected, including basalts, hyaloclastites and peridotite xenoliths. Subaerial samples from Franklin Island were collected from the western side of the island, near the Adelie penguin rookery, and represent three separate flows from the lowest 100 m of elevation. Additional information on the volcanic stratigraphy of Franklin Island can be found in LeMasurier and Thompson (1990). Samples BFT-1 and BFT-2 from Beaufort Island were collected during a helicopter landing on Beaufort Island by the TAMDEF research team and represent materials obtained from the highest elevations, approximately 670 m.

Seven volcanic edifices were dredged north of Ross Island (Fig. 2-2). Dredge 1 sampled a small, conical feature approximately 3.5 km southeast of the southern tip of Franklin Island. Dredge 2 sampled a small pyramidal feature, ~ 2 km E-W and 3.5 km N-S, located 50 km N-NE of Franklin Island (Fig. 2-3a). This feature is also referred to as 'Potter Peak'. Dredge 3 sampled a small, ~1.5 km diameter, submarine volcano on a broad area of shallow bathymetry roughly 10 km N of the northern end of Franklin Island (Fig. 2-3b). Dredge 4 sampled a large seamount measuring more than 15 km E-W and roughly 20 km in length along an N-NW to S-SE trend located ~10 km E of Beaufort Island (Fig. 2-4). Dredge 5 sampled another large seamount ~ 50 km N of Beaufort Island and ~50 km W-SW of Franklin Island (Fig. 2-5). This seamount is less than 10 km across and ~25 km in length along a N-S trend. Dredges 6 and 7 were taken from cones in close proximity to the location of Dredge 3. Dredge 6 sampled a small topographical high with
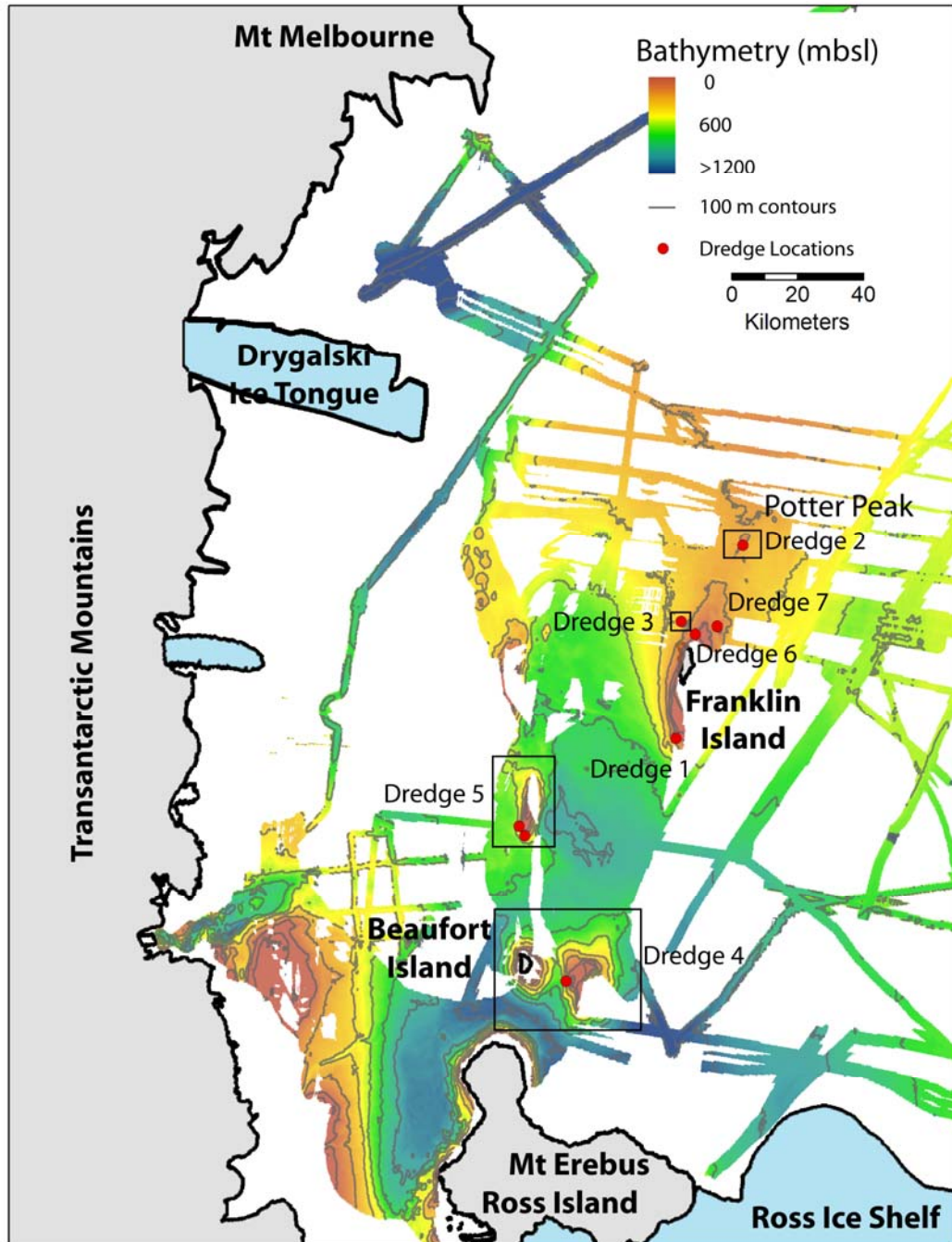
Figure 2-2. Sample locations and limits of the available high resolution bathymetry in the Ross Sea. Large data gaps are due to poor ice conditions at the time of data acquisition. Features sampled by dredge 1, 3, 6 and 7 are smaller than the location symbols. Boxes outline detailed areas in following figures.

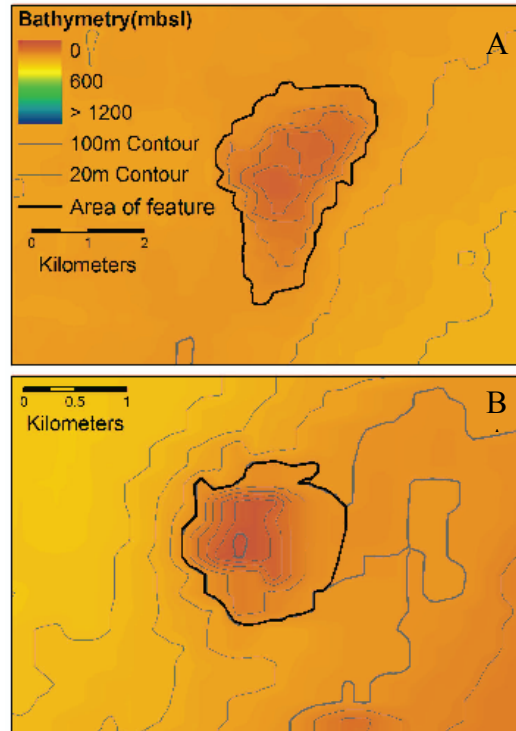**Figure 2-3**. Contour maps generated from bathymetry for seamounts sampled by A.) dredge 2 and B.) dredge 3. These features are located on the FIVR, and the 400 mbsl contour was used as the base. See text for additional details of volume determinations.
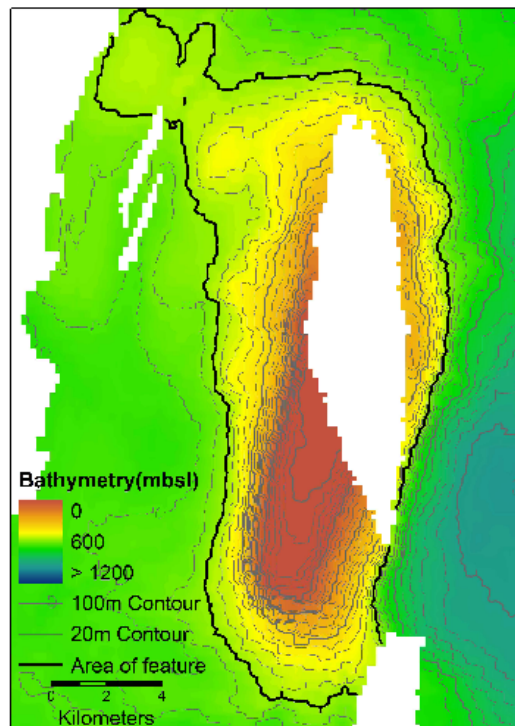

Figure 2-4. Contour map of feature sampled by dredge 5 generated from bathymetry. Base of feature is located along the 600 mbsl contour.
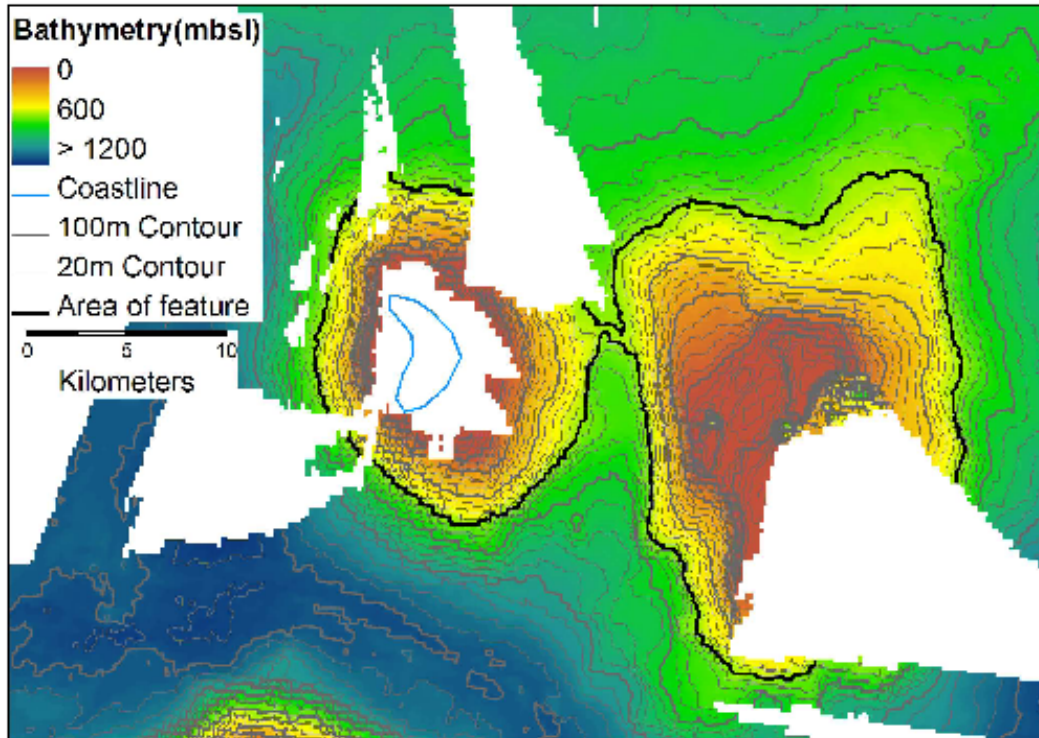
Figure 2-5. Contour maps generated from bathymetry near Beaufort Island and the seamount sampled by dredge 4 Central data gap for Beaufort Island was filled by stitching together data from topographic maps. The base contour for both features is 600 mbsl. Deep area in the southwest of the figure is the moat located around Ross Island.

a N-S elongation and a strong positive magnetic anomaly. The cone is less than 1 km in diameter, but is associated with a ridge up to 5 km long and over 1 km wide. Dredge 7 was located only 7 km N of Franklin Island.

A series of tests were used to determine the most appropriate samples for Ar analysis. Rocks with at least one fresh, recently broken surface were given first priority, as this surface was assumed to be created as the dredge broke the material loose from the submarine edifice. Cobble- to boulder-sized rounded rocks were eliminated because of the possibility that they are glacial erratics. Samples with abundant biological growth were also avoided. Three to five rocks with little or no signs of alteration and the least

18

amount of vesicularity from each location were chosen for major oxide and trace element

analysis, except for dredge 2, which had only two samples meeting the selection criteria.

Total Alkalis vs. Silica
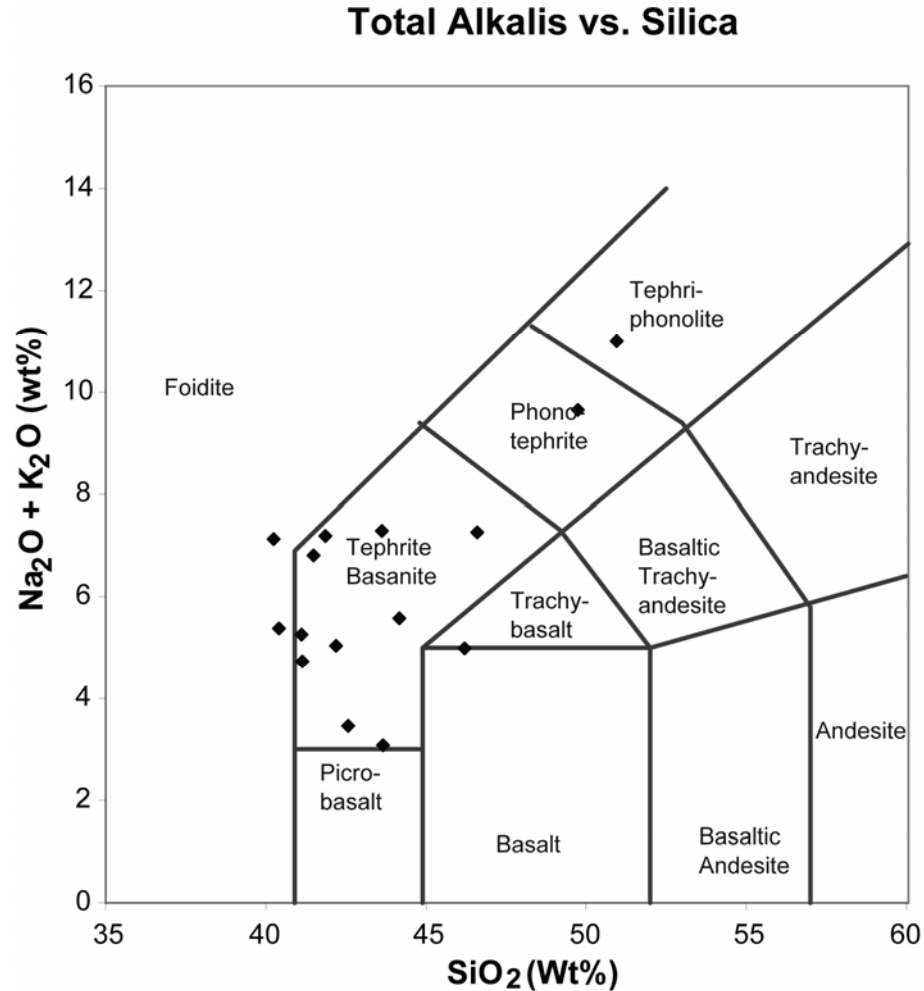
Figure 2-6. Silica vs total alkali classification for the dated samples. All samples are primitive lavas except for the two samples from Beaufort Island which plot along the phonolitic evolution trend and one sample from Franklin Island that plots along the border for trachybasalt.

The SiO_2 wt % versus total alkalis major oxide compositions for the chosen

samples are shown in Fig. 2-6. Most samples are classified as basanites. Samples are

crystal poor, with most phenocrysts being less than a millimeter in length. Olivine and

clinopyroxene are the predominant phases, although oxides ranging from tens to

19

hundreds of micrometers in size are also abundant; plagioclase phenocrysts are subordinate in a few of the samples. Xenocrystic olivine and spinel are present in many samples and typically occur in large aggregates centimeters in size, or exhibit textures in thin section which clearly indicate non-equilibrium and the breaking apart of aggregated mantle xenoliths. Centimeter-scale granitic xenoliths have been observed in some samples but are extremely rare overall. The matrix of the samples analyzed consists of glass or very fine-grained oxides and clinopyroxene, along with plagioclase in several samples. None of the samples contained large enough grains of amphibole or plagioclase to determine mineral ages, and therefore all of the ages we report here are based on whole rock analyses.

2. $^{40}Ar/^{39}Ar$ analysis

The few samples with granitic xenoliths were carefully inspected during the crushing process to avoid any contamination. Sample chips (~ 2 mm in size) were cleaned with super-deionized water in an ultrasonic cleaner to remove surface material. The pieces then retained for analyses underwent a final microscopic inspection. To the extent possible, mafic xenocrysts were avoided by excluding any sample chips that contained microscopically visible crystals, rather unlike the aphyric lavas of the WARS. However, in the case that fine-grained xenocrysts were not completely removed from the groundmass, we expect negligible effect on the radiogenic ^{40}Ar as the olivine and clinopyroxene contain little to no potassium.

Sample chips and neutron flux monitors were encased in pure aluminum foil and set into a quartz cylinder. The cylinder was then irradiated for a total of 6 MWhrs at the McMaster University research reactor. Analyses were performed in the Argon

Geochronology Laboratory at the University of Michigan, using the laser step-heating method as outlined in Frey et al. [2004]. Biotite from the Fish Canyon Tuff (FCT-3), with an age of 28.16 ± 0.28 Ma (2σ) by Renne [1998], was used as the neutron flux monitor. J-values were determined based on the specific location of sample chips within the quartz cylinder during irradiation and varied between 5.9E-4 to 6.3E-4. Chips were laser heated for 13 steps of 30 seconds each, with the exception of DRE7-120 which required a 14th step to complete fusion.

Ages were calculated by total gas, plateau, and inverse isochron methods. Although inverse isochrons were generated using Ar released from all steps, they were also generated based on only those fractions that defined a plateau (i.e., > 50 % ^{39}Ar released). Previous studies [*Armstrong*, 1978; *Esser, et al.*, 2004; *Esser, et al.*, 1997] have shown that many samples from the Erebus Volcanic Province have ^{40}Ar/^{36}Ar$_i$ values greater than the atmospheric value of 295.5, the assumed value for total gas and plateau calculations. Isochron ages were preferred for most samples because this method does not assume a set value for the ^{40}Ar/^{36}Ar$_i$ and provides a more accurate assessment of the true initial argon ratios. Several samples, particularly those with ages younger than 2 Ma, had low abundances of radiogenic ^{40}Ar leading to poor constraints of the x-intercept, representing ^{39}Ar/^{40}Ar, and used in the isochron calculations. For these samples, the isochron age was still used as the preferred age if the ^{40}Ar/^{36}Ar$_i$ was greater than 300. However, if the initial ^{40}Ar/^{36}Ar was in agreement with atmospheric argon values, the plateau age was our preferred age.

3. Flow volume calculations

Multibeam bathymetric data were collected using a Kongsberg Simrad EM120 multibeam echosounder (12 kHz) system on the research vessel *Nathaniel B. Palmer* during the 2004 NBP04-01 cruise [*Wilson, et al.*, 2004]. Data were imported into ArcGIS9.2 as a NetCDF file provided by the University of Texas Institute for Geophysics (UTIG). Additional information on data collection and processing can be found in Wilson et al. [2004] and Lawver et al. [2007]. Although cruise NBP04-01 greatly improved the geographic coverage of the multibeam mapping, large data gaps still persist due to the large icebergs, calved from the Ross Ice Shelf, that grounded on and covered seafloor volcanic edifices and the unfavorably shifting ice conditions during the cruise (Fig. 2-2). Contours generated at 20 m intervals, were used to determine the feature outlines used in area and volume calculations. Feature edges, defined at the most prominent break in slope between the steep-sided volcanic edifices and the surrounding flat seafloor, were identified using these contour maps.

The break in slope occurs at 600 meters below sea level (mbsl) for seamounts sampled by dredge 4 and dredge 5, as well as for the base of Beaufort Island. Although there are small gaps in bathymetric coverage for these three features, contours could be interpolated around them assuming continuity of the preserved shape. Magnetic anomalies on regional aeromagnetic maps [*Chiappini, et al.*, 2002], support interpretation of the edifice edges used in this study (Fig. 2-7). Calculating the Beaufort Island volume required joining together both bathymetry data and digitized subaerial topography data. This provides additional errors in volume calculations, as topography is not exactly known, but allows a reasonable estimate to be made in areas lacking complete data. A
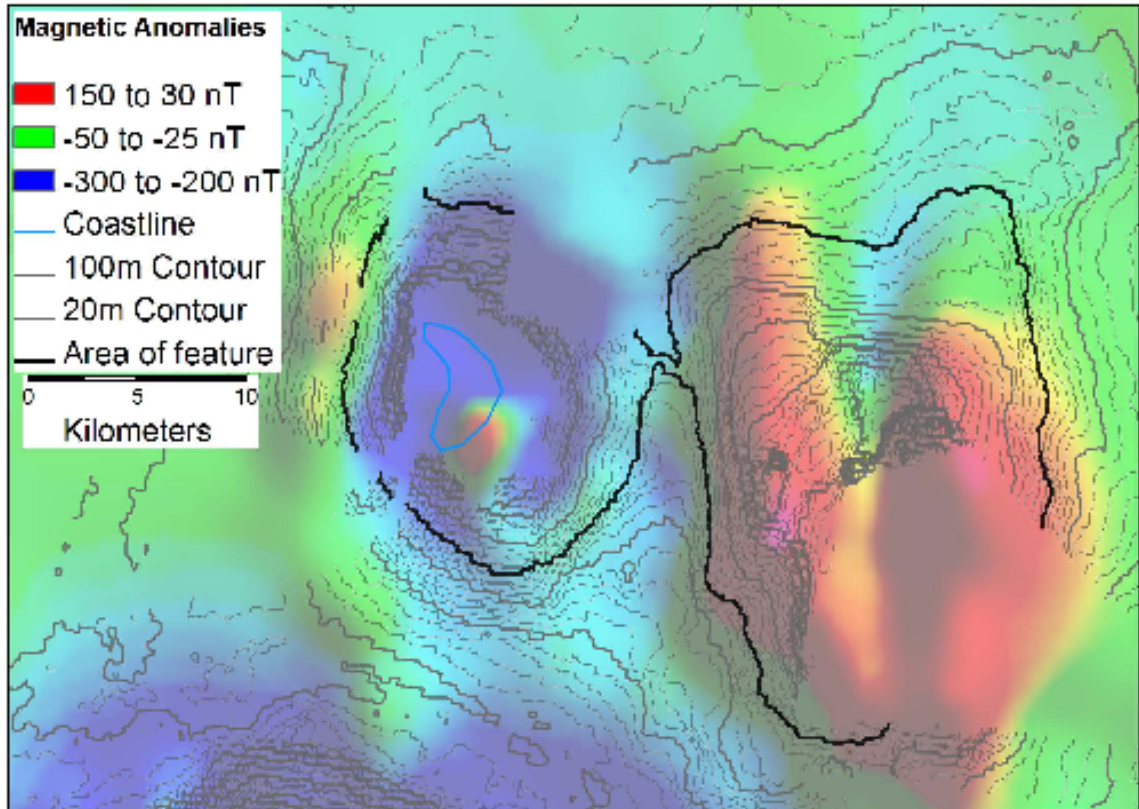
Figure 2-7. Example of magnetic anomalies associated with volcanic edifices in the Ross Sea. Beaufort Island on the left was erupted during reverse magnetic polarity. The seamount sampled by dredge 4 was erupted during normal magnetic polarity (modified from Chiappini et al., 2002).

400 mbsl base level was used for the seamounts sampled by dredge 2 and 3. This shallower depth is the surface of a prominent volcanic ridge observed on regional aeromagnetic maps [*Chiappini, et al.*, 2002], henceforth referred to as the Franklin Island Volcanic Ridge (FIVR) [*Smith, et al.*, 2004]. For large areas of the Ross Sea, data gaps prevent any reasonable estimates of flow volumes. The vast majority of the FIVR remains unmapped by high-resolution bathymetry. Dredges 1, 6, 7 and Franklin Island are all in close proximity to each other and cannot be segregated into individual features using the data presently available.

Areas and volumes for the volcanic edifices were initially calculated using the Zonal Statistics tool in ArcGIS 9.2 to sum the thickness of each raster cell (2870 m^2); however, small data gaps present on most features prevented complete summations. For more accurate estimates, 3-dimensional representations, or Triangular Irregular Networks (TINs), were created from the contour maps and volumes calculated using the Spatial Analysis extension of ArcGIS, similar to the methods of Frey et al. [2004]. TINs allow for more accurate volume determinations below a continuous sloping feature rather than summing average thickness over the area of a raster cell.

RESULTS

1. Geochronology

Results for the 18 samples dated are shown in Table 2-1. Three factors were tested to determine whether the dates generated are geologically significant: (1) The plateau must represent > 50% of the ^{39}Ar released; (2) the plateau and isochron ages must agree within error; and/or (3) the MSWD of the calculation used must be < 2. At least two of these three tests must be met for us to consider a particular determination as chronologically significant. Of the 18 samples analyzed, thirteen met these requirements. Eight of these geologically significant samples (ANT1-9, ANT5A-19, BFT1, DRE1-31, DRE3-73, DRE4-75, DRE6-107, and DRE7-120) yield ages that agree within error at the one sigma level for all three methods of calculation; samples DRE1-32, DRE3-59, DRE4-76, and DRE5-85 agreed within 2 sigma errors. The remaining samples either failed to produce a reliable isochron or had differing plateau and isochron ages due to higher $^{40}\text{Ar}/^{36}\text{Ar}_i$ values calculated from the isochron than assumed in total gas and

24

Table 2-1. Calculated $^{40}Ar/^{39}Ar$ Ages

Sample ID	Total Gas Age (Ma)	Plateau Age (Ma)	% ^{39}Ar in Plateau	MSWD	Isochron Age (Ma)	$^{40}Ar/^{39}Ar_i$	MSWD	Preferred Age (Ma)
ANT1-6	3.553 ± 0.035	--	--	--	3.297 ± 0.042	304.1 ± 1.8	2.65	3.30 ± 0.04
ANT1-9	3.489 ± 0.024	3.422 ± 0.020	92.3	1.09	3.404 ± 0.039	297.3 ± 3.3	1.18	3.40 ± 0.04
ANT5A-19	3.774 ± 0.037	3.753 ± 0.048	95	2.11	3.707 ± 0.158	297.4 ± 6.3	2.32	3.70 ± 0.16
BFT1	6.778 ± 0.025	6.759 ± 0.021	83.7	1.71	6.797 ± 0.046	274.0 ± 9.6	1.14	6.80 ± 0.05
BFT2	6.805 ± 0.030	--	--	--	6.768 ± 0.032	304.4 ± 3.7	2.32	6.77 ± 0.03
04DRE1-31	0.132 ± 0.026	0.134 ± 0.024	100	1.16	0.159 ± 0.047	293.0 ± 4.0	1.22	0.134 ± 0.024
04DRE1-32	0.193 ± 0.018	0.168 ± 0.015	99.6	0.94	0.123 ± 0.026	308.2 ± 6.1	0.55	0.123 ± 0.026
04DRE2-42	1.288 ± 0.041	1.002 ± 0.053	58.7	1.93	--	--	--	1.00 ± 0.05
04DRE3-59	1.574 ± 0.085	0.520 ± 0.078	60.3	1.91	0.188 ± 0.176	300.5 ± 2.5	1.17	0.188 ± 0.176
04DRE3-73	0.174 ± 0.026	0.157 ± 0.021	100	1.4	0.090 ± 0.066	307.6 ± 1.1	1.36	0.090 ± 0.066
04DRE4-75	1.972 ± 0.046	1.939 ± 0.039	100	1.14	1.884 ± 0.059	296.6 ± 1.0	1.12	1.94 ± 0.04
04DRE4-76	1.941 ± 0.035	1.937 ± 0.037	64.5	0.98	2.069 ± 0.093	288.1 ± 4.8	0.78	1.94 ± 0.04
04DRE5-80	3.778 ± 0.039	--	--	--	3.959 ± 0.079	294.1 ± 1.0	3.1	3.96 ± 0.08
04DRE5-85	4.153 ± 0.030	4.047 ± 0.034	69.1	1.48	3.752 ± 0.140	315.9 ± 9.5	0.54	3.75 ± 0.14
04DRE6-103	8.556 ± 0.078	--	--	--	6.406 ± 0.895	303.7 ± 3.8	208	--
04DRE6-107	0.564 ± 0.025	0.509 ± 0.024	95.9	1.62	0.498 ± 0.037	296.0 ± 1.1	1.76	0.509 ± 0.024
04DRE7-116	2.775 ± 0.211	--	--	--	--	--	--	--
04DRE7-120	0.591 ± 0.035	0.556 ± 0.038	70.5	2.04	0.507 ± 0.043	297.9 ± 1.4	1.51	0.556 ± 0.038

plateau calculations. Although they do not meet the criteria for chronologic significance, samples ANT1-6, BFT2, and DRE5-80 are included in the following discussion because of several favorable factors. ANT1-6 yielded a stratigraphically reasonable age relative to the two other samples from Franklin Island. BFT2 and DRE5-80 each yielded ages within error of the other sample from the same location.

Samples DRE6-103 and DRE7-116 are not included in following discussions due to clear problems in the produced spectra. The arc shape observed on the spectrum diagram of DRE6-103 indicates that the sample may have been influenced by later reheating event (possibly from a later volcanic flow or intrusion) leading to an erroneously old age. Sample DRE7-116 displays the classic saddle-shape pattern on the spectrum diagram described by Lanphere and Dalrymple [1976] as an indication of excess or inherited argon. The youngest age observed in the spectra, 2.76 ± 0.21 Ma, can therefore only be interpreted as a maximum age and may be significantly older than the true age of the rock.

Subaerial samples collected from Franklin and Beaufort Islands yielded older ages than most of the submarine samples in this study. ANT5A-19 represents the stratigraphically lowest flow from Franklin Island sampled for this study and has the oldest age of 3.70 ± 0.05 Ma. ANT1-9 is a mid-level sample with a slightly younger age of 3.40 ± 0.04 Ma. ANT1-6 is a dike which cross-cuts a hyaloclastite unit and has the youngest age of 3.30 ± 0.04 Ma. Two samples from the same locality on Beaufort Island, 505 m elevation, were analyzed. These samples yielded much older ages of 6.80 ± 0.05 for sample BFT-1 and 6.77 ± 0.03 Ma for sample BFT-2.

In most cases, samples from the same dredge yielded very similar ages. Dredge 5 samples yielded the oldest ages, slightly older than those from Franklin Island. Sample DRE5-80 has an age 3.96 ± 0.08 Ma and DRE5-85 is 3.75 ± 0.14 Ma, indistinguishable within error. Dredge 4 sampled the next oldest submarine feature with both DRE4-75 and DRE4-76 giving an age of 1.94 ± 0.04 Ma. Dredges 6 and 7 each had only one sample with a geologically meaningful age of 509 ± 24 Ka for DRE6-107 and 556 ± 38 ka for DRE7-120. Dredges 1 and 3 samples were very close in age and yielded the youngest dates from the submarine sample set. Dredge 1 had two samples which agree within error, 134 ± 24 ka for sample DRE1-31, and 123 ± 26 ka for sample DRE1-32. DRE3-59 yielded an age of 188 ± 176 ka and DRE3-73 is 90 ± 66 ka, both clearly with poor precision.

Ca/K and Cl/K were measured during the laser step-heating to monitor mineralogical and potential alteration effects (Fig. 2-8). For example, all samples exhibit increasing values of Ca/K in the higher temperature fractions, interpreted to reflect degassing of pyroxene in the groundmass. Samples BFT2 and DRE4-76 also have slight increases in this ratio over more moderate temperature fractions, likely to be caused by degassing of plagioclase. These two samples have more abundant and slightly larger grains of plagioclase in the groundmass than other samples. The observed increases in Ca/K values do not correlate with calculated ages for these fractions. A high spike in Cl/K is also observed in the first step of the Ar release profile for all samples, and for the second step of a few samples. In all cases, this represents less than 5% of released [39]Ar, and for most samples these steps are not considered in the plateau and isochron calculations. Cl decreases dramatically by the second and third steps, except for samples

27
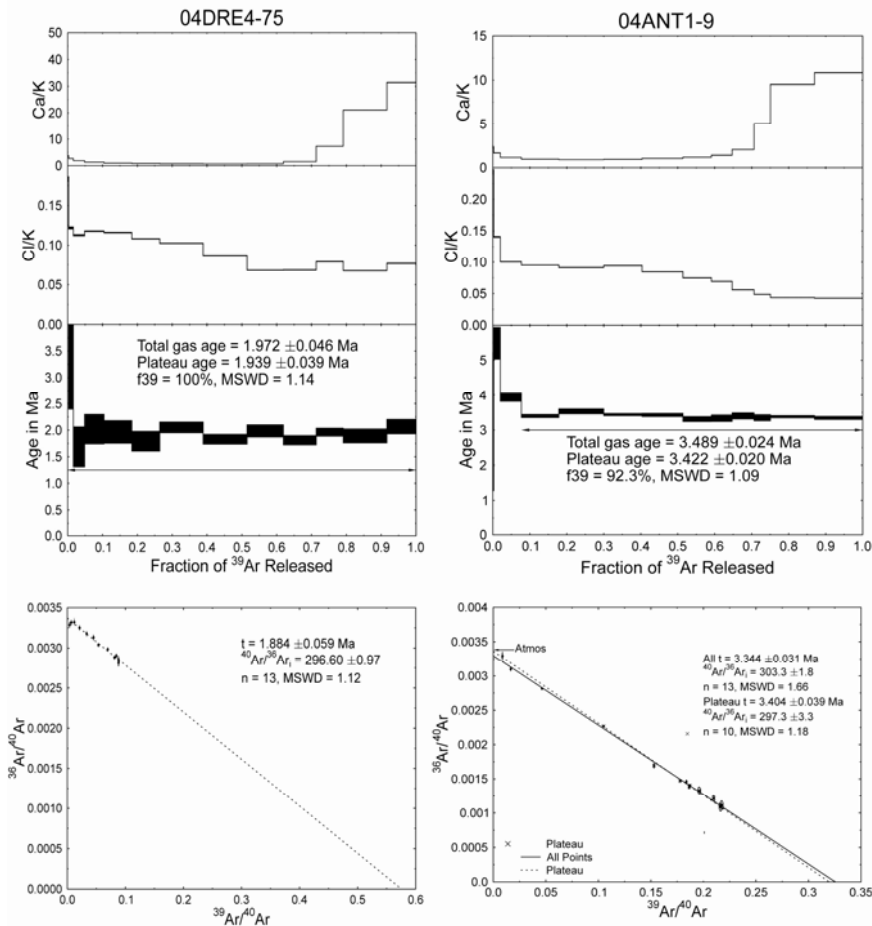
Figure 2-8. Examples of age calculations using total gas, plateau, and inverse isochron methods. The preferred age for sample 04DRE4-75 was calculated using the plateau method due to low abundances of 40Ar. The preferred age for 04ANT1-9 was calculated using the isochron method due to the higher 40Ar/36Ar, or lower 36Ar/40Ar, than expected atmospheric. See text for additional descriptions.

ANT1-6 and DRE6-107, in which the decreases are more gradual. Seawater interaction

and/or secondary mineralization are the most obvious explanation for observed Cl spikes

in the lowest temperature fractions for samples DRE1-31, DRE3-73, DRE4-76, and

DRE6-103. Younger ages are associated with these steps, meaning that a small amount of

Ar loss was triggered by these processes. However, most samples in which Cl/K values

are elevated show older ages, best explained by degassing of melt inclusions [*Esser, et al.*,

1997] and/or apatite needles which commonly occur as inclusions, and in the groundmass to a lesser extent, of several samples.

Discrepancies between total gas and isochron ages may be explained by the presence of extraneous argon in several samples. Total gas- and plateau-age calculations assume an initial $^{40}Ar/^{36}Ar$ value of 295.5. Five samples show significantly higher values based on the isochron calculations. Sample DRE5-85, for example, has the highest $^{40}Ar/^{36}Ar_i$ value calculated at 315, when including all points in the isochron, but also when using only the points defining the plateau on the isochron. The problem of extraneous argon has been observed in other studies of the McMurdo volcanic group [*Armstrong*, 1978; *Esser, et al.*, 2004; *Esser, et al.*, 1997]. Armstrong [1978] attributed excess argon to xenocrystic sources, as peridotite nodules are commonly observed in hand samples, and calculated that three percent of xenocrystic augite could increase a K-Ar age by as much as 0.5 Ma. While textures indicative of xenolith disaggregation are indeed observed in some thin sections, suggesting that dissolution of augite is not an unreasonable explanation, our study shows that there is no correlation between degassing of pyroxene (as represented by increasing Ca/K ratio), and what would be increasingly higher calculated ages. The preservation of peridotite nodules up to 10 cm in diameter supports the hypothesis of very rapid magma transport limiting assimilation of surrounding mantle material and therefore making contamination negligible. The higher initial Ar ratio is then attributed to inheritance, rather than excess argon caused by diffusion or dissolution of xenocrystic materials. Observations of extraneous argon in samples collected throughout the volcanic province instead suggest that high $^{40}Ar/^{36}Ar_i$ ratios may instead be a signature of the regional mantle source. Additional studies could

29

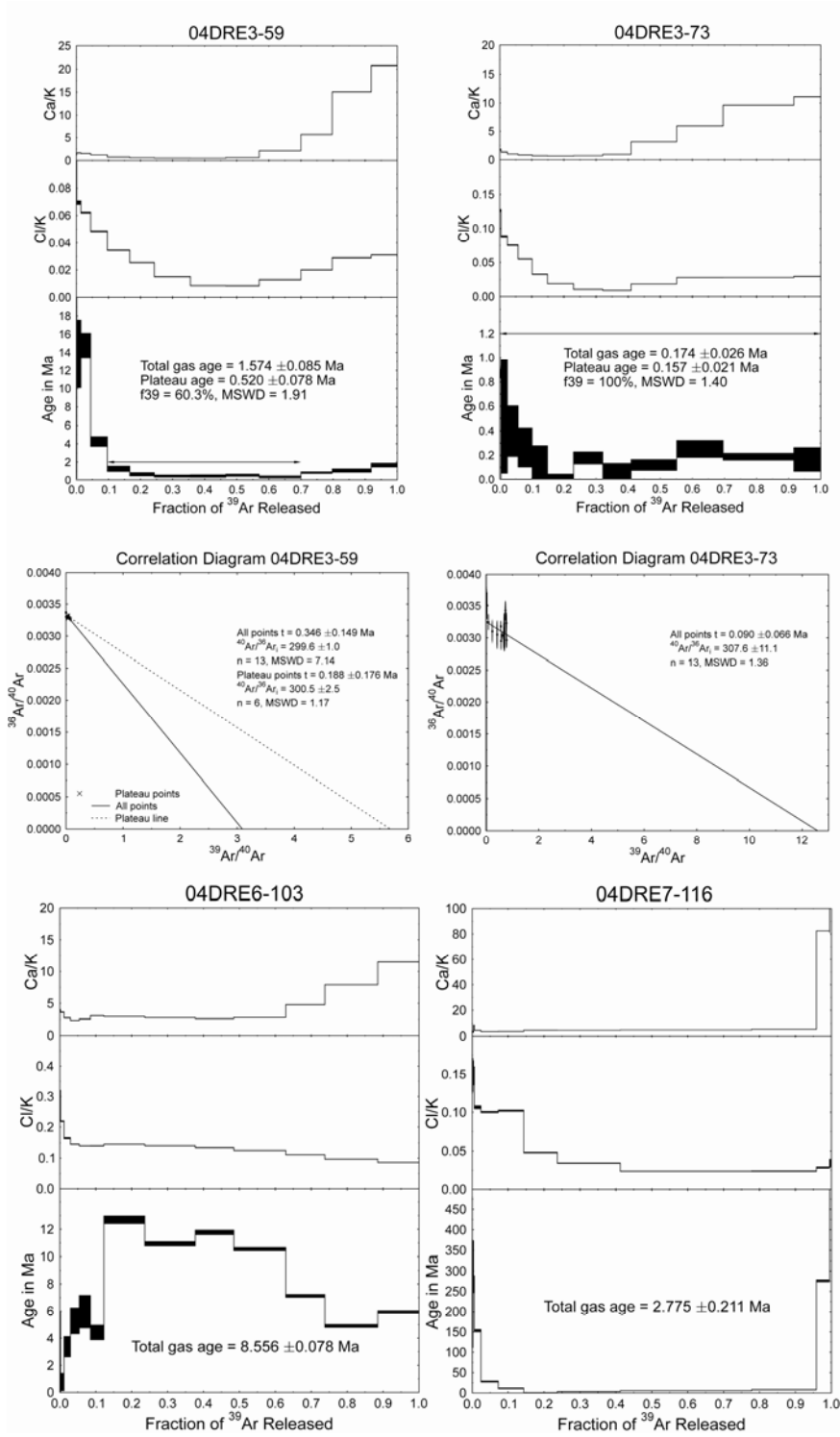**Figure 2-9.** Examples of problematic spectra. Ages calculated for samples from dredge 3 are likely near zero ages. See text for further explanation. Spectra generated by sample 04DRE6-103 displays an arc shape commonly associated with samples which have undergone a later stage heating event after eruption. 04DRE7-116 spectra display a classic saddle shape most likely a result of excess argon in the sample.

address this hypothesis by analyzing other noble gases to determine, for example, whether $^3He/^4He$ signatures correlate with $^{40}Ar/^{39}Ar$ in primitive melt inclusions or fresh erupted glass material.

Age determinations for the two samples from dredge 3 are complicated by several factors (Fig. 2-9). First, isochron ages are difficult to calculate because of the extremely low abundance of radiogenic ^{40}Ar. A line plotted through the points all near the y-axis could intercept the x-axis over a large range in $^{39}Ar/^{40}Ar$ values, creating significant errors in the age. Second, it is possible that the samples are very near zero age. The spectrum diagram for DRE3-73 supports this hypothesis. The shape of the spectrum produced by step-heating is very similar to the shape of the Cl/K curve. As discussed above, the high initial Cl/K is probably due to the presence of melt inclusions in the sample. Because all of these steps are concordant within one sigma, they are included in the plateau age calculation, although these slightly higher initial steps may lead to an erroneously old age. The true age would then be younger than 156 ka. For consistency with our methods of calculation, we report the isochron ages, however, these ages should be treated as maximum ages for the lavas recovered by dredge 3.

2. Flow Volumes

Calculated submarine flow volumes are summarized in Table 2-2. Potter Peak, sampled by dredge 2, and the feature sampled by dredge 3 are both relatively small in size with 0.176 and 0.069 km^3 of magmatic materials, respectively (Fig. 2-3). These features were fully mapped during the cruise and have relatively small errors related mainly to the initial bathymetry measurements. The seamount sampled by dredge 5 has a volume of 22.3 km^3. The volcanic edifice sampled by dredge 4 is the largest feature with

Table 2-2. Flow volume calculations using ArcGIS9.2

Feature	Latitude	Longitude	Base (mbsl)	Area (km^2)	Volume (km^3)
Dredge 2	-76.7322	168.7641	400	5.24	0.176
Dredge 3	-75.9754	168.2267	400	1.48	0.0690
Dredge 4	-76.9825	167.4890	600	314	58.8
Dredge 5	-76.5785	166.7026	600	156	22.3
Beaufort Island	-76.9833	167.0167	600	169	42.3
Beaufort Island - above sea level			0	10	2.0

a volume of 58.8 km^3. Beaufort Island contains only 42.3 km^3, smaller than the feature

sampled by dredge 4, even though it reaches 767 m above sea level. Less than 5% of

Beaufort Island's total volume lies above current sea level. The volume calculated for the

dredge 4 seamount has the largest uncertainty due to the lack of data over roughly 25% of

the feature's area. The feature sampled by dredge 5 has a smaller data gap, only ~ 10%

of the area. Beaufort Island is mapped over all except for about 10% of the area, but has

a fairly symmetrical base and is therefore thought to be well approximated. The lack of

complete data prevents us from determining specific errors, and the volumes for these

features are considered estimates.

DISCUSSION

1. Time-Space Distribution of Erebus Volcanic Province Eruptive Activity

One of the most intriguing findings of geochronologic studies of Cenozoic

magmatism in the Victoria Land region is the lack of spatial localization or geographic

progression of magmatism. Although this may partially be the result of discontinuous

sampling between major edifices due to ice cover, this finding has continued to hold true

with additional studies. Fig. 2-10 shows a generalized overview of localities within the

Erebus and Melbourne Volcanic Provinces which had volcanic eruptions over the same

time span as the features dated in this study LeMasurier and Thomson [1990]; and more

recent studies on Mt. Melbourne and Mt. Morning [*Cooper, et al.*, 2007; *Esser and Kyle*, 2002; *Esser, et al.*, 2004; *Esser, et al.*, 1997; *Harpel, et al.*, 2004; *McIntosh and Esser*, 2005; *Paulsen and Wilson*, 2009; *Rocchi, et al.*, 2002]. Early Miocene volcanic rocks are found on the lowermost flanks of Mt Morning and in the Melbourne Volcanic Province. Minna Bluff, Black Island, and Beaufort Island all had activity in the Late Miocene.
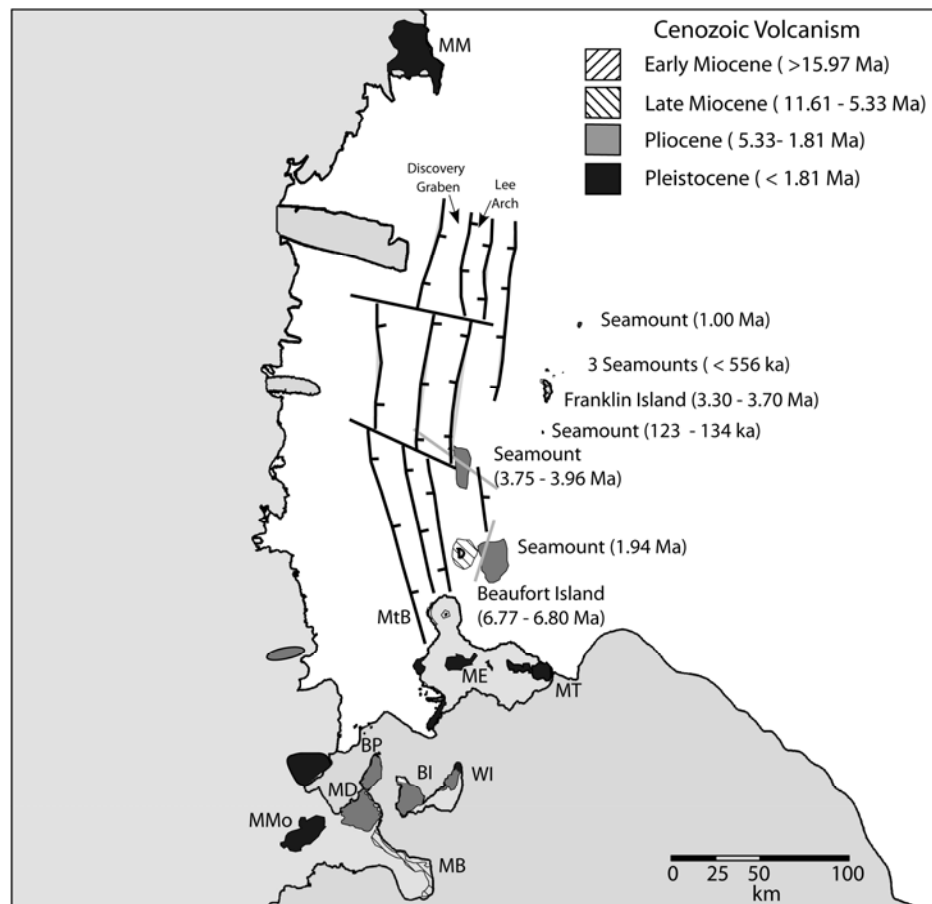
Figure 2-10. Generalized summary of primary ages of volcanism from localities within the Erebus and Melbourne Volcanic Provinces. P - The Pleiades, MP - Malta Plateau, MM - Mt. Melbourne, MtB - Mt. Bird, ME - Mt. Erebus, MT - Mt. Terror, BP - Brown Peninsula, BI - Black Island, WI - White Island, MMo - Mt. Morning, MD - Mt. Discovery, MB - Minna Bluff. Ages from this study and [Cooper, et al., 2007; Esser and Kyle, 2002; Esser, et al., 2004; Harpel, et al., 2004; LeMasurier and Thomson, 1990; McIntosh and Esser, 2005; Paulsen and Wilson, 2009]. Black lines represent mapped faults from [Hall, 2006; Henrys, et al., 2007]. Grey lines are locations of seismic lines in Fig. 2-11.

33

Slightly younger, Pliocene age volcanism is found throughout the Erebus Volcanic Province, including flows at Mt Bird on Ross Island, Mt. Discovery, Black Island, Brown Peninsula, Mt. Morning, and Franklin Island. Volcanism of Pliocene age is also found to the north along Cape Washington near Mt Melbourne. By the Pleistocene, major volcanoes including, Mt Morning, Mt Terror, Mt. Melbourne and Mt. Erebus became active, with the latter two remaining active today. Tens to perhaps hundreds of smaller Pleistocene edifices are scattered over a wide area including The Pleiades, Shield Nunatak and the Mt Melbourne region in the north, the seamounts sampled by dredges 1, 2, 3, 6, and 7 along the Terror Rift, Mt. Terror, White Island, and on numerous parasitic cones at Mt. Morning in the south.

Although there appears to be no geographic progression of volcanism, this general summary of isotopic ages for magmatism in the Melbourne and Erebus Volcanic Provinces leads to several key deductions. There is no age progression in the volcanism N-S along the rift shoulder or in the Terror Rift, nor eastward away from the rift shoulder associated with the opening of the VLB or Terror Rift. This suggests that the volcanism is not associated with any rift progression southward into the continent from the Adare Basin [*Cande and Stock*, 2006], or with propagation of Terror Rift, but instead has expanded across a broad region during the Pliocene and Pleistocene. The new submarine features overlap the ages of the previously analyzed subaerial features throughout both volcanic provinces. Miocene and younger age volcanism has now been dated along a ~650 km span, continuing from the Erebus Volcanic Province in the south to the Melbourne Volcanic Province to the north. The amount of magmatism has been generally

increasing since the Miocene, with the most voluminous and widespread volcanic edifices constructed in the Pliocene and Pleistocene.

2. Flow Volumes and Eruption Rates

While the volumes of Potter Peak and dredge 3 are very small and likely represent a short-lived, monogenetic eruptive episodes, the seamounts of dredge 4 and dredge 5 and Beaufort Island are much larger cumulative volumes potentially erupted over a longer period of time. Beaufort Island and the area sampled by dredge 5 both display prominent negative magnetic anomalies, while the area sampled by dredge 4 displays a strong positive magnetic anomaly (Fig. 2-5). The ages of these features are consistent with formation during times of reverse and normal polarity, respectively. In some areas, magnetic anomalies continue past the break in slope used as the edge of the features, and are interpreted to represent additional volcanic material extending beneath the regional sediment cover. These are not included in eruption volume calculations because data to establish definitive subsurface limits are lacking. Seismic lines show that volcanic material potentially extends deeper than 1 km below the present day sea floor for dredge 4 (Fig.2-11). The resolution of these features rapidly diminishes at greater depths, but an additional 1 km of thickness for dredge 4 below sediment cover, as inferred from the seismic data, would more than double the volume of magmatic material.

The samples recovered from the dredge 4 seamount came from near the top of the edifice and should represent some of the youngest eruptive material. Cande and Kent [1995] reported normal polarity between 1.77 Ma and 1.95 Ma, consistent with the 1.94 Ma ages we report on two samples from dredge 4. Preservation of a strong positive magnetic signature [*Chiappini, et al.*, 2002] also suggests rapid build-up of the bulk of
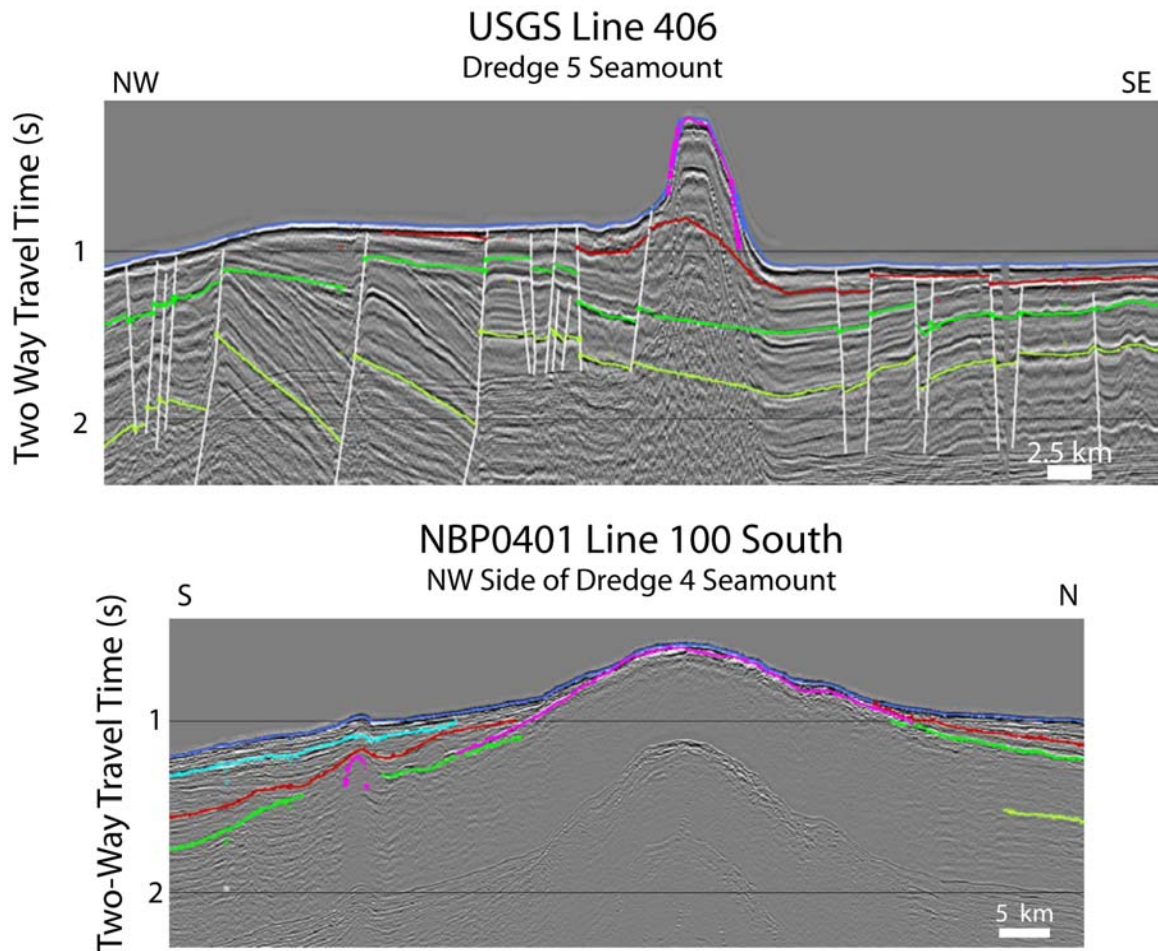
Figure 2-11. Seismic lines across the volcanic features sampled by dredges 5 and 4. Feature extends below the seafloor and is obscured by the seafloor multiples. Lines from [Hall, 2006].

the seamount between 1.95 Ma and 1.92 Ma. If the majority of volcanism was erupted

prior to 1.95 Ma, with only a few tens of meters of the 1.94 Ma flow on the upper surface

of the seamount, then the overall magnetic signature of the feature would be a negative

anomaly. If even a small portion of the 400-m thick erupted material included in this

calculation had been erupted during a time of reversed polarity, prior to 1.95 Ma or more

recently than 1.77 Ma, the combined magnetic signal would be closer to neutral than is

observed. This may be the case in a small area on the northern flank of the seamount

which has slightly more neutral magnetic signatures relative to the rest of the feature

[*Chiappini, et al.*, 2002], and may represent an older flow buried beneath the younger seamount-building flows.

A similar argument can be made for rapid formation of Beaufort Island. The two samples analyzed from Beaufort Island represent some of the youngest activity from this edifice, 6.77 – 6.80 Ma, due to their location near the summit. Cande and Kent [1995] reported reversed polarity from 6.57 Ma to 6.94 Ma. The strength of the negative anomaly supports rapid emplacement of the majority of Beaufort Island within the ~400 kyrs of this reversal. However, a conduit with a positive magnetic anomaly is observed in the center of the feature off the SW side of the island. This material most likely represents younger intrusive material which cooled after 6.57 Ma, but could also represent a younger flow which breached the surface at a lower elevation than the samples analyzed in this study.

The eruption of these large volumes over short periods is reasonable when compared to other basaltic volcanism in the world. If the seamount sampled by dredge 4, the largest volume feature, was formed between 1.94 and 1.95 Ma, the average rate of output was 6E-3 km^3/yr. This is a minimum eruption rate considering the unknown amount of glacial erosion and the undeterminable amount of material at depth. Beaufort Island has an average volcanic output rate of 2E-4 km^3/yr, assuming that the majority of activity took place between 6.94 and 6.74 Ma. These rates are similar to many other localities listed in the global compilation of magmatic volumes in White et al. [2006]. The most similar rate of rift-related volcanism is in Kenya which ranges from 3.5E-3 to 1.6E-2 km^3/yr [*Crisp*, 1984]. This rate is also very similar to the 1E-3 to 4E-3 km^3/yr eruption rate estimates for Mt. Erebus by Esser et al. [2004], and also to the Great Rift of

the Eastern Snake Plains which erupted ~31 km^3 of basalt over 13 kyrs at an average rate

of 2.4E-3 km^3/yr [*Kuntz, et al.*, 1986]. These eruption rates and volumes alone do not

help to link the Terror Rift magmatism to either an active or passive source, but when

considering their generation by only 0.10 to 0.22 GPa of decompression in the area,

discussed below, they support a hypothesis of origination from a modified mantle source

with a solidus close to the regional geotherm.

3. Glacial Erosion of Volcanic Edifices

Grounded ice of the Antarctic Ice Sheet has repeatedly advanced across the Ross

Sea region since at least the Oligocene [*Barrett*, 2009]. Over the past 5 Myr, 38 cycles of

ice advance/retreat are recorded in the AND-1B sedimentary rock core from south of

Ross Island [*Naish, et al.*, 2009]. Even the youngest features sampled in this study have

therefore undergone some extent of glaciation and could have been substantially eroded

during these glacial advance/retreat cycles. Behrendt et al. [1996] presented magnetic

models for inferred late Cenozoic magmatic bodies in selected regions of the WARS,

including the western Ross Sea region of this study. Morphologic profiles across the

magmatic bodies from seismic reflection data showed volcanic edifices with preserved

sharp relief, suggesting they were not glacially eroded and therefore of "post-latest

deglaciation age" [*Behrendt, et al.*, 1996]. Seismic profiles over the two Ross Sea

magnetic anomalies modeled by Behrendt et al. [1996] are shown in Fig. 2-11, which

show the seamounts sampled by dredge 4 and 5 of this study. The 3.9 Ma dredge 4 body

has relatively low, smooth relief on this seismic profile, but the swath bathymetry shows

it has much more substantial relief just east of the seismic line. The 1.9 Ma dredge 5 body

is steep-sided, with high relief. 'Potter Peak' and the small vents near Franklin Island

sampled by dredges 1, 3, 6 and 7 still show clear volcanic cone morphologies. All the seafloor volcanic features are interpreted to have been covered by grounded ice at the Last Glacial Maximum [*Shipp, et al.*, 1999] at about 11,000 ka, and likely were covered in numerous older glacial cycles. The preservation of volcanic edifices through millions of years of glaciation indicates that morphology is not a reliable indicator of age, and rugged relief is not a useful criterion for assigning a 'post-deglaciation' age. It is still possible, however, that some material has been removed from the volcanic vents, hence the volumes calculated for the features sampled in this study are still considered to be minimum estimates, even though there appears to have been only minimal glacial removal of material.

4. Relationship Between Volcanism and Tectonic Evolution

A recent study by Paulsen and Wilson [2009] demonstrated that Plio-Pleistocene parasitic cones in the Mt. Morning region developed along NE trending fissures controlled by a regional stress field. Several features in the Ross Sea show similar north to northeast trends. The seamount sampled by dredge 5 has an elongate shape, more than 2.5 longer along a NNE trend than the width. The FIVR also occurs along a NNE trend, and the smaller cones on the ridge sampled by dredges 1 and 7 have very minor elongations. 'Potter Peak' and the large seamount sampled by dredge 4 show elongations along a NNE trend with a roughly 1.5:1 length to width ratio for both features. With such low axial ratios, it could also be argued that these edifices are approximately circular. The small seamounts sampled by dredges 3 and 6, as well as Beaufort Island, are more circular features. From a regional perspective, the individual volcanic features appear to align along two general trends. Beaufort Island and the dredge 5 seamount lie on a N-S

trend between Mt. Erebus and Mt. Melbourne. Another volcanic feature located north of the dredge 5 seamount, not sampled by dredging, occurs along the same trend (Fig. 2). The dredge 4 edifice, the small seamount of dredge 1, the FIVR, and 'Potter Peak' lie along a subparallel NNE-SSW trend to the east.

The elongated individual edifices and the regional volcanic lineaments could mark the trends of pre-existing Terror Rift faults that were used for magma ascent to the seafloor. Alternatively, the elongated volcanic edifices may indicate fissure-fed eruptions controlled by a regional stress field of the same orientation as documented at Mt Morning. Comparison of the volcanic elongations and lineaments (Fig. 2-10) shows that Beaufort Island and the other volcanic bodies along the ~N-S trend are aligned along the margin of the major fault zone defining the eastern boundary of the Terror Rift [*Hall*, 2006; *Hall, et al.*, 2007], suggesting structural control on the eruptive conduits. The main Franklin Island region NNE-SSW trend falls east of the dominant zone of Terror rift faulting, and may be more compatible with fissure development controlled by regional stresses [*Smith, et al.*, 2004].

Although rifting to form the VLB occurred mainly in Paleogene-early Miocene times, the Terror Rift is a superimposed structural zone along the central VLB that is younger than the VLB deformation [*Cooper, et al.*, 1987; *Salvini, et al.*, 1997]. The onset of Terror Rift deformation has been associated with a regional seismic disconformity known to be younger than 17 Ma from drillcore constraints from the Cape Roberts Project [*Fielding, et al.*, 2006]. A major angular unconformity truncates faults and fault-related folds formed during the main phase of Terror Rift deformation in the north-central Terror Rift, where fault geometry is not obscured by younger volcanism [*Hall, et al.*,

40

2007]. Terror Rift faults also cut and displace this unconformity, reaching, and possibly displacing, the seafloor [*Hall, et al.*, 2007; *Rossetti, et al.*, 2006]. Based on age constraints for the seismic reflectors from AND-1B drillcore strata, the main Terror rift phase occurred in the mid-late Miocene, followed by less pervasive faulting of Plio-Pleistocene to recent age [*Henrys, et al.*, 2007; *Naish, et al.*, 2009]. The new age data, in context of the regional eruptive history summarized here, suggest that the onset of more voluminous volcanism occurred just after the main-phase Terror Rift deformation. It appears that only minor rifting accompanied the widespread Plio-Pleistocene volcanism. Generation of the Ross Sea volcanism may therefore be related to decompression resulting from Terror Rift extension.

We show immediately below that decompression melting of typical anhydrous peridotite due to Terror Rift extension cannot generate the volcanism documented in this study. The initial crustal structure in the VLB prior to Terror Rift extension is assumed to be similar to the crust in the present day Coulman High and Central High (~ 25 km thick). The lack of sufficient seismic data across the VLB limits the accuracy of extension magnitude estimates for the Terror Rift, which controls the degree of exhumation of the lower crust below the volcanic province. Henrys et al. [2007] reported 10 to 15 km lateral extension based on the available limited seismic information. Using this estimate, and assuming that the majority of upper crustal thinning is due to mid-late Miocene extension along the Terror Rift, we calculate an approximate decrease in pressure at the base of the crust of only 0.10 to 0.22 GPa, assuming the crustal densities determined by Trey et al. [1999]. Considering both the McMurdo geotherm and NVL geotherms determined by Berg et al. [1989] and Perinelli et al.[2006], respectively, this change in pressure is

insufficient to cross the anhydrous peridotite solidus and generate partial melting without

also invoking an additional heat source such as a plume or mantle upwelling along the

craton margin (Fig. 2-12). Neither thermobarometry study noted the presence of an

anomalous heat source, as would be expected for plume-related magmatism, and instead

defined a more typical rift geotherm than a hotspot geotherm [*Berg, et al.*, 1989; *Perinelli,*
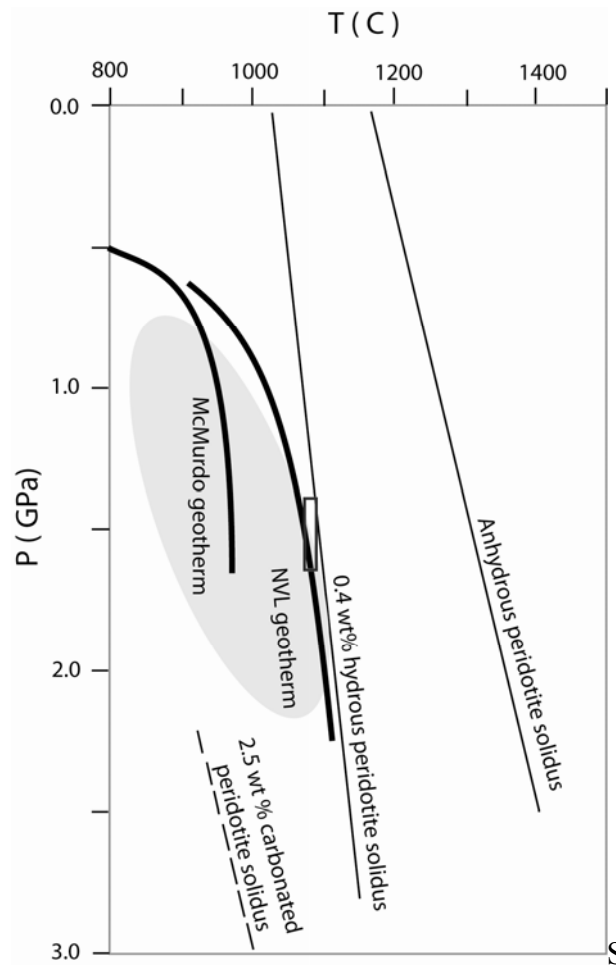
et al., 2006].

Figure 2-12. Box outlines an example of 0.22 GPa of decompression. Grey shading represents PT conditions determined from NVL xenoliths. Figure modified from Perinelli et al. [2006]. McMurdo geotherm is from Berg et al. [1989]. The 2.5 wt% carbonated peridotite solidus is approximated from high pressure determinations in Dasgupta et al. [2007; *Dasgupta, et al.*, 2006].

A modified mantle source (carbonated and/or hydrous peridotite) has a lower solidus and would therefore melt under smaller decreases in pressure than anhydrous peridotite. Perinelli et al. [2006] demonstrated that the solidus of a hydrous peridotite (<0.4 wt% H_2O) is very close and even meets the Ross Sea geotherm at pressures > 2 GPa. The 0.10 to 0.22 GPa of decompression calculated for Terror Rift extension between the Miocene and onset of Terror Rift volcanism is adequate to cross their proposed 0.4 wt% solidus at pressures greater than ~1.5 GPa. The experimentally determined solidus of peridotite + 2.5 wt % carbonate [*Dasgupta, et al.*, 2007; *Dasgupta, et al.*, 2006] falls well below the McMurdo and NVL geotherms, but lower concentrations of carbonate would yield higher temperature solidii, between the anhydrous peridotite solidus and the 2.5 wt % carbonated peridotite solidus. These compositions could also generate partial melting with limited decompression. This suggests that the mantle below the VLB contains at least 0.4 wt% H_2O or minor amounts of carbonate in order for Terror Rift related decompression to generate the observed volumes of volcanism.

CONCLUSIONS

Volcanic activity at Franklin Island and Beaufort Island, as well as several seamounts along the Terror Rift in the Ross Sea, Antarctica, ranges in age from 6.80 Ma to 90 ka. These ages overlap volcanism previously dated in both the Melbourne and Erebus Volcanic Provinces to the north and south of the study area, respectively. Our new documentation of the extent of volcanism on the sea floor shows that there is very widespread Pliocene and Pleistocene volcanism along the Terror Rift post-dating the

Miocene phase of major extension. This timing is consistent with a model of decompressional melting; however, the change in pressure due to main-phase mid-late Miocene extension in the Terror Rift is insufficient for melting of an anhydrous mantle peridotite source rock along the regional geotherm. A modified mantle source must be invoked in order for melting to be produced due to extensional deformation. Lava volumes and estimated minimum eruption rates are consistent with other rift systems and with proposed rates for the rapid build up of nearby Mt. Erebus and Ross Island.

REFERENCES

Armienti, P., L. Civetta, F. Innocenti, P. Manetti, A. Tripodo, L. Villari, and G. Vita (1991), New petrological and geochemical data on Mt. Melbourne volcanic field, northern Victoria Land, Antarctica, *Memorie della Societa Geologica Italiana*, *46*, 397-424.

Armstrong, R. L. (1978), K-Ar dating: Late Cenozoic McMurdo Volcanic Group and dry valley glacial history, Victoria Land, Antarctica, *New Zealand Journal of Geology and Geophysics*, *21(6)*, 658-698.

Barrett, P. J. (2009), A History of Antarctic CenozoicGlaciation-View from the Margin, in *Developments in Earth & Environmental Sciences*, edited by F. Florindo and M. Siegert, pp. 33-83.

Behrendt, J. C. (1999), Crustal and lithospheric structure of the West Antarctic Rift System from geophysical investigations - a review, *Global And Planetary Change*, *23*, 25-44.

Behrendt, J. C., D. D. Blankenship, C. A. Finn, R. E. Bell, R. E. Sweeney, S. M. Hodge, and J. M. Brozena (1994), CASERTZ aeromagnetic data reveal late Cenozoic flood basalts in the West Antarctic rift system, *Geology*, *22*, 527-530.

Behrendt, J. C., R. Saltus, D. Damaske, A. McCafferty, C. A. Finn, D. Blankenship, and R. E. Bell (1996), Patterns of late Cenozoic volcanic and tectonic activity in the West Antarctic rift system revealed by aeromagnetic surveys, *Tectonics*, *15*, 660-676.

Berg, J. H., R. J. Moscati, and D. L. Herz (1989), A petrologic geotherm from a continental rift in Antarctica, *Earth and Planetary Science Letters*, *93*, 98-108.
Cande, S. C., and D. V. Kent (1995), Revised Calibration Of The Geomagnetic Polarity Timescale For The Late Cretaceous And Cenozoic, *Journal Of Geophysical Research-Solid Earth*, *100*, 6093-6095.

Cande, S. C., and J. M. Stock (2006), Antarctica: Contributions to global earth sciences. "Constraints on the Timing of Extension in the Northern Basin, Ross Sea, 319-326.

Cande, S. C., J. M. Stock, R. D. Muller, and T. Ishihara (2000), Cenozoic motion between East and West Antarctica, *Nature*, *404*, 145-150.

Chiappini, M., F. Ferraccioli, E. Bozzo, and D. Damaske (2002), Regional compilation and analysis of aeromagnetic anomalies for the Transantarctic Mountains - Ross Sea sector of the Antarctic, *Tectonophysics*, *347*, 121-137.

Cooper, A. F., L. J. Adam, R. F. Coulter, G. N. Eby, and W. C. McIntosh (2007), Geology, geochronology and geochemistry of a basanitic volcano, White Island, Ross Sea, Antarctica, *Journal Of Volcanology And Geothermal Research*, *165*, 189-216.

Cooper, A. K., F. J. Davey, and J. C. Behrendt (Eds.) (1987), *Seismic stratigraphy and structure of the Victoria Land basin, western Ross Sea, Antarctica*, 27-66 pp., The Circum-Pacific for Energy and mineral Resources, Houston, TX.

Crisp, J. A. (1984), Rates of Magma Emplacement and Volcanic Output, *Journal of Volcanology and Geothermal Research*, *20*, 177-211.

Dasgupta, R., M. M. Hirschmann, and N. D. Smith (2007), Partial melting experiments of peridotite CO2 at 3 GPa and genesis of alkalic ocean island basalts, *Journal Of Petrology*, *48*, 2093-2124.

Dasgupta, R., M. M. Hirschmann, and K. Stalker (2006), Immiscible transition from carbonate-rich to silicate-rich melts in the 3 GPa melting interval of eclogite plus CO2 and genesis of silica-undersaturated ocean island lavas, *Journal Of Petrology*, *47*, 647-671.

Davey, F. J., and G. Brancolini (1995), The late Mesozoic and Cenozoic structural setting of the Ross Sea region, *Antarctic Research Series*, *68*, 167-182.

Davey, F. J., and L. De Santis (2006), A multi-phase rifting model for the Victoria Land Basin, western Ross Sea, *Antarctica: Contributions to Global Earth Sciences*, 303-308.

Decesari, R. C., D. S. Wilson, B. P. Luyendyk, and M. Faulkner (2007), Cretaceous and Tertiary extension throughout the Ross Sea, Antarctica, paper presented at Tenth International Symposium on Antarctic Earth Sciences, United States Geological Survey and The National Academies.

Di Vincenzo, G., S. Rocchi, F. Rossetti, and F. Storti (2004), Ar-40-Ar-39 dating of pseudotachylytes: the effect of clast-hosted extraneous argon in Cenozoic fault-generated friction melts from the West Antarctic Rift System, *Earth And Planetary Science Letters*, *223*, 349-364.

Esser, R. P., and P. R. Kyle (2002), 40Ar/39Ar chronology of the McMurdo Volcanic Group at The Pleiades, northern Victoria Land, Antarctica, *Royal Society of New Zealand Bulletin*, *35*, 415-418.

Esser, R. P., P. R. Kyle, and W. C. McIntosh (2004), Ar-40/Ar-39 dating of the eruptive history of Mount Erebus, Antarctica: volcano evolution, *Bulletin Of Volcanology*, *66*, 671-686.

Esser, R. P., W. C. McIntosh, M. T. Heizler, and P. R. Kyle (1997), Excess argon in melt inclusions in zero-age anorthoclase feldspar from Mt. Erebus, Antarctica, as revealed by the Ar-40/Ar-39 method, *Geochimica Et Cosmochimica Acta*, *61*, 3789-3801.

Esser, R. P., W.C.McIntosh, M. T. Heizler, and P. R. Kyle (1997), Excess argon in melt inclusions in zero-age anorthoclase feldspar from Mt. Erebus, Antarctica, as revealed by the 40Ar/39Ar method, *Geochimica e Cosmochimica Acta*, *61*, 3789-3801.

Fielding, C. R., S. A. Henrys, and T. J. Wilson (Eds.) (2006), *Rift history of the western Victoria Land Basin: a new perspective based on integration of cores with seismic reflection data*, Springer-Verlag, New York.

Frey, H. M., R. A. Lange, C. M. Hall, and H. Delgado-Granados (2004), Magma eruption rates constrained by Ar-40/Ar-39 chronology and GIS for the Ceboruco-San Pedro volcanic field, western Mexico, *Geological Society Of America Bulletin*, *116*, 259-276.

Hall, J. M. (2006), Structural Evolution of the Terror Rift, Western Ross Sea, Antarctica: Interpretation from 2D Reflection Seismic, 202 pp, The Ohio State University, Columbus, OH.

Hall, J. M., T. J. Wilson, and S. Henrys (2007), Structure of the central Terror Rift, western Ross Sea, Antarctica, paper presented at Tenth International Symposium on Antarctic Earth Sciences, United States Geological Society and The National Academies, Santa Barbara, CA.

Harpel, C. J., P. R. Kyle, R. P. Esser, W. C. McIntosh, and D. A. Caldwell (2004), Ar-40/Ar-39 dating of the eruptive history of Mount Erebus, Antarctica: summit flows, tephra, and caldera collapse, *Bulletin Of Volcanology*, *66*, 687-702.

Henrys, S., T. Wilson, J. M. Whittaker, C. R. Fielding, J. M. Hall, and T. R. Naish (2007), Tectonic history of mid-Miocene to present southern Victoria Land Basin, inferred from seismic stratigraphy in McMurdo Sound, Antarctica, paper presented at Tenth International Symposium on Antarctic Earth Sciences, United States Geological Survey, Santa Barbara, CA.

Kuntz, M. A., D. E. Champion, E. C. Spiker, and R. H. Lefebvre (1986), Contrasting magma types and steady-state, volume-predictable, basaltic volcanism along the Great Rift, Idaho, *Geological Society of America Bulletin*, *97*, 579-594.

Kyle, P., and H. L. Muncy (1989), Geology and geochronology of McMurdo Volcanic Group rocks in the vicinity of Lake Morning, McMurdo Sound, Antarctica, *Antarctic Science*, *1(4)*, 345-350.

Kyle, P. R. (1990), Erebus Volcanic Province, in *Volcanoes of the Antarctic Plate and the Southern Oceans*, edited by W. E. LeMasurier and J. W. Thompson, pp. 81-88, American Geophysical Uniion, Washington, D.C.

Kyle, P. R., J. A. Moore, and M. F. Thirlwall (1992), Petrologic Evolution Of Anorthoclase Phonolite Lavas At Mount Erebus, Ross Island, Antarctica, *Journal Of Petrology*, *33*, 849-875.

Lanphere, M. A., and G. B. Dalrymple (1976), Identification Of Excess Ar-40 By Ar-40-Ar-39 Age Spectrum Technique, *Earth And Planetary Science Letters*, *32*, 141-148.

Lawver, L. A., M. B. Davis, and T. J. Wilson (2007), Neotectonic and other features of the Victoria Land Basin, Antarctica, interpreted from multibeam bathymetry data, paper presented at Tenth International Symposium on Antarctic Earth Sciences, United States Geological Survey, Santa Barbara, CA.

Lawver, L. A., and L. M. Gahagan (2003), Evolution of Cenozoic seaways in the circum-Antarctic region, *Palaeogeography Palaeoclimatology Palaeoecology*, *198*, 11-37.

LeMasurier, W. E. (2008), Neogene extension and basin deepening in the West Antarctic rift inferred from comparisons with the East African rift and other analogs, *Geology*, *36*, 247-250.

LeMasurier, W. E., and J. W. Thomson (Eds.) (1990), *Volcanoes of the Antarctic Plate and Southern Oceans*, 487 pp., American Geophysical Union, Washington, D.C. McIntosh, W. C., and R. P. Esser (2005), 40Ar-39Ar Geochronology Results from McMurdo Sound Area, Antarctica: New Mexico Bureau of Geology and Mineral Resources, *Open-File Report, OF-AR-34*, p. 50.

Naish, T., R. Powell, R. Levy, G. Wilson, R. Scherer, F. Talarico, L. Krissek, F. Niessen, M. Pompilio, T. Wilson, L. Carter, R. DeConto, P. Huybers, R. McKay, D. Pollard, J. Ross, D. Winter, P. Barrett, G. Browne, R. Cody, E. Cowan, J. Crampton, G. Dunbar, N. Dunbar, F. Florindo, C. Gebhardt, I. Graham, M. Hannah, D. Hansaraj, D. Harwood, D. Helling, S. Henrys, L. Hinnov, G. Kuhn, P. Kyle, A. Laufer, P. Maffioli, D. Magens, K. Mandernack, W. McIntosh, C. Millan, R. Morin, C. Ohneiser, T. Paulsen, D. Persico, I. Raine, J. Reed, C. Riesselman, L. Sagnotti, D. Schmitt, C. Sjunneskog, P. Strong, M. Taviani, S. Vogel, T. Wilch, and T. Williams (2009), Obliquity-paced Pliocene West Antarctic ice sheet oscillations, *Nature*, *458*, 322-U384.

Paulsen, T. S., and T. J. Wilson (2009), Structure and age of volcanic fissures on Mount Morning: A new constraint on Neogene to contemporary stress in the West Antarctic rift, southern Victoria Land, Antarctica, *Geological Society of America Bulletin*, *in press*.

Perinelli, C., P. Armienti, and L. Dallai (2006), Geochemical and O-isotope constraints on the evolution of lithospheric mantle in the Ross Sea rift area (Antarctica), *Contributions To Mineralogy And Petrology*, *151*, 245-266.

Renne, P. R., C. C. Swisher, A. L. Deino, D. B. Karner, T. L. Owens, and D. J. DePaolo (1998), Intercalibration of standards, absolute ages and uncertainties in Ar-40/Ar-39 dating, *Chemical Geology*, *145*, 117-152.

Rocchi, S., P. Armienti, M. D'Orazio, S. Tonarini, J. R. Wijbrans, and G. DiVincenzo (2002), Cenozoic magmatism in the western Ross Embayment: Role of mantle plume

versus plate dynamics in the development of the West Antarctic Rift System, *Journal of Geophysical Research, 107*.

Rocholl, A., M. Stein, M. Molzahn, S. R. Hart, and G. Worner (1995), Geochimcal evolution of rift magmas by progressive tapping of a stratified mantle source beneath the Ross Sea Rift, Northern Victoria Land, Antarctica, *Earth and Planetary Science Letters, 131*, 207-224.

Rossetti, F., F. Storti, M. Busetti, F. Lisker, G. Di Vincenzo, A. L. Laufer, S. Rocchi, and F. Salvini (2006), Eocene initiation of Ross Sea dextral faulting and implications for East Antarctic neotectonics, *Journal of the Geological Society of London, 163*, 119-126.

Salvini, F., G. Brancolini, M. Busetti, F. Storti, F. Mazzarini, and F. Coren (1997), Cenozoic geodynamics of the Ross Sea region, Antarctica: Crustal extension, intraplate strike-slip faulting, and tectonic inheritance, *Journal of Geophysical Research, 102(B11)*, 24,669-624,696.

Shipp, S., J. B. Anderson, and E. W. Domack (1999), Late Pleistocene-Holocene retreat of the West Antarctic ice-sheet system in the Ross Sea; Part 1, Geophysical results, *Geological Society of America Bulletin, 111(10)*, 1486-1516.

Siddoway, C. (2008), Tectonics of the West Antarctic rift system: New light on the history and dynamics of distributed intracontinental extension (invited paper), paper presented at Tenth International Symposium on Antarctic Earth Sciences, United States Geological Survey and the The National Academies Press, Santa Barbara, CA.

Smith, A., T. J. Wilson, M. Davis, L. A. Lawver, and S. B. Mukasa (2004), Franklin Volcanic Field: Characteristics of a Submarine Volcanic Province in the Western Ross Sea, Antarctica, *Eos Trans. AGU, 85*, T11A-1231.

Storti, F., M. L. Balestrieri, F. Balsamo, and F. Rossetti (2008), Structural and thermochronological constraints to the evolution of the West Antarctic Rift System in central Victoria Land, *Tectonics, 27*.

Tessensohn, F., and G. Worner (1991), The Ross Sea rift system, Antarctica; structure, evolution and analogues, paper presented at International Symposium on Antarctic Earth Sciences, Cambridge, United Kingdom.

Trey, H., A. K. Cooper, G. Pellis, B. della Vedova, G. Cochrane, G. Brancolini, and J. Makris (1999), Transect across the West Antarctic rift system in the Ross Sea, Antarctica, *Tectonophysics, 301*, 61-74.

White, S. M., J. A. Crisp, and F. J. Spera (2006), Long-term volumetric eruption rates and magma budgets, *Geochemistry Geophysics Geosystems, 7*.

Wilson, T. J., L. A. Lawver, S. A. Henrys, S. Mukasa, H. Horgan, M.Weiderspahn, M. Davis, J. Whittaker, A. Lowe, and M. Watson (2004), Cruise Report NBP0401 19 January to 18 February 2004 - McMurdo Station to McMurdo Station, Ross Sea, Antarctica, *Institute of Geological and Nuclear Sciences Science Report*, *2004/03*, 85.

Worner, G. (1999), Lithospheric dynamics and mantle sources of alkaline magmatism of the Cenozoic West Antarctic Rift System, *Global and Planetary Change*, *23*, 61-77.

CHAPTER 3

GEOCHEMICAL EVIDENCE OF A CARBONATED OR METASOMATIZED MANTLE SOURCE FOR CENOZOIC LAVAS FROM ROSS SEA REGION OF THE WEST ANTARCTIC RIFT SYSTEM

ABSTRACT

Samples from seven seamounts in the Terror Rift region of the Ross Sea were dredged during the 2004 NBP-0401 research cruise on research icebreaker *Nathaniel B. Palmer.* Analyses of these samples provide the first geochemical information from submarine lavas in the Ross Sea. Subaerial samples from Franklin and Beaufort Islands as well as various localities near Mt Melbourne in Northern Victoria Land (NVL) were also analyzed for comparison. These alkaline basalts are similar in major and trace element composition to samples from throughout the West Antarctic Rift System (WARS). The major element compositions of the Ross Sea lavas more closely match experimental melts of carbonated peridotite than anhydrous peridotite, which is an expected mantle plume composition. This information, along with new interpretations of the enriched trace element signatures, supports a new hypothesis of contributions from the lithospheric and asthenospheric mantle for Cenozoic WARS magmas. Nd and Sr isotopic compositions from twenty-four samples plot near the HIMU mantle endmember and contradict Pb and Hf isotopic compositions that plot between the HIMU and DMM endmembers. The addition of these samples to previous sample suites allows us to test a larger dataset for previously hypothesized temporal and regional variations of the mantle source isotopic signature.

We propose varying proportions of a lithospheric mantle source that has been modified by ~400 Myrs of subduction and flux melting during the Paleozoic and Mesozoic and an asthenospheric source for the Ross Sea and northern Victoria Land (NVL) region of the WARS. Subduction-related magmas and fluids removed fluid-mobile elements, including Pb, from the mantle wedge. The less radiogenic Pb isotopic signatures of Cenozoic lavas reflect the mixing of the original HIMU-like isotopic signature of the source and the signature of subduction magmas and fluids. The lithospheric component of the Ross Sea and NVL lavas has increased since the Miocene and is likely the result of rifting-induced decompression and heat applied to the base of the lithosphere by upwelling of hot asthenosphere. This model explains the minor isotopic variations in the WARS lavas as a result of variations in the mantle lithosphere along the ancient subduction margin and eliminates the need for a complex mantle source stratified with numerous endmember compositions.

INTRODUCTION

West Antarctica (Fig. 3-1) is comprised of several tectonic blocks which were once amalgamated with the Chatham Rise, Campbell Plateau, and New Zealand to form the long-lived subduction zone along the paleo-Pacific margin of the supercontinent Gondwana. The Granite Harbour Intrusive suite provides evidence of subduction related magmatism by ~530 Ma, initially along the Trans-Antarctic mountains (TAM) region [*Rocchi, et al.*, 1998]. This subduction continued, perhaps episodically, through the Mesozoic and began a progressive west to east cessation between 110 Ma in western present day Marie Byrd Land (MBL) and 94 Ma in eastern MBL [*Mukasa and Dalziel*, 2000].
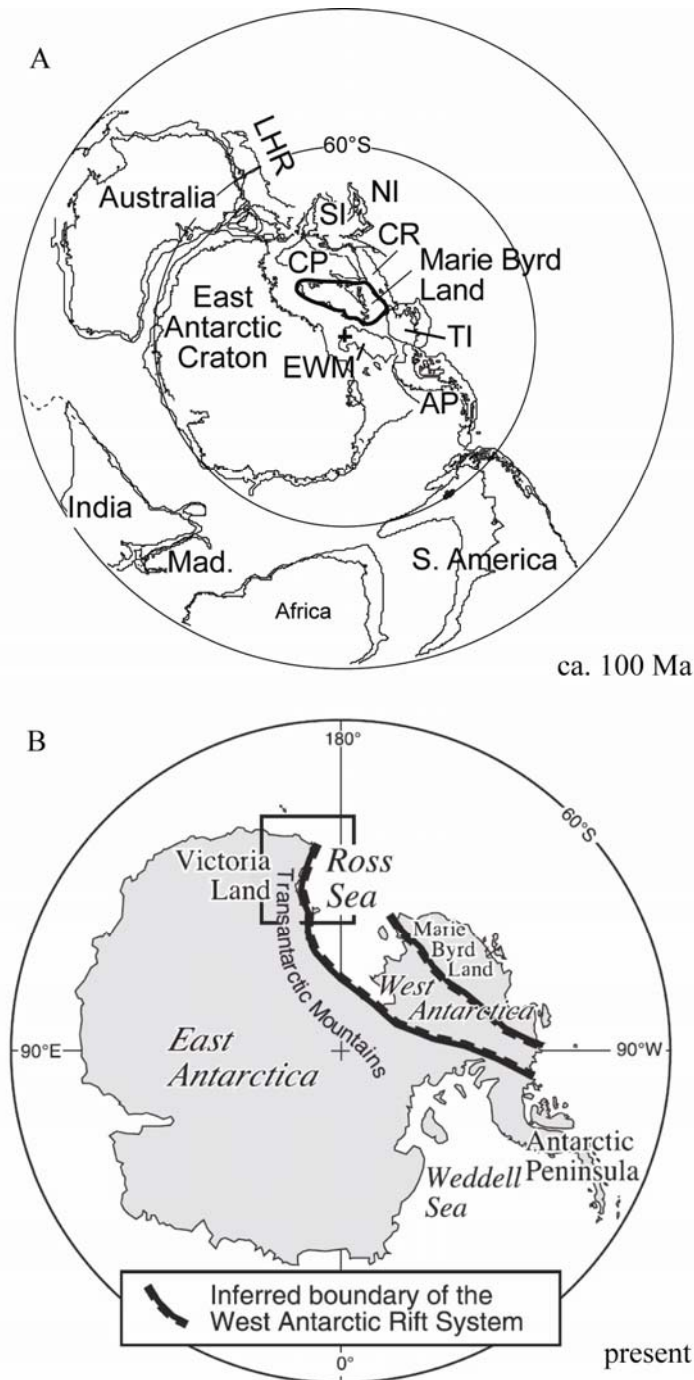
Figure 3-1. A.) Tectonic reconstruction of the paleo-Pacific margin of Gondwana ca. 100 Ma. AP – Antarctic Peninsula; CP – Campbell Plateau; CR – Chatham Rise; EWM – Ellsworth-Whitmore block; LHF – Hord How Rise; NI – North Island, New Zealand; SI – South Island, New Zealand; TI – Thurston Island block. Figure modified from [*Mukasa and Dalziel*, 2000]. B.) Present day orientation of the Antarctic continent and inferred boundary of the West Antarctic Rift system. Figure A from [*Rocchi, et al.*, 2002].

Supercontinent break-up along this paleo-Pacific margin of Gondwana followed this period of convergence. The most recent studies estimate the complete separation of New Zealand, Campbell Plateau, and Chatham Rise from West Antarctica by ~ 83 Ma [*Eagles, et al.*, 2004; *Brown, et al.*, 2006]. Initiation of West Antarctic Rift System (WARS) extension and opening of the Ross Sea embayment began in the Cretaceous with primarily amagmatic processes [*Salvini, et al.*, 1997]. Rift-related magmatism in Northern Victoria Land (NVL) began ~48 Ma [*Rocchi, et al.*, 2002] and in MBL at ~30 Ma [*Hart, et al.*, 1997]. Behrendt [1999] estimated the volume of Cenozoic eruptive products in the WARS to be more than 10^6 km^3, with a sizeable fraction of this material thought to be beneath the West Antarctic Ice Sheet. Volcanism of similar age and composition is found in all tectonic blocks that were previously located along the paleo-Pacific Gondwanan margin, although they are now separated by ocean basins and distances upwards of 2000 km. Finn et al. [2005] termed this area the Diffuse Alkaline Magmatic Province (or DAMP spot).

Previous explanations of WARS magmatism have included (1) a single plume beneath MBL [*Behrendt, et al.*, 1994; *Hole and LeMasurier*, 1994; *Behrendt, et al.*, 1996; *Behrendt*, 1999], (2) an injected subduction signature mixed with multiple other enriched mantle sources [*Hart, et al.*, 1995], and (3) decompressional melting of a fossilized plume head below the entire region [*Rocholl, et al.*, 1995; *Panter, et al.*, 2000]. Hole and LeMasurier [1994] postulated that a mantle plume roughly 1500 by 2500 km was responsible for volcanism in MBL over the past 25-20 Ma, based on enrichments in incompatible trace element concentrations and the HIMU-like isotopic signature of analyzed lavas. Behrendt [1999] and Behrendt et al. [1994; 1996] also hypothesized the

possible presence of a plume located beneath MBL in order to explain the large volumes of lavas present under the West Antarctic Ice Sheet. Coeval volcanism in the Erebus Volcanic Province led Kyle et al. [1992] and Esser et al. [2004] to invoke a mantle plume model on the NVL side of the WARS as well. This requires a second plume at least 500 km in diameter, in close proximity to the MBL plume, as one way to explain the young volcanism on both edges of the WARS.

The proposal of a mantle source injected with material containing a subduction signature was made by Hart et al. [1997] based on one of the first studies to include Pb isotopic compositions. However, the Pb isotopic dataset is considerably smaller compared to the cumulative Sr and Nd isotopic datasets published in various studies throughout the WARS [*Futa and LeMasurier*, 1983; *Hole and LeMasurier*, 1994; *Hart, et al.*, 1995; *Rocholl, et al.*, 1995; *Hart, et al.*, 1997; *Panter, et al.*, 2000; *Rocchi, et al.*, 2002]. Studies on MBL lavas with both sets of data have demonstrated that $^{207}Pb/^{204}Pb$ and $^{208}Pb/^{204}Pb$ isotopic signatures are decoupled from the $^{87}Sr/^{86}Sr$ isotopic signatures [*Hart, et al.*, 1995; *Hart, et al.*, 1997]. The mechanism for this decoupling was not explained, and the authors concluded that the source of WARS magmatism was still uncertain. The observation of isotopic decoupling in the mantle source has not been further addressed by subsequent studies of the WARS until this study.

More recent explanations for WARS volcanism have focused on the concept of a fossilized plume head or stratified mantle source beneath the region. The Jurassic Ferrar dolerites are thought by some to have been sourced from a plume [*Storey, et al.*, 2001; *Riley, et al.*, 2003], the remnants of which could have underplated the base of the Antarctic lithosphere. Asthenospheric mantle combined with this presumed ancient

plume material, have been proposed as the sources of volcanism associated with thinning of the WARS lithosphere. Rocholl et al. [1995] called for at least three mantle end-members (MORB-type or DMM, EM, and HIMU-like) in the source components, and suggested that some of the geochemical differences are the result of variations in the degrees and depths of melting. They attribute the differences in melting depth to the distance of volcanism from the rift shoulder. Hart et al. [1997] also called for a stratified mantle source for volcanism in MBL. They noted that melts generated at the deepest levels yielded HIMU isotopic signatures while those generated at shallower depths yielded isotopic signatures more similar to FOZO, as defined by Hart et al. [1986]. Panter et al. [2000] suggested that lavas with isotopic compositions closest to the HIMU mantle end member were instead the result of smaller degree partial melts than those with a more FOZO type isotopic signature, and melts which yielded a mixture of isotopic signatures were the result of higher degrees of melting. If the mantle source was stratified, with fossil mantle plume material defining a layer below the lithospheric mantle, polybaric melting would generate melts with isotopic signatures that are mixtures of both layers.

Lack of exposure over much of the WARS and sparse sampling have so far impeded and complicated determinations of the source characteristics for magmas, and even impacted our ability to understand the nature of the rifting styles and overall tectonic evolution of the rift. Much of the region is covered by thick ice or water; therefore, sampled edifices tend to be focused in several distinct regions separated by hundreds or thousands of kilometers of virtually no exposure. This study provides information on several previously unsampled submarine and on-land locations within the Ross Sea as well as additional chemical analyses on samples in the Mt Melbourne region

of northern Victoria Land. Patterns of chemical characteristics are easier to determine based on these larger data sets than on the previous, smaller and geographically limited studies. The new results help address questions about the composition of the mantle source(s) below the WARS.

METHODS

Seven seamounts, Franklin Island, Beaufort Island, and several mainland locations surrounding Mt Melbourne were sampled in the field area shown in Figure 3-2. Submarine samples were obtained by dredging seven volcanic edifices associated with a variety of seafloor structures identified by mapping with multibeam bathymetry during the 2004 NBP-0401 research cruise on research icebreaker *Nathaniel B. Palmer*. Tensions were monitored while the dredge was towed behind the ship, with the highest tensions, ranging from 3200 to 9000 lbs, interpreted as breaking "*in situ* outcrops" on the volcanic edifices. A variety of materials were collected, including basalts, hyaloclastites and peridotite xenoliths. Additional details of the dredged features can be found in Wilson et al. [2004]. Samples chosen for analysis had one fresh surface, interpreted to be a recent break resultant of dredging. Subaerial samples from Franklin Island were collected by members of the cruise with a zodiac from *Nathaniel B. Palmer*. Samples from Beaufort Island were collected by helicopter during GPS installations for another study by members of our party. The remaining samples from various localities in northern Victoria Land were collected during numerous field seasons by Prof Wesley LeMasurier.
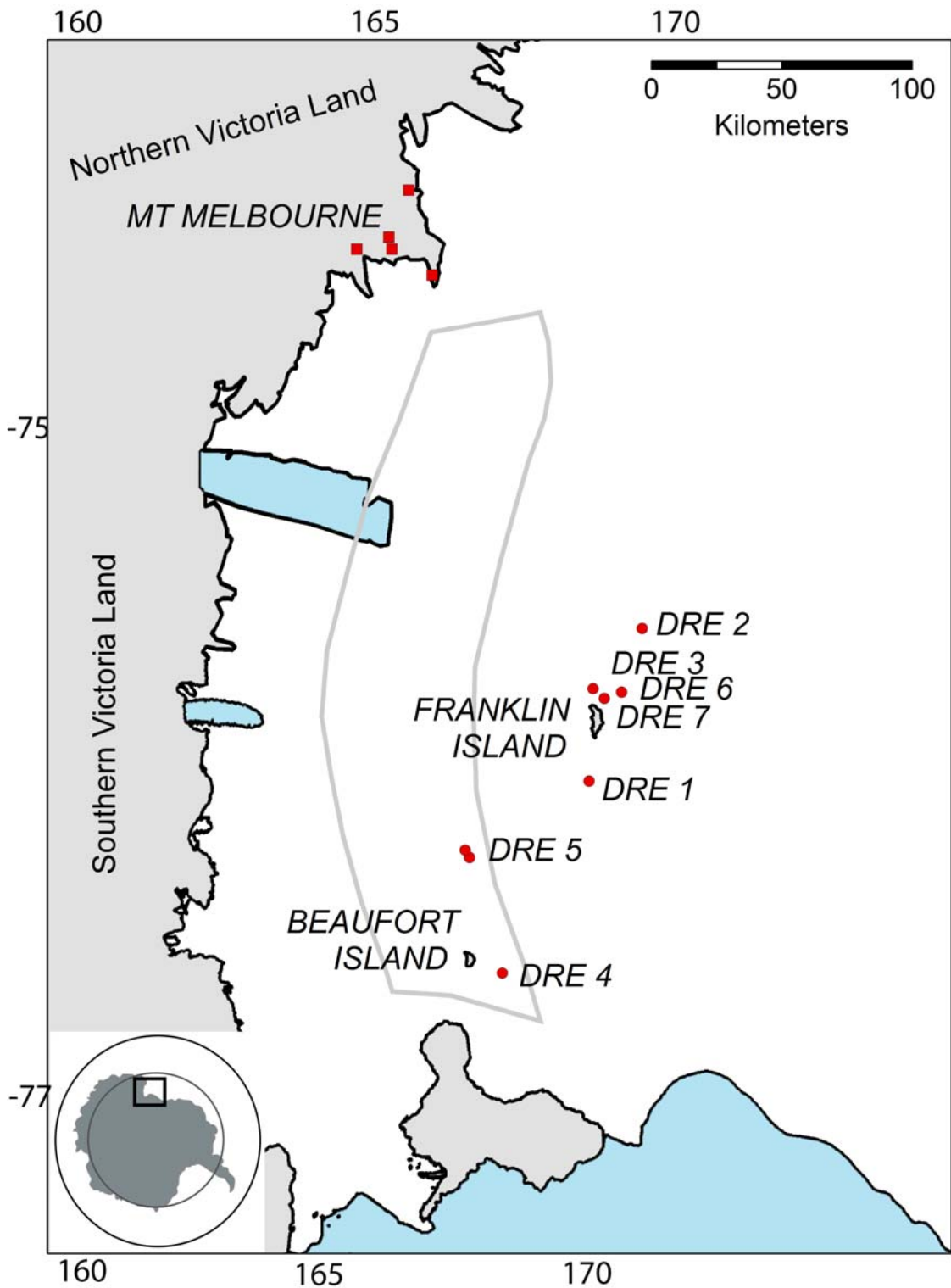
Figure 3-2. Location of samples from the Ross Sea and Victoria Land. Grey box outlines the Terror Rift.

Mineral compositions were determined on diamond-polished thin sections with the Cameca SX 100 electron microprobe at the University of Michigan Electron Microbeam Analysis Laboratory (EMAL). Beam power was set to 15 kV, and current was set to 60 μA. Typical counting times were 20 seconds for major elements and 30 seconds for minor elements. Diopside was used as a standard to generate a calibration for Ca and Si, enstatite for Mg, almandine for Fe and Al, albite for Na, rhodonite for Mn, uvaroite for Cr, and geikite for Ti. Ferrous and ferric iron concentrations in pyroxene were approximated by charge balancing to six oxygen atoms. Two separate analyses were performed for each sample to assess reproducibility of the calculations.

Sample chips for detailed chemical analyses were washed ultrasonically in deionized water and soaked in dilute (2.5N) HCl before crushing to a < 150 μm grain size. Major elements, Rb, Sr, and Zr were analyzed by x-ray fluorescence (XRF) and trace elements were measured by laser ablation inductively coupled plasma mass spectrometer (LA-ICP-MS) at the XRF and ICP-HEX-MS Laboratories of Michigan State University following the methods of Hooper et al., 1993, and at the Washington State University Geoanalytical Laboratory following the methods of Knaack et al. (1994) and Johnson et al. (1999). Three samples were analyzed by both laboratories to determine reproducibility. Pb concentrations were also determined by isotope dilution during isotopic analyses for six samples for comparison with ICP-MS analyses. Major elements and most trace elements agreed within 10%. Rb, Ho, V, Cr, and Nb varied within 15%. Pb showed up to 23% variation. Samples were sorted by major element data, removing those with high loss on ignition (over 3.5%) or low totals (less than 96 wt%) from further consideration during the isotopic analyses.

Analysis of Pb, Sr, and Nd isotopic compositions were completed on the VG Sector thermal ionization mass spectrometer (TIMS) at the University of Michigan according to the procedures of Mukasa et al. [1987; 1991]. Hf isotopic compositions were conducted on the Nu Plasma multi-collector inductively coupled plasma mass spectrometer (MC-ICP-MS), also at the University of Michigan, following the columns chemistry and analytical methods of Choi et al. [2006]. Instrumental mass fractionation of Pb was corrected by a factor of 0.12 percent per atomic mass unit (amu) based on replicate analyses of the standard NBS-981. The Sr and Nd isotopic ratios were normalized to $^{86}Sr/^{88}Sr$ to 0.1194 and $^{146}Nd/^{144}Nd$ to 0.7219, respectively. Replicate analyses of NBS-987 and La Jolla standards gave $^{87}Sr/^{86}Sr = 0.710255 \pm 0.000011$ (N = 30, 2σm) and $^{143}Nd/^{144}Nd = 0.511848 \pm 0.000019$ (N = 30, 2σm). A mean $^{176}Hf/^{177}Hf$ of 0.282166 ± 0.000021 (N = 14, 1σ$_m$) was determined from measured values of standard JMC-475. Sample values were normalized using standard-sample bracketing.

RESULTS

1. Petrography

The dredged samples, with few exceptions, are porphyritic with few phenocrysts, hypocrystalline, and are highly vesicular. The extent of chemical alteration varies widely amongst the dredged samples, and vesicles commonly are lined with secondary carbonate. Ultramafic xenoliths and xenocrysts are present to varying extents in all samples, and a few samples have rare granitic xenoliths. We followed a careful crushing and sorting procedure to ensure sample purity prior to any analysis. Multiple samples processed from each dredge location are chemically and mineralogically similar, with the exception of Dredge 4, which has two very different samples, and Dredge 2, which has only one

sample meeting the selection criterion, specifically evidence of a recently broken surface as a result of dredging the submarine outcrop.

Two samples from Dredge 1 (DRE1-31, DRE1-32) are porphyritic with phenocrysts of olivine and clinopyroxene in a microcrystalline matrix of predominantly clinopyroxene and oxides. Olivine phenocrysts range in size up to a few hundred micrometers and have Mg#s between 68 and 77. Clinopyroxene phenocrysts ($Na_{0.04}Ca_{0.90}Mg_{0.70}Fe^{2+}_{0.20}Fe^{3+}_{0.06}Ti_{0.06}Al_{0.21}Si_{1.82}O_6$) are comparable in size but are less abundant than olivine. Phenocrysts have abundant melt inclusions as well as spinel-magnetite solid solution and apatite mineral inclusions. Clinopyroxene ($Na_{0.04}Ca_{0.90}Mg_{0.61}Mn_{0.01}Fe^{2+}_{0.22}Fe^{3+}_{0.08}Ti_{0.09}Al_{0.30}Si_{1.76}O_6$) is the dominant groundmass phase and is invariably less than 20 μm in length. A few grains of xenocrystic olivine (Mg# = 87.5 – 89.7) display resorption textures (Fig. 3-3a) indicative of being out of equilibrium with the magma from which the basaltic rock formed.
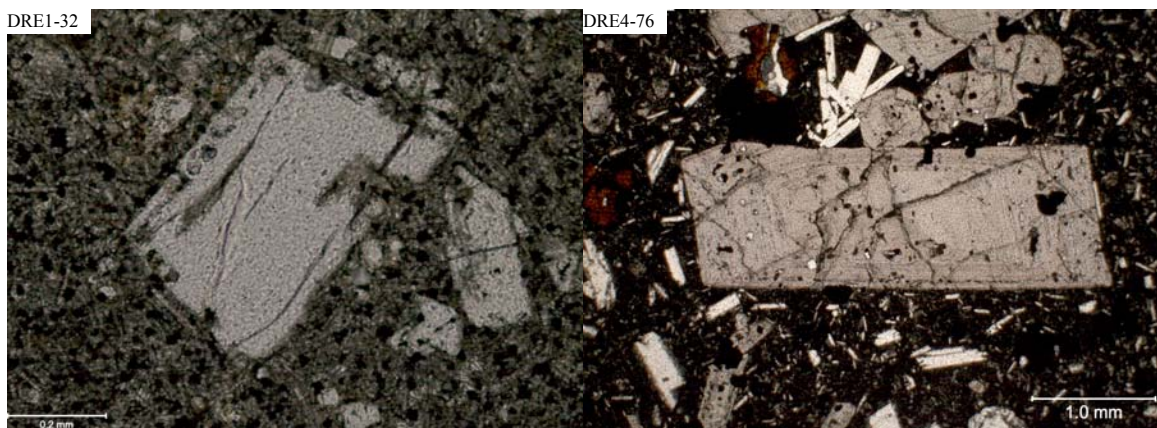

Figure 3-3. A.) Example of phenocryst texture B.) Example of common zonation in Ti-augite.

Only one sample (DRE2-42) from Dredge 2 was judged to be fresh enough to process for petrologic and geochemical analyses. It is one of the rare nonvesicular lava

sampled during dredging from the submarine volcanic edifices. Highly zoned Ti-rich clinopyroxene is the dominant phenocryst phase with grains up to 1 mm in size. Grains show reverse zoning with average compositions ranging from $Na_{0.04}Ca_{0.87}Mg_{0.51}Mn_{0.02}$ $Fe^{2+}_{0.42}Fe^{3+}_{0.01}Ti_{0.05}Al_{0.21}Si_{1.87}O_6$ at the core to $Na_{0.04}Ca_{0.87}Mg_{0.65}Mn_{0.01}Fe^{2+}_{0.23}Fe^{3+}_{0.03}$ $Ti_{0.08}Al_{0.32}Si_{1.77}O_6$ at the rim. Groundmass phases consist of clinopyroxene $(Na_{0.05}Ca_{0.86}Mg_{0.66}Mn_{0.01}Fe^{2+}_{0.24}Fe^{3+}_{0.02}Ti_{0.08}Al_{0.29}Si_{1.79}O_6)$, oxides, olivine (Mg# 67-69), and plagioclase. Xenocrystic olivine (Mg# = 85, Mg ~ 28 wt%, Fe~10 wt%) and clinopyroxene $(Na_{0.08}Ca_{0.73}Mg_{0.66}Mn_{0.01}Fe^{2+}_{0.16}Fe^{3+}_{0.25}Ti_{0.16}Al_{0.44}Si_{1.52}O_6)$ are both present and are often clustered together showing only minor disaggregation.

Dredge 3 had two samples (DRE3-59 and DRE3-73) which met the acceptance criteria. DRE3-73 is extremely crystal poor with a microcrystalline matrix of primarily clinopyroxene and only a few phenocrysts of olivine, each less than 0.5 mm in length. This sample is also the most vesicular in the entire sample suite. DRE3-59 has dramatically different crystallinity and only minor vesicularity. Clinopyroxene grains 75 to 100 μm in length are the dominant phenocrysts. Olivine grains are slightly less abundant, but are coarser grained, falling in the range of 200 – 300 μm in size. Clinopyroxene phenocrysts from DRE3-59 are zoned with average compositions of $Na_{0.03}Ca_{0.96}Mg_{0.61}Fe^{2+}_{0.07}Fe^{3+}_{0.14}Ti_{0.13}Al_{0.49}Si_{1.56}O_6$ at the core and $Na_{0.02}Ca_{0.95}Mg_{0.71}$ $Fe^{2+}_{0.10}Fe^{3+}_{0.10}Ti_{0.08}Al_{0.29}Si_{1.74}O_6$ at the rims. Phenocrysts of olivine in this sample are the most primitive analyzed in this study (Mg # = 86-88). Groundmass clinopyroxene in the two samples, within error, has the same chemical compositions -- $Na_{0.03}Ca_{0.95}Mg_{0.66}$ $Fe^{2+}_{0.06}Fe^{3+}_{0.15}Ti_{0.10}Al_{0.37}Si_{1.66}O_6$. Olivine compositions range between Mg# = 84 and Mg# = 87, and spinel-magnetite solid solution ranging in composition from

$Mg_{0.11}Fe^{2+}_{1.30}Fe^{3+}_{0.81}Ti_{0.43}Al_{0.30}O_4$ to $Mg_{0.66}Fe^{2+}_{0.38}Fe^{3+}_{0.33}Ti_{0.46}Al_{1.12}O_4$. One highly resorbed xenocrystic olivine is zoned with an Mg # = 89 at the core and only an Mg# = 82 at the rim.

The Dredge 4 samples, DRE4-75 and DRE4-76, both have abundant olivine and less abundant phenocrystic clinopyroxene, which differ from the composition of groundmass clinopyroxene. Groundmass phases in DRE4-76 are predominantly clinopyroxene, olivine, oxides, and plagioclase while DRE4-75 has clinopyroxene, olivine, and oxides but lacks plagioclase. Olivine phenocrysts from both samples have Mg # of 81-82 and are up to 2 mm in length, although most range between 0.1 to 0.4 mm. Clinopyroxene phenocrysts are highly zoned. One grained analyzed has an Mg-rich core, $Na_{0.03}Ca_{0.84}Mg_{0.76}Mn_{0.01}Fe^{2+}_{0.16}Fe^{3+}_{0.13}Ti_{0.07}Al_{0.25}Si_{1.76}O_6$, and less Mg-rich rim with a composition of $Na_{0.04}Ca_{0.94}Mg_{0.70}Fe^{2+}_{0.12}Fe^{3+}_{0.10}Ti_{0.06}Al_{0.24}Si_{1.78}O_6$. There are also two thin rims with sharp increases in Mg (Fig. 3-3b). Groundmass clinopyroxene with an average composition of $Na_{0.04}Ca_{0.92}Mg_{0.68}Mn_{0.01}Fe^{2+}_{0.14}Fe^{3+}_{0.11}Ti_{0.08}Al_{0.29}Si_{1.74}O_6$ is the most abundant phase in DRE4-75, with lesser oxides, which are close to the magnetite end of the spinel-magnetite solid solution. The groundmass of DRE4-76 has clinopyroxene grains with similar composition, $Na_{0.03}Ca_{0.89}Mg_{0.69}Fe^{2+}_{0.05}Fe^{3+}_{0.06}Ti_{0.08}Al_{0.37}Si_{1.72}O_6$, oxides, olivine with Mg # ~ 75, and plagioclase with an average composition of $Or_2Ab_{28}An_{70}$.

Finally, two samples from Dredge 5, DRE5-80 and DRE5-85, are very similar except for the slightly larger grains in the groundmass of DRE5-85. The predominant phenocryst phase in both samples is olivine, which exhibits dramatic zoning from cores with Mg# ~ 83 and rims with Mg# = 69-73. The majority of the olivine phenocrysts are

roughly 500 μm in length. Many of the phenocrysts contain melt inclusions, most of which appear to be connected to the surface of the grains. Highly zoned Ti-augite, $Na_{0.04}Ca_{0.88}Mg_{0.65}Fe^{2+}_{0.06}Fe^{3+}_{0.11}Ti_{0.13}Al_{0.38}Si_{1.65}O_6$, though rare, is also present, and is comparable in size to groundmass oxides, all less than 100 μm in length. Plagioclase with an average composition of $Or_3Ab_{35}An_{62}$, oxides with an average composition of $Mg_{0.28}Fe^{2+}_{1.35}Fe^{3+}_{0.54}Ti_{0.64}Al_{0.15}O_4$, and olivine (Mg # ~ 71) are also common in the groundmass. Analysis of the plagioclase is difficult, due to most grains being <10 μm in width, even though lengths are up to ~50 μm. Groundmass crystals are oriented in a weak trachytic flow texture.

2. *Major and trace elements*

A complete overview of the major and trace element concentrations is summarized in Table 3-1. A majority of the samples in the suite studied fall in the fields for basanite and primitive foidites on a total alkalis versus silica diagram (Fig. 3-4). The two samples from Beaufort Island are evolved and plot on a trend towards phonolite. Sample ANT1-6 from Franklin Island is also slightly evolved but plots at the boundary between basalt and trachybasalt. MgO concentrations range from 13.70 wt%, typical of primitive mantle melts, to only 1.28 wt% in BFT1. For most samples the MgO concentrations are lower than expected for mantle melts given their corresponding low SiO_2 concentrations.
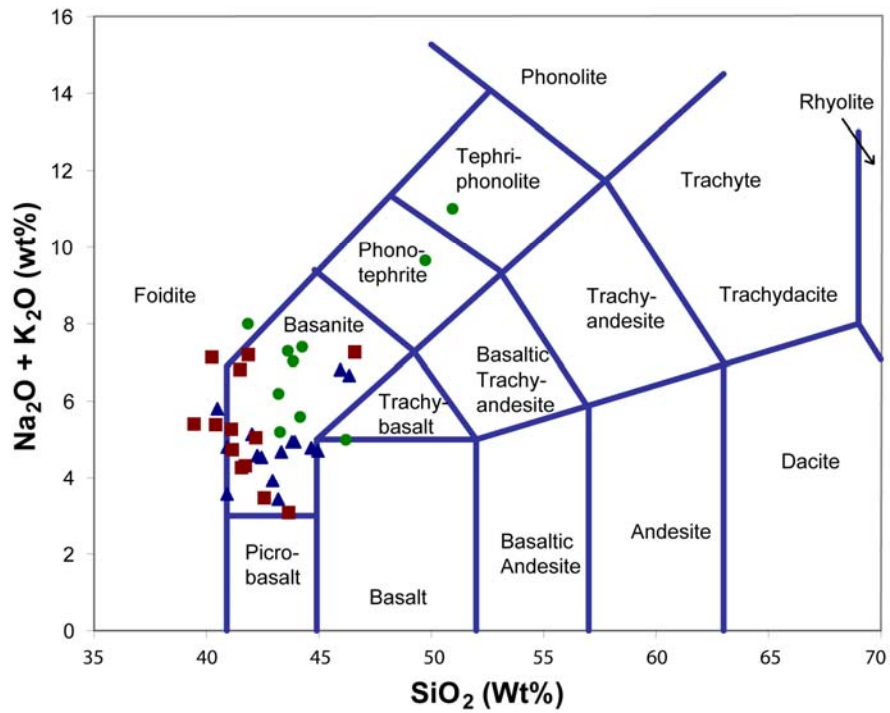
Figure 3-4. Alkalis vs SiO₂ classification diagram. Circles = island samples. Triangles = NVL samples. Squares = dredged samples.
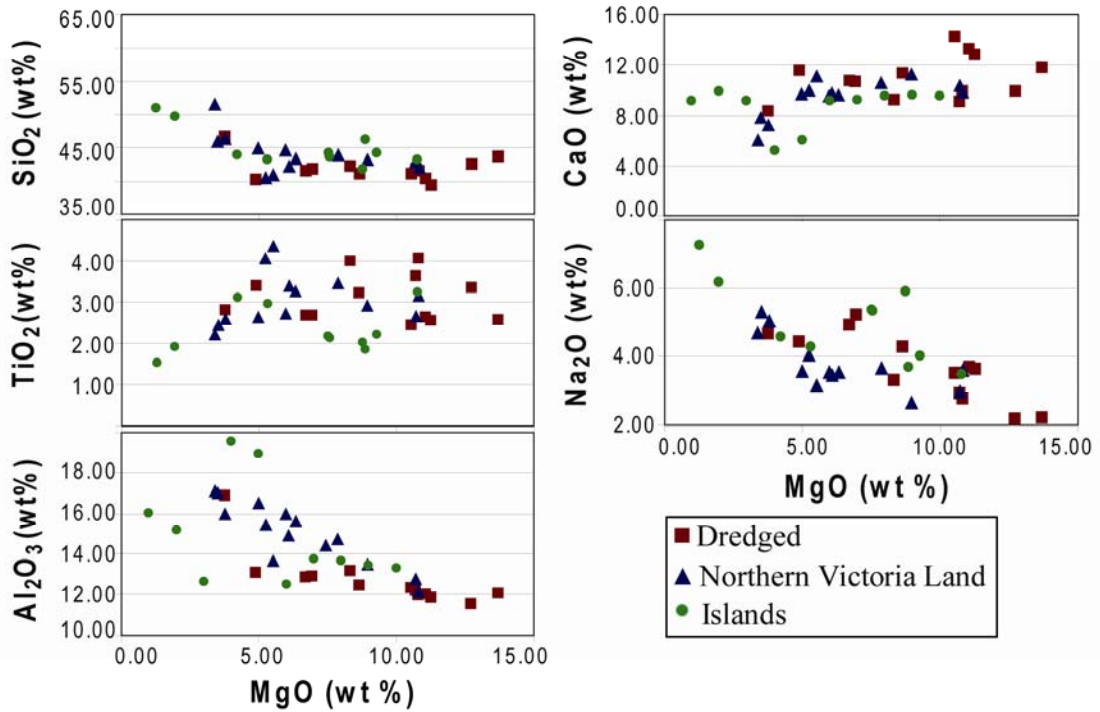
Figure 3-5. Major element variations for all samples.

SiO$_2$ plotted versus MgO shows evidence of olivine and clinopyroxene fractionation in the full sample set (Fig. 3-5). There is more scatter in the TiO$_2$ and Al$_2$O$_3$ versus MgO plots, but they also show the general decreasing and increasing patterns expected for crystal fractionation. Clinopyroxene grains from all the samples analyzed are Si-undersaturated and have high amounts of Al and Ti. Na$_2$O has an unusually steep trend considering the lack of plagioclase in most samples, but can be explained as variability of Ti concentration in the pyroxene phenocrysts. A general primary melt composition can be determined by removing the effects of these trends, and is represented by the compositions of samples DRE3-56 and DRE3-73 (Fig. 3-6).

All samples are enriched in incompatible elements. To focus solely on the differences in magma sources rather than the effect of crystal fractionation, only the nineteen samples with SiO$_2$ < 45 wt% and MgO > 7 wt% are included in the following discussion. Primitive mantle-normalized trace element abundance patterns for the nineteen samples exhibit enriched shapes with a wide range in concentrations (Fig. 3-7). The most striking feature of the plots is the strong negative anomaly for Pb. Negative anomalies for fluid-mobile elements (Rb, Th, and U) are also present to varying degrees.

Samples 12-19-01-5, DRE4-75, VC-44, NV-11B, and NV-14C show the most pronounced negative anomalies for Rb and Pb and an overall concave down shape for LILE. In contrast, the remaining samples show either less pronounced negative Rb anomaly or flat distribution pattern for LILE. Each of these three groups represent similar ranges of SiO$_2$, MgO, and Al$_2$O$_3$ suggesting that differences in the EDD is not the result of crystal fractionation or magma evolution processes.
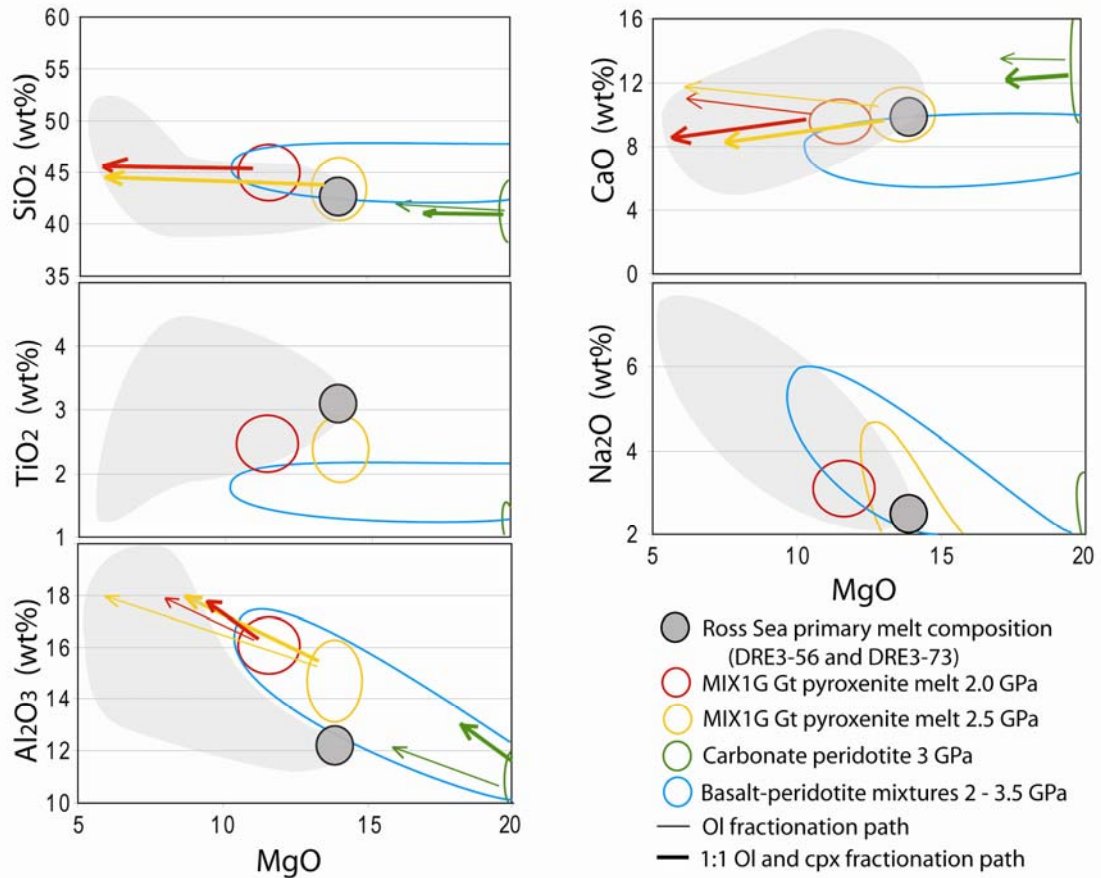
Figure 3-6. Comparisons of primary melt compositions with experimental melt compositions. MIX1G and carbonated peridotite data from [*Hirschmann, et al.*, 2003], basalt-peridotite mixtures from [*Kogiso, et al.*, 1998; *Kogiso, et al.*, 2003]. Light grey shading represents magma compositions from this study. Dark grey shading represents the most primitive magma from this study. Thin and thick lines indicate the effect of olivine and olivine + clinopyroxene fractionation, respectively, for the carbonated peridotite and pyroxenite experimental melts. Olivine and clinopyroxene compositions used in this calculation are average values for the phenocrysts analyzed from samples DRE3-59 and DRE3-73.

Chondrite-normalized rare earth element (REE) distributions display a steep pattern (Fig. 3-8). The shape is similar for all samples and varies only in concentration, with La_N ranging between 124 and 872 and La_N/Lu_N between 12.6 and 24.4. The strong enrichment in light REE relative to MORB compositions is typical for melting of a mantle source containing residual garnet [*Harrison and Wood*, 1980]. This is in contrast to geodynamical studies which show melting just below anomalously thin crust [*Trey, et*

al., 1999], but agrees with thermobarometry results which suggest melting at pressures up to 4 to 5 GPa [*Perinelli, et al.*, 2006].

3. Pb, Sr, Nd, and Hf isotopes

Isotopic ratios represent narrow ranges for all analyzed isotopic systems. $^{206/204}$Pb, $^{207/204}$Pb, and $^{208/204}$Pb isotopic compositions for the Ross Sea samples range from 19.28 ± 0.02 to 20.04 ± 0.05, 15.34 ± 0.07 to 15.63 ± 0.07, and 38.27 ± 0.01 to 39.44 ± 0.01, respectively. $^{87/86}$Sr isotopic ratios range from 0.70212 ± 0.00001 to 0.70394 ± 0.00001. $^{143/144}$Nd ratios range from 0.51282 ± 0.00001 to 0.51301 ± 0.00001. $^{176/177}$Hf ratios are amazingly homogenous ranging only between 0.282983 ± 3E-6 and 0.283065 ± 5E-6.
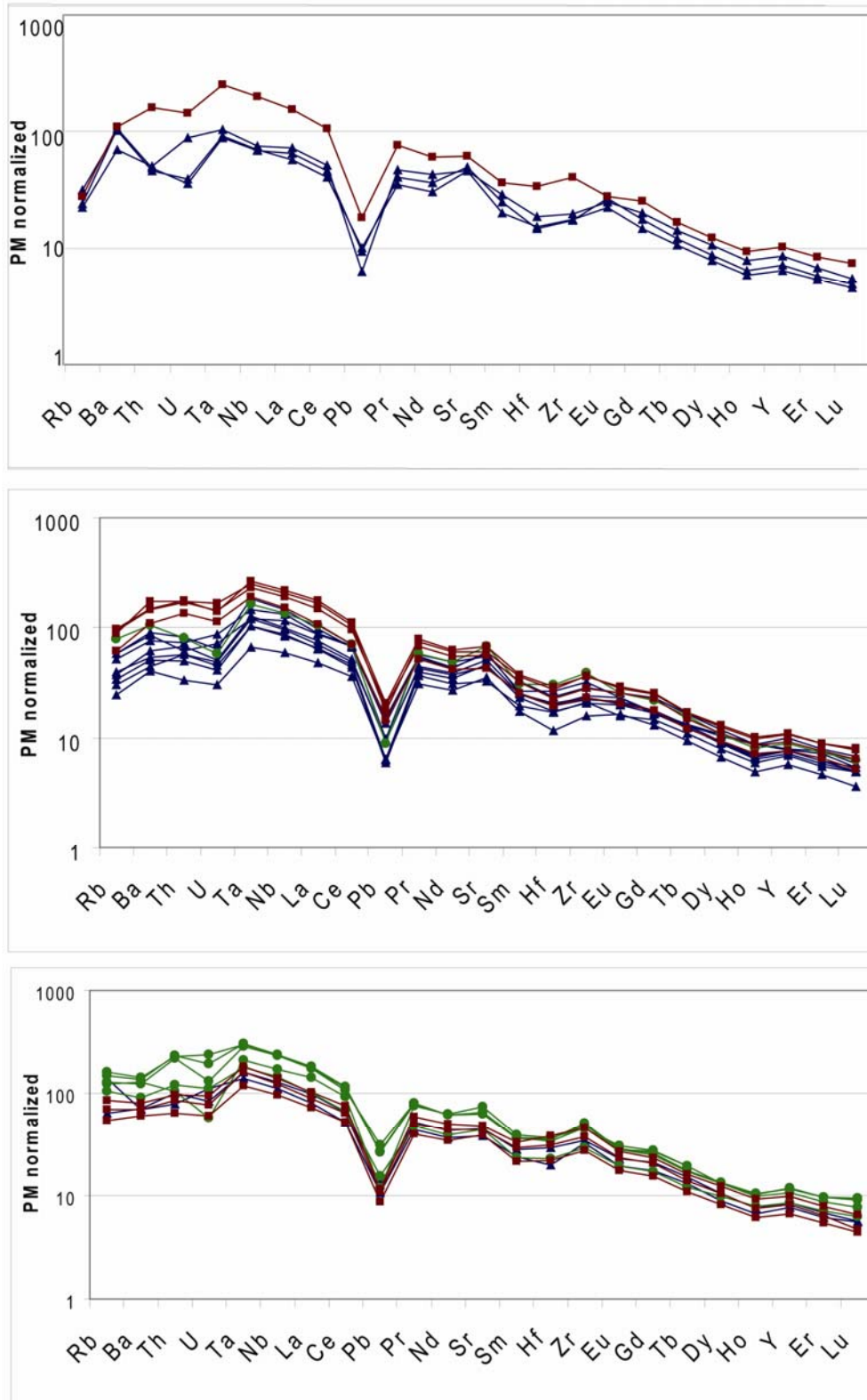
Figure 3-7. Element distribution diagram for all samples with $SiO_2 < 45$ wt % and MgO ≥ 5 wt%. All elements are normalized to primitive mantle values found in Hofmann, 1988. Circles = island samples. Triangles = NVL samples. Squares = dredged samples.
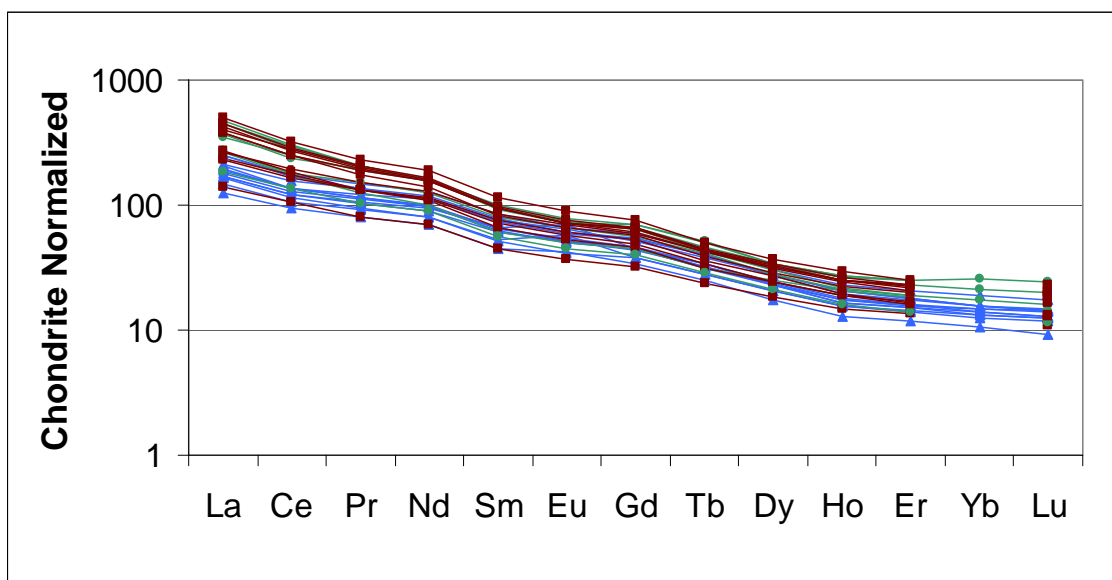
Figure 3-8. Rare-earth element diagram for all samples with SiO_2 < 45 wt % and MgO > 7 wt%. All elements are normalized to chondrite values of McDonough and Sun, 1995.

DISCUSSION

1. Magma source composition

Experimental melts derived from a carbonated peridotite mantle source which has undergone olivine ± clinopyroxene fractionation more closely match the estimated major element compositions for primary melts in our study compared to other varieties of fertile peridotite or even SiO_2-deficient garnet pyroxenite (Fig. 3-6). It is possible, as hypothesized by Rocholl et al. [1995], that ancient mantle plume material, potentially fertile peridotite in composition, would be preserved admixed with crystallized basalt melts in the upper mantle beneath the WARS from earlier episodes of upwelling and melting. The partial melt experiments by [*Kogiso, et al.*, 1998; *Hirschmann, et al.*, 2003; *Kogiso, et al.*, 2003] for various peridotite and pyroxenite compositions were conducted at comparable pressures to the melting of the mantle below the Ross Sea, 1.5 – 3 GPa, but at higher temperatures, 1400-1525ºC, than the Ross Sea geotherm, which has a

temperature range of 1100-1150ºC at the estimated pressures [*Berg, et al.*, 1989; *Perinelli, et al.*, 2006]. This needs to be considered during any comparisons between experimental melts and primary melt compositions for the rocks in the WARS. Kogiso et al. [1998] provide experimental data from melting of fertile peridotite and fertile peridotite with basaltic veins. At pressures less than 3 GPa (~90 km depth), the experimental melts for both source compositions are all too rich in SiO_2, Al_2O_3, and Na_2O to be the appropriate sources for magmas in the Ross Sea. At all pressures, the CaO concentrations in the experimental source compositions are lower than the estimated primary melt composition. Clinopyroxene fractionation would lower the CaO concentrations further.

Hirschmann et al. [2003] summarized melt compositions from anhydrous peridotite, SiO_2-deficient garnet pyroxenite, and carbonated peridotite sources which are worth assessing in our study. Experiments were completed at the same general pressure and temperature conditions as summarized above. Anhydrous peridotite yields melts that are too rich in SiO_2 relative to other major element concentrations to be the source of the Ross Sea lavas. The SiO_2-deficient garnet pyroxenite source has a similar composition to the eclogite produced by metamorphism and partial melting of subducted oceanic crust. Melts from that potential source are similar to the estimated primary melt compositions when generated at pressures greater than 2.5 GPa (~75 km depth), except for having higher concentrations of Al_2O_3. The effect of olivine ± clinopyroxene fractionation from the original melts would drive liquids to even higher concentrations of Al_2O_3, rather than matching the trend of observed magma compositions. The concentration of CaO in the melt would also be driven lower by clinopyroxene fractionation, matching only a few of the observed magma compositions. The lower temperatures of the Ross Sea geotherm is

71

expected to lead to lower degrees of melting and lower concentrations of Al_2O_3, but also

higher concentrations of SiO_2, unlike the analyzed lavas.

Carbonated peridotites yield the best match between the experimental melt

compositions and the primary melts for WARS magmatism. Although the primitive Ross

Sea composition plot at lower MgO (wt %) than the initial experimental melts of

carbonated peridotite in Figure 3-6, the difference can easily be explained by crystal

fractionation. Analyzed Ross Sea lavas with the highest CaO, lowest SiO_2, lowest Al_2O_3

concentrations match those of the primary Ross Sea melts which have undergone olivine

fractionation. The variability of these major elements in the analyzed lavas can also be

explained by incorporating different proportions of olivine and clinopyroxene during

magma evolution. Clinopyroxene fractionation would lower CaO and increase SiO_2 and

Al_2O_3. Both olivine and clinopyroxene phenocrysts are present in these lavas supporting

the occurrence of these processes. Some involvement of garnet pyroxenite can not be

entirely ruled out for higher Al_2O_3, lower CaO samples, but the majority of the

compositions have too low Al_2O_3 and too high CaO to match the fractionation patterns of

garnet pyroxenite and are better explained by a carbonated peridotite source.

2. Source formation processes

The overall enrichment of incompatible elements in the Ross Sea submarine lavas,

shown on the element distribution and REE diagrams (Figs. 3-7 and 3-8), is similar to the

enrichments observed elsewhere in the WARS [*Kyle and Rankin*, 1976; *LeMasurier, et*

al., 1994; *Hart, et al.*, 1995; *Hart, et al.*, 1997; *Panter, et al.*, 2000; *Rocchi, et al.*, 2002],

suggesting either an unusually homogenous source beneath the entire region with varying

degrees of partial melting or only a slightly heterogeneous source. The slightly positive

anomaly for Nb and the slightly negative anomalies for Rb and Pb observed on the

element distribution diagrams (EDD) of the Ross Sea samples, and common to many OIB,

have previously been used as evidence for melts generated in the lithosphere rather than

asthenospheric mantle melts. Pilet et al. [2008] discuss the recent interpretations of these

trace element signatures and argue for lithospheric melt sources rather than the traditional

interpretation of asthenospheric melting. Halliday et al. [1995] made a similar argument

for lithosphere-derived melts based on the variable Ce/Pb ratios and uniform Ce/U

observed in many OIB (Fig. 3-9), opposite that expected from asthenospheric mantle

derived melts. These traits are also observed in the Ross Sea lavas and support a

potential lithospheric source for the Ross Sea lavas.
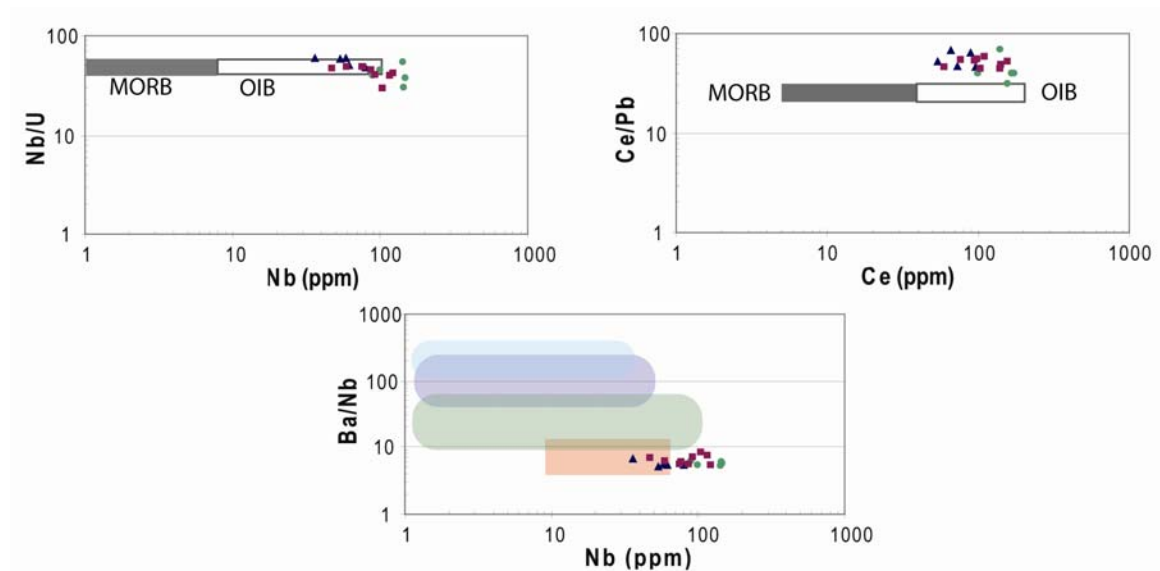
Figure 3-9. Comparisons of trace element ratios to typical MORB and OIB magmas, both interpreted as asthenospheric melting. Red shading represents Hawaiian lavas [*Dixon, et al.*, 2008], green shading represents Basin and Range [*Dungan, et al.*, 1986], dark blue represents Great Basin [*Kempton, et al.*, 1991], and light blue represents Masota, western Mexico[*Carmichael, et al.*, 1996] lavas.

Figure 3-10 illustrates the difficulty in distinguishing a lithospheric or sthenospheric source for the WARS lavas. Kempton et al. [1991] used plots of high field strength elements (HFSE) and large-ion lithophile elements (LILE) ratios to determine if magmas from the Great Basin region of the Basin and Range province were generated from lithospheric melts modified by arc fluids, increasing LILE concentrations relative to HFSE, or asthenospheric melts, containing higher concentrations of HFSE relative to LILE. This concept can be applied to other studies of magmas from the Mascota region of western Mexico [*Carmichael, et al.*, 1996], Hawaii [*Dixon, et al.*, 2008], and the Basing and Range proper [*Dungan, et al.*, 1986] as well. Most studies plot only one set of ratios (most often K_2O/TiO_2 vs Zr/Ba) to support source interpretations. When additional elements are used, as in Figure 3-10, these plots are inconsistent.

The WARS lavas plot primarily within fields for asthenospheric melts from the Basin and Range and Hawaii (CITE) when considering K_2O/TiO_2 vs Zr/Ba, but overlap fields for lithospheric melts from Mascota, Mexico (CITE) when considering Rb/Hf vs Y/Rb. Plots of Rb/Hf vs Nb/Sr do not overlap either previously defined fields. These complex datasets support generation from a modified magma source which has undergone multiple types of melting. Melting associated with subduction-related fluids may have altered LILE concentrations. In the case of the WARS, the extensive melt history of the area may have led to depletions of LILE compared to the other regions. Melting associated with extension may be sampling decompressing asthenosphere as well as the thinning, metasomatized lithosphere. Subsequent magmas would yield compositions which show evidence of multiple processes. WARS magmas show
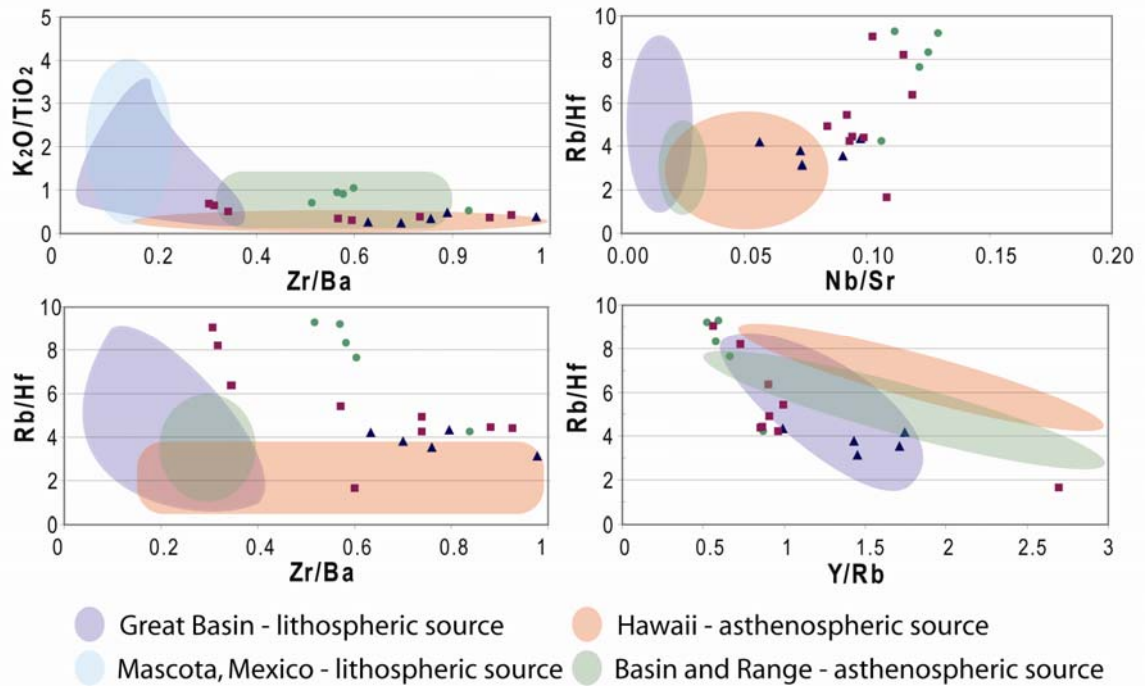
Figure 3-10. Comparisons of HFSE and LILE ratios of WARS lavas to previously defined values for asthenospheric and lithospheric melts. See text for further discussion and sources.

evidence of both lithospheric and asthenospheric melts. Variable accessory phases in the magma source, proportion of lithospheric contributions, and/or extent of subduction modification may be responsible for WARS lava compositions differing from other localities. A conclusive determination of either an asthenospheric or lithospheric source is impossible to determine using this trace element data, but the depletion of fluid mobile elements for some WARS lavas suggest that residual lithospheric sources are at least partially involved in the magma generation.

The convex shape of the more incompatible portion (left side) of the EDD was noted by Hart et al. [1997] and interpreted to be the result of an originally depleted source that underwent subsequent enrichment. They also mention the alternative explanation that the originally enriched mantle source of the WARS lavas underwent a secondary melting

event subsequent to preferential removal of some elements. Under this alternative scenario, the LILE and fluid-mobile elements were removed during an earlier episode of flux melting. The most recent melting, which produced the Ross Sea lavas, occurred in the residual mantle materials already depleted in fluid-mobile elements. This would explain the overall enrichment of incompatibles but the slight differences in the LILE patterns. The striking negative Pb anomaly has been observed in all areas of the WARS and may also be related to this region's history as an active margin. More than 500 Myrs of arc volcanism could have removed significant amounts of Pb from the remaining mantle wedge material. A slightly less pronounced negative anomaly is present for K and Rb, and even less pronounced for U; all elements would have also been removed to varying extents during flux melting [*Kelley, et al.*, 2005].

Trace element ratios (Fig. 3-11) of the Ross Sea lavas do not appear to fit perfectly the fields for either HIMU or EM melts as defined by Halliday et al. [1995]. The trends suggest either removal or addition of only some elements to the magma source. Th, Pb, and U are fluid mobile elements and would have gone into subduction-related fluids and magmas passing through the lithosphere during the Paleozoic and Mesozoic [*Kelley, et al.*, 2005]. Although there could be multiple explanations for these features, the simplest explanation for the severe negative Pb anomaly is by a removal process rather than an "injection" or mixing of multiple enriched sources.

The Sr and Nd isotopic compositions plot near the HIMU mantle end member (Fig. 3-12). In contrast, the Pb and Hf isotopic ratios plot between HIMU and DMM. This decoupling of the Pb isotopic system from Nd and Sr was noted previously by Hart et al. [1995], but our study adds the additional dimension of Hf isotopic ratios, and these

compositions strengthen the argument for a modified HIMU-like source. The origin of a

HIMU signature has been debated in the geochemical community for many years [*Hart,*

et al., 1986; *Halliday, et al.*, 1995; *Panter, et al.*, 2006]. The traditional interpretation is

based on the typically elevated Pb isotopic ratios and calls on ancient ocean crust (with a

high $^{238}U/^{204}Pb$ ratio) to have been sequestered in the mantle, potentially at the core-

mantle boundary, for hundreds of millions of years, until remobilized by ascending

mantle plumes [*Hart, et al.*, 1986]. This material may continue to be cycling through the

asthenosphere beneath the WARS, or may be frozen as melt veins in the mantle

lithosphere. A newer interpretation focuses HIMU-like signatures being generated in the

lithosphere [*Halliday, et al.*, 1995; *Panter, et al.*, 2006], and also has been invoked by a

study of the East African Rift [*Paslick, et al.*, 1995]. Together, these studies suggest that

mantle material that has been sequestered in sub-continental lithosphere could generate

the same trace element and isotopic trends as if it had been stored in the lower mantle.

The isotopic signatures combined with trace element data from the Ross Sea lavas

support this more recent interpretation.
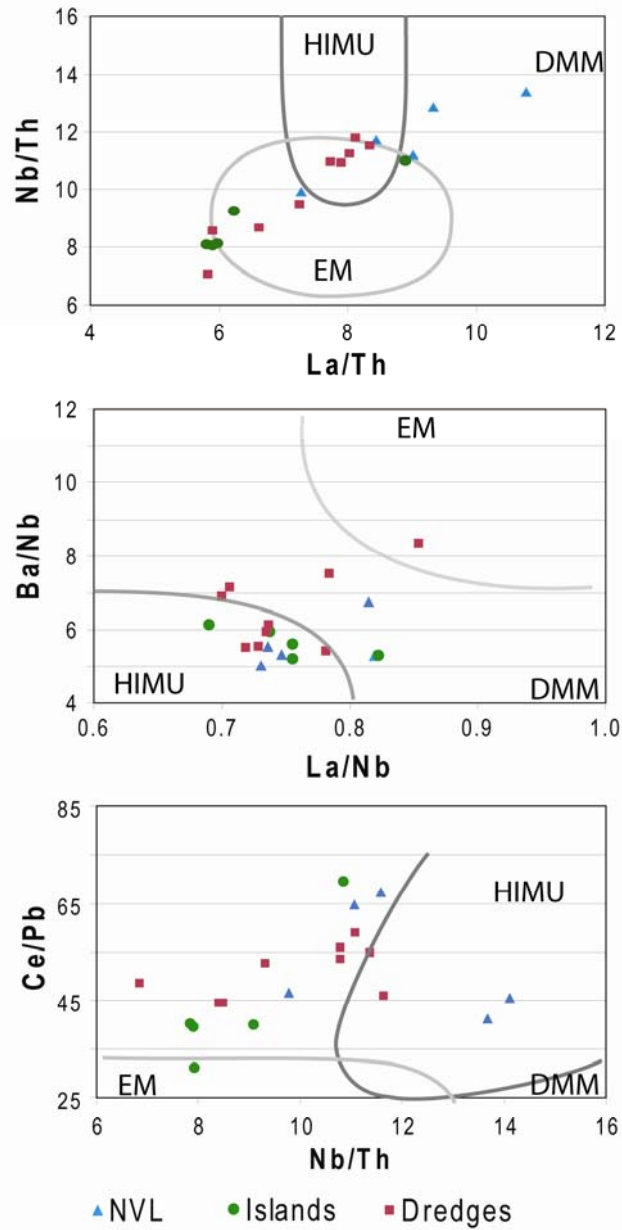
Figure 3-11. Trace-element ratios from Ross Sea lavas compared to typical ratios for mantle source endmembers. Only samples with $SiO_2 < 45$ wt% and $MgO > 7$ wt% are plotted.
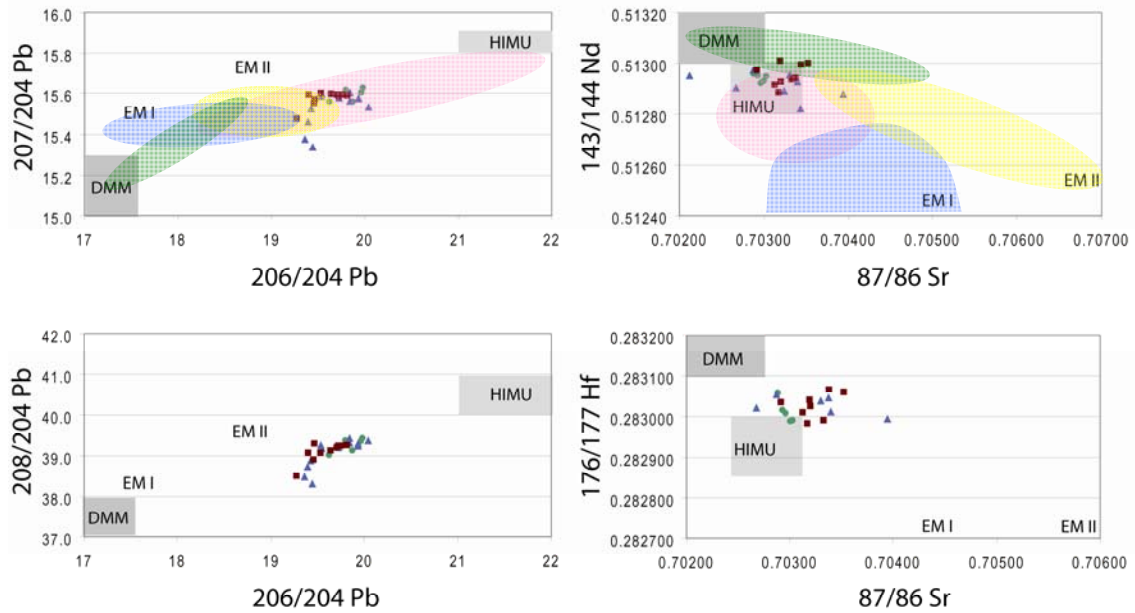
Figure 3-12. Isotopic compositions from a sample subset. Endmember definitions from [*Hart, et al.*, 1986; *Ballentine, et al.*, 1997]. Pink: global HIMU, yellow: EMII, blue: EMI, and green: DMM.

3. Isotopic evidence for Pb loss in the mantle

A simple calculation of mixing relationships illustrates the decoupling of isotopic systems. We assume that the Pb and Hf isotopic ratios represent a higher proportion of a subduction component relative to the enriched HIMU contribution. This is the expected result for a mantle which had Pb (and Hf) removed during an initial stage of melting and was replaced by a source of lower concentration and a different isotopic ratio. The basic mixing equation,

$$R_M = R_{SUB}f_{SUB} + R_{HIMU}(1 - f_{SUB}) \qquad \text{Eq. 3-1}$$

can be used to determine the required proportion of Pb with a depleted isotopic ratio, R_{SUB}, that would have been contributed to the mantle source by a subduction or metasomatizing agent to generate the observed Pb isotopic ratios of the Cenozoic WARS magma source (Fig. 3-13). Because it is impossible to determine the exact isotopic

composition of the long-since-subducted altered and aged paleo-Pacific oceanic crust that

would have facilitated flux melting upon dehydration, typical MORB values from the
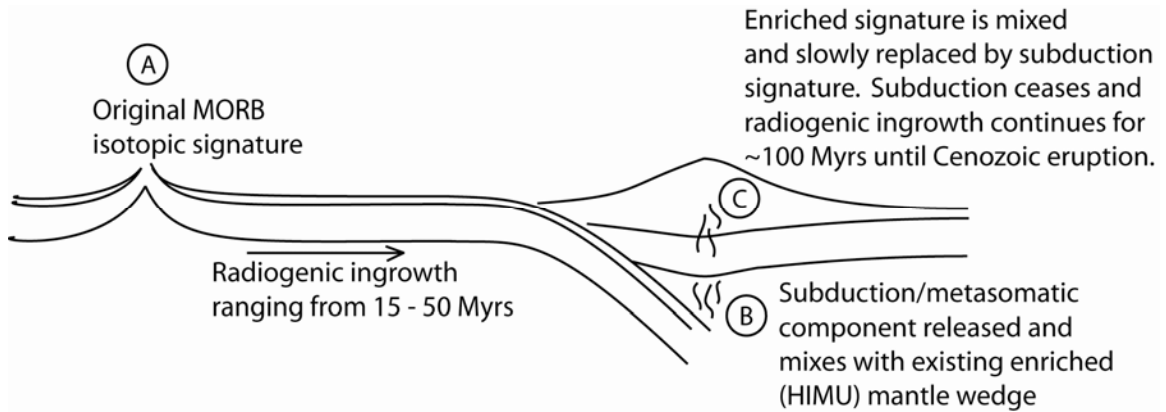
Figure 3-13. Illustration of the different stages of mantle evolution for the WARS magmatic sources, used in the simple isotopic mixing calculations. A) Eruption of the MORB, oceanic lithosphere is subducted below the Antarctic portion of Gondwana after only 15 – 50 Myrs. B) Flux melting takes places releasing modified MORB signature into overlying mantle and lithosphere. C) After arc volcanism ceases, radiogenic in-growth of source takes place for up to 110 Myrs.

Geochemical Earth Reference Models (GERM) database were used, modified for the

radiogenic in-growth between the time of eruption and time of subduction. R_{HIMU}

represents the accepted range for the HIMU mantle end member. The isotopic ratio of the

mixture, R_M, is based on the observed isotopic composition of Cenozoic volcanism

throughout the WARS, back-calculated to remove radiogenic in-growth that resulted after

cessation of subduction. Calculations show that the mantle source beneath the WARS

requires addition of 30 – 60% of the subduction component in order to generate the Pb

isotopic ratios observed in the Cenozoic lavas. Results from using Hf isotopic

compositions in the mixing calculation are similar to those for Pb. Some 25 – 45% of the

subduction component is required to generate the Hf isotopic ratios observed in the Ross

Sea lavas of the WARS.

The Nd isotopic system is not expected to match, if the isotopic signature of the original source was modified by fluid removal and progressive addition of the subduction component to the residual source. Nd should retain the radiogenic isotopic ratios from the pre-modified mantle source, because Nd is less mobile [*Cherniak*, 2001; *Cherniak*, 2003; *Johnston and Schwab*, 2004]. The isotopic ratio would not be modified by the small amounts of Nd being added by frozen melts and/or fluids percolating into the mantle wedge during subduction-related metasomatism. Using Equation 3-1, we estimate that less than 16% of the subduction component is required to generate the observed Nd isotopic ratios. Varying the mixing components to extreme values would still require less than 20% of the subduction component. Although Sr ratio calculations are expected to agree closely with Nd, Sr was not included in these calculations because the isotopic ratios are similar for both the subduction component and the HIMU end member.

Table 3-1. Variables for isotopic mixing equation. The upper portion of the table reports the initial variables used in Equation 1. The bottom portion shows the complete ranges used for each variable in the equation.

Initial Calculation	$^{207/204}Pb$	$^{208/204}Pb$	$^{144/143}Nd$	$^{176/177}Hf$
Subduction component	15.49	37.85	0.51329	0.28340
HIMU	15.85	40.5	0.51280	0.28280
Cenozoic mantle source	15.69	39.32	0.512729	0.28302
Complete Ranges				
Subduction component	15.48 - 15.49	37.82 - 38.07	0.51311 - 0.51347	0.28330 - 0.28350
HIMU	15.80 - 15.90	40 - 41	0.51270 - 0.51285	0.28270 - 0.28290
Cenozoic mantle source	15.64 - 15.74	38.98 - 39.66	0.51266 - 0.51288	0.28298 - 0.28304

We caution that this simple mixing calculation method has inherent limitations, because the exact concentration of Pb in each source is unknown and the two sources are not likely to be equal. There are also limitations in using exact values for the subduction input and for HIMU, which in reality represent ranges of isotopic ratios and probably vary slightly throughout the region. To test the impact of these limitations, each of the factors was varied to higher and lower values than the average, as summarized in Table

3-2. All of the calculated fractions remained within the reported ranges. More importantly, when Pb isotopic ratios of the endmembers are varied between reasonable values, the Nd isotopic system would be expected to vary correspondingly. The calculated f_{SUBS} for both systems then change in the same direction but remain dissimilar. Although the exact fractions of source components in the mixture cannot be determined, the concept is strongly supported by the values calculated here. The decoupling illustrated here also warrants caution when trying to determine mantle source compositions based on only one or two isotopic systems.

4. Previous magma source models

Although the volume and enriched geochemical signatures of Cenozoic WARS magmatism have been used previously as support for the mantle plume model, the vast geographic extent of these coeval magmas weakens this explanation. The mantle plume concept is still widely accepted in the MBL portion of the WARS, largely because of the estimated eruption rates in this area as well as geophysical evidence of extensive crustal doming [*Behrendt*, 1999; *LeMasurier, et al.*, 2003; *Riley, et al.*, 2003]. However, geophysical evidence is not supportive of the plume model for the Cenozoic volcanism in NVL [*Berg, et al.*, 1989; *Perinelli, et al.*, 2006]. The large size of the DAMP spot seismic anomaly and active magmatism over thousands of kilometers for 30 Myrs leads to doubt over the feature being generated by a mantle plume [*Finn, et al.*, 2005]. Because of these complications and the fact that the geochemical data presented in this study are best explained by other processes, we have eliminated the active mantle plume hypothesis as an explanation for the Ross Sea volcanism.

The hypothesis that WARS magmatism was produced by two-stage melting punctuated by a considerable amount of time is a more passive interpretation but is still focused on an enriched mantle plume source – i.e., ancient mantle plume material underplating the lithosphere or stratifying the upper mantle source beneath the Ross Sea during the first episode of melting or upwelling, and second-stage melting due to rift-induced decompression. These models suggest that MBL melts are polybaric with different depths yielding different isotopic ratios [*LeMasurier, et al.*, 2003]. HIMU-like lavas were derived from the asthenospheric mantle and lavas with more ambiguous isotopic signatures originated from the shallower lithospheric mantle [*Hart, et al.*, 1997; *LeMasurier, et al.*, 2003]. While we agree that polybaric melting is likely to have occurred, the Pb isotopic evidence and elemental anomalies support a model whereby the dominant process has been selective removal of certain materials from the original source rather than pure mixing of two enriched mantle end members.

Studies that have invoked a stratified mantle have also reported regional and temporal variations to support the concept of polybaric melting. Rocholl et al. [1995] observed minor variations in isotopic ratios between samples from the rift shoulder, in NVL, and samples from within the rift itself or the Ross Sea, and attributed them to the depth of melting partly influenced by differences in lithospheric thickness. Wörner et al. [1999] called for at least two endmembers in the southern Victoria Land (SVL) source, concluding that the slight variations in isotopic ratios were caused by both temporal and regional differences in the source components. However, these conclusions were based on a small number of samples.

Hypotheses advocating regional and temporal variations can be given a fresh assessment based on the now-possible compilation of a larger age and isotopic ratio dataset from throughout the WARS. Figure 3-14 uses Nd isotopic ratios to illustrate the variations. Although a slight difference in ratios for rift-shoulder and within-rift lavas – both from NVL – could be argued, this variation appears to be related more to having older samples from the rift shoulder than from within the rift. Both sample sets from Victoria Land and Zealandia (the major islands of New Zealand and surrounding submerged continental lithosphere) show a change towards more depleted or MORB-like isotopic ratios through time. This trend is easily explained by decompression melting with continued rifting and crustal thinning, if the proposed concept of a less radiogenic subduction-modified lithosphere source for the subsequent lavas is correct. The hotter asthenosphere upwells to fill this new space and assists in additional melting of the modified lithospheric materials [*Faccenna, et al.*, 2008]. The process generating the observed isotopic signatures took place during the period of subduction along the Gondwanan margin and would have influenced the Zealandia lithosphere as well. Although Zealandia has not undergone the complete rifting of NVL, other mechanism leading to melting of the mantle lithosphere during the Cenozoic would generate the same trend. This explanation does not hold true for data on samples from the MBL region of the WARS. The MBL tectonic plate may have remained more intact than other areas of the WARS, not experiencing the intense lithospheric thinning that has taken place in the Ross Sea, or have more contribution from asthenospheric upwelling.
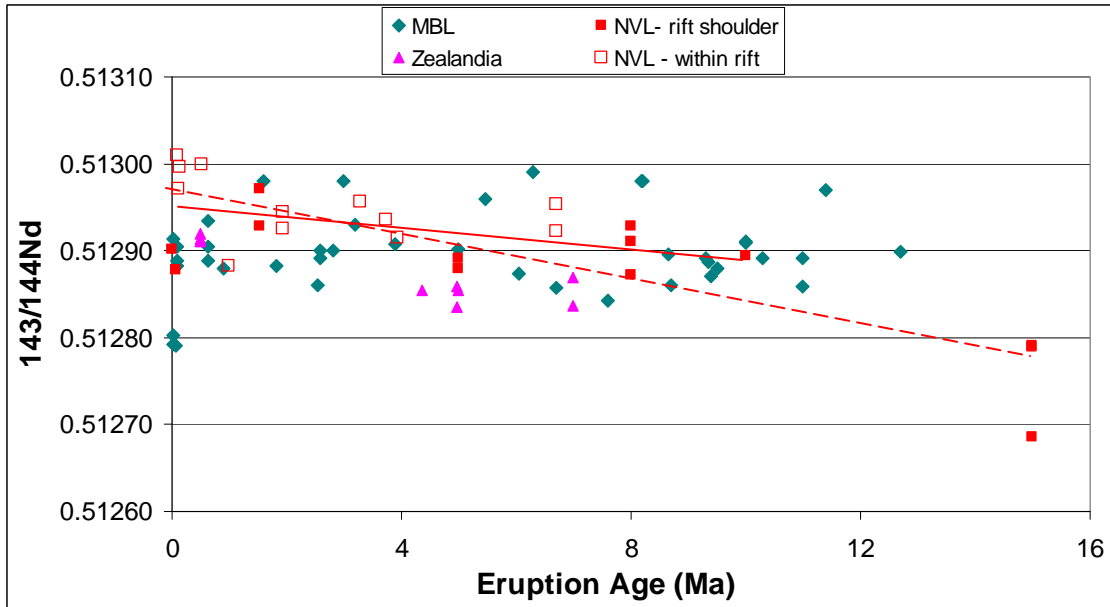
Figure 3-14. Regional data compilation. Solid line show trend for data 0 – 10 Ma. Dashed line shows trend for all data points. Data from this study and [*Hart, et al.*, 1995; *Rocholl, et al.*, 1995; *Hart, et al.*, 1997; *Rocchi, et al.*, 1998; *Panter, et al.*, 2000; *Panter, et al.*, 2006].

The history of subduction along the paleo-Pacific margin of Gondwana that we invoke here can also explain the anomalous seismic structures observed below the WARS. Numerous tomographic studies [*Sieminski, et al.*, 2003; *Finn, et al.*, 2005; *Watson, et al.*, 2006] have attributed slow seismic anomalies below the WARS to hotter mantle temperatures in this region. An alternative explanation is that the seismic anomaly is due to chemical variations. As the lithosphere thinned during rifting, the mantle underwent decompression; small amounts of either water or carbon could account for larger amounts of melting than expected in an anhydrous mantle setting. This may not be unrealistic given the long subduction history experienced by the mantle beneath the entire subduction margin of Gondwana. Several authors [*Zipfel and Worner*, 1992; *Coltorti, et al.*, 2004; *Perinelli, et al.*, 2006; *Cooper, et al.*, 2007] have noted the presence of hydrous phases, including amphiboles and phlogopite, in mantle xenoliths from Victoria Land, which supports the hydrated mantle hypothesis. Pyroxenite veins, frozen in place after

previous melting events, would also have a lower melting temperature and could be, at least in part, the sources of WARS magmatism during a second episode of melting, this time facilitated by decompression due to Cenozoic rifting.

5. *New magma source model*

Our proposed model calls for a multistage modification of the mantle source. Ancient magmatism emplaced an enriched signature into the lithospheric mantle that either already possessed a HIMU signature or was placed early enough to generate that radiogenic signature through time by radioactive decay. The asthenospheric mantle may also have a HIMU signature today, though this is not required. Between 550 and ~110 Ma, subduction took place along the Gondwanan margin, and flux melting preferentially removed LILE and fluid mobile elements, including Pb, from the lithospheric mantle. Simultaneously, transient melt crystallized to form veins (potentially of gt-pyroxenite composition) throughout the mantle lithosphere, and at the end of subduction, some eclogite/SiO_2-deficient gt-pyroxenite may have also adhered to base of lithosphere. An amagmatic period followed allowing the lithospheric mantle source to "enrich" by simple radiogenic ingrowth, because of an increased U/Pb ratio. WARS rifting began in the late Mesozoic, thinning the lithosphere and changing patterns of mantle convection after the end of subduction [*Finn, et al.*, 2005]. Magmas were generated from both decompression of hot, and potentially hydrated, asthenosphere and thermal erosion of the metasomatized lithosphere. During the latest stages of Cenozoic rifting, melting became more localized as a result of broad extension transitioning to the opening of separate basins [*Rossetti, et al.*, 2006]. Decompression and thermal erosion in the Ross Sea basins is not significant enough to melt pure peridotite sources, but could initiate melting of carbonated peridotite

and/or gt-pyroxenite present in the lithospheric mantle. This is especially true if minor

amounts of water are also present as supported by the observation of amphiboles and

phlogopite in the region's mantle xenoliths. Partial melts of carbonated peridotites are the

best chemical match for the Ross Sea lavas and likely are the dominant source

components for WARS magmatism.

CONCLUSION

Alkaline basalts from samples dredged from seven seamounts in the Ross Sea,

Franklin and Beaufort Islands, and Mt Melbourne are chemically similar to other

volcanics throughout the WARS. A mantle plume model has been invoked previously to

explain Cenozoic WARS magmatism, but comparisons to experimental melts of fertile

peridotite do not match the major element concentrations of the Ross Sea lavas.

Experimental melts of carbonated peridotite provide a better match and are likely the

dominant source, although gt-pyroxenite could also be involved. These source

compositions are expected to be present in the mantle lithosphere due to the region's

long-lived subduction history. The Ross Sea lavas possess an overall enrichment of

incompatible elements; however, the large negative Pb anomaly and the concave shape of

LILE on the EDD support a model whereby fluid mobile elements are removed from the

residual mantle lithosphere source during the subduction related volcanism along the

paleo-Pacific Gondwanan margin. Heterogeneity in the extent of LILE removal suggest

melts are polybaric with varying degrees of asthenospheric and lithospheric contributions.

The decoupling of the Pb isotopic system from the Nd isotopic system agrees with this

model. Pb isotopic signatures were modified as the original Pb, with HIMU-like isotopic

signature, was removed from the mantle wedge and replaced by Pb with a less radiogenic signature. Nd is less fluid mobile and was relatively unaffected by this process. Although there are differences in the Nd isotopic signature between major regions of the WARS (ie., MBL and NVL), there is no geographic variation within NVL. A temporal variation of Nd isotopic signatures in NVL may be the result of an increased proportion of the modified lithospheric mantle source melting as a result of additional heat supplied by hot asthenosphere upwelling after rifting and crustal thinning.

Table 3-2. Major and trace element and isotopic ratio data for samples analyzed in this study.

Sample	Victoria Land													
	NV-15B	NV-15	NV-14C	NV-14A	NV-13A	NV-12A	NV-11B	NV-6E	VC-21	NV-4B	VC-44	VC-3	NV-3B	NV-3I
Location	Cape Washington		Oscar Point (1km W)		Shield Nunatak	Edmonson Point	Baker Rocks	Downshire Cliffs		Foyn Island	Malta Plateau	Cotter Cliffs (base)	Possession Island	
Age (Ma) [a]														
SiO_2 (wt %)	42.02	40.92	44.66	43.32	43.19	56.53	44.96	39.25	41.46	42.94	40.91	46.35	42.26	45.95
TiO_2	3.16	3.50	2.73	3.27	2.91	0.94	2.65	3.55	2.99	2.67	4.36	2.59	3.40	2.44
Al_2O_3	12.15	12.06	15.96	15.61	13.48	15.96	16.51	12.56	13.43	12.79	13.68	15.96	14.93	16.99
Fe_2O_3	13.01	14.01	12.07	13.28	12.76	9.23	12.17	13.33	13.18	12.42	15.61	11.49	13.56	11.14
MnO	0.18	0.19	0.18	0.18	0.17	0.22	0.19	0.16	0.17	0.18	0.20	0.23	0.21	0.22
MgO	10.82	9.08	5.97	6.33	8.95	1.01	4.98	9.21	6.52	10.70	5.53	3.78	6.09	3.51
CaO	9.84	9.86	9.57	9.61	11.25	3.54	9.71	10.09	10.28	10.38	11.09	7.23	9.79	7.81
Na_2O	3.61	3.43	3.55	3.55	2.66	5.80	3.58	3.53	3.47	2.98	3.14	5.05	3.44	5.31
K_2O	1.52	1.37	1.23	1.12	0.77	3.81	1.12	0.86	1.42	0.94	0.42	1.61	1.14	1.85
P_2O_5	0.76	1.29	0.66	0.79	0.69	0.29	1.06	0.68	0.65	0.54	1.17	1.23	0.91	1.21
Rb (ppm)	34	24	17	18	13	78	13	21	75	16	12	21	20	42
Ba	425	328	616	307	244	1207	647	323	419	269	425	576	371	498
Th	8.2	5.6	3.8	4.1	2.7	14.3	4.0	4.6	6.4	4.6	4.2	9.3	5.5	11.2
U	1.7	1.2	0.8	0.8	0.6	2.7	0.7	1.0	2.3	0.9	1.8	2.0	1.0	2.3
Ta	5.9	4.8	3.4	3.8	2.5	8.7	3.3	4.4	5.1	3.8	3.9	7.5	4.7	8.3
Nb	80	62	44	52	36	121	43	58	68	53	47	102	61	109
La	62	51	35	40	29	83	40	43	49	39	45	76	47	84
Ce	103	95	65	74	58	148	74	78	84	70	82	136	83	144
Pb	2.2	1.5	1.8	1.1	1.1	8.4	1.7	1.7	1.9	1.0	1.1	3.3	1.6	3.3
Pb (ID)	3.9		2.7											
Pr	12.6	12.6	8.5	9.6	7.4	17.8	9.8	10.3	10.6	8.8	11.4	17.0	10.7	17.4
Nd	51	54	37	41	32	70	44	44	44	36	51	69	46	68
Sr	817	844	846	839	642	433	900	800	695	592	843	848	925	987
Sm	10.9	11.6	7.8	8.9	6.7	14.6	9.6	9.7	9.1	7.6	11.1	13.7	9.6	12.9
Hf	7.9	7.7	4.1	4.7	3.1	12.4	4.0	5.6	5.3	4.6	5.0	7.8	5.2	8.6
Zr	336	319	172	201	153	538	169	225	311	203	193	359	217	420
Eu	3.3	3.4	3.3	2.9	2.4	4.5	3.9	2.9	2.8	2.3	3.7	3.9	3.1	3.7
Gd	11	11	8	9	7	14	9	9	9	7	10	13	9	13
Tb	1.4	1.4	1.0	1.2	0.9	2.0	1.1	1.2	1.2	1.0	1.4	1.7	1.2	1.7
Y	34	35	25	30	23	53	28	30	30	27	34	43	28	39
Dy	6.6	7.0	5.0	5.7	4.3	10.2	5.6	5.9	5.7	5.1	6.8	8.1	5.6	7.4
Ho	1.1	1.1	0.8	1.0	0.7	1.7	0.9	1.0	1.0	0.8	1.1	1.4	0.9	1.2
Er	2.8	2.8	2.2	2.6	1.9	4.6	2.4	2.6	2.5	2.3	2.9	3.7	2.4	3.4
Yb	2.5	2.5	2.0	2.3	1.7	4.6	2.1	2.4	2.4	2.1	2.5	3.5	2.2	3.3
Lu	0.4	0.4	0.3	0.3	0.2	0.7	0.3	0.3	0.4	0.3	0.4	0.5	0.3	0.5
Ni	388	461	281	213	193	162	282	435	373	411	382	303	296	411
Cu	132	111	182	65	57	119	198	226	206	101	176	95	101	264
Zn	93	102	84	85	79	124	89	75	80	78	99	98	87	95
V	184	187	166	180	226	0	132	235	240	209	291	99	215	108
Cr	227	198	75	85	343	4	62	225	218	395	10	4	35	18
$^{206}Pb/^{204}Pb$	19.44	19.36	19.93	19.43	19.39	-	19.53	-	-	-	19.84	-	19.84	20.04
$^{207}Pb/^{204}Pb$	15.34	15.38	15.58	15.52	15.46	-	15.58	-	-	-	15.56	-	15.60	15.53
$^{208}Pb/^{204}Pb$	38.30	38.48	39.23	38.88	38.73	-	39.26	-	-	-	39.32	-	39.43	39.37
$^{87}Sr/^{86}Sr$	0.70287	0.70340	0.70330	0.70267	0.70338	-	0.70394	-	-	-	0.70324	-	0.70343	0.70212
$^{143}Nd/^{144}Nd$	0.51297	0.51293	0.51296	0.51290	0.51294	-	0.51288	-	-	-	0.51289	-	0.51282	0.51295
$^{176}Hf/^{177}Hf$	0.28305	0.28301	0.28304	0.28302	0.28305	-	0.28300	-	-	-	-	-	-	-

[a] $^{40}Ar/^{39}Ar$ ages for DRE samples from Rilling et al., in press

Table 3-2.

Sample	Islands											Dredges		
	NV-5B	AW82-284	NV-17A	BFT-1	BFT-2	BFT-5	NV-16B	04ANT1-6	04ANT1-8	04ANT1-9	04ANT5A-19	04DRE1-31	04DRE1-32	04DRE2-42
Location	Cape Adare, N. end	Beaufort Island					Franklin Island					Dredge 1 Seamount		Dredge 2 Seamount
Age (Ma) [a]		6.76 ± 0.05	6.73 ± 0.03					3.28 ± 0.04		3.38 ± 0.04	3.68 ± 0.16	0.133 ± 0.024	0.122 ± 0.026	1.00 ± 0.05
SiO_2 (wt %)	40.48	43.85	43.21	50.95	49.74	43.27	41.84	46.20	44.26	44.17	43.62	41.49	41.86	46.60
TiO_2	4.05	3.12	2.97	1.53	1.90	3.23	2.02	1.85	2.17	2.20	2.13	2.68	2.69	2.81
Al_2O_3	15.43	16.04	15.16	19.57	18.91	12.52	12.62	13.74	13.66	13.43	13.31	12.85	12.92	16.89
Fe_2O_3	13.81	11.62	11.65	7.78	8.71	13.53	12.29	12.14	11.87	12.58	11.64	14.49	14.54	10.22
MnO	0.21	0.20	0.21	0.20	0.22	0.20	0.27	0.21	0.26	0.22	0.26	0.27	0.27	0.21
MgO	5.24	4.21	5.31	1.28	1.95	10.77	8.76	8.87	7.53	9.28	7.57	6.72	6.94	3.77
CaO	10.01	9.13	9.93	5.15	6.01	9.20	9.18	9.23	9.57	9.62	9.56	10.72	10.64	8.31
Na_2O	4.05	4.58	4.28	7.25	6.18	3.47	5.89	3.69	5.36	4.01	5.34	4.92	5.23	4.65
K_2O	1.75	2.45	1.90	3.75	3.47	1.72	2.11	1.30	2.04	1.57	1.95	1.89	1.96	2.61
P_2O_5	1.12	1.03	0.76	0.63	0.73	1.28	0.85	0.45	0.88	0.62	0.88	1.30	1.32	0.84
Rb (ppm)	31	66	42	129	112	42	69	50	86	56	79	47	52	62
Ba	541	774	627	1066	1034	528	739	471	864	546	824	1031	898	812
Th	6.7	8.5	6.5	15.3	14.6	9.2	17.9	9.8	18.4	9.8	18.8	14.0	14.3	11.0
U	1.3	1.2	1.2	4.0	3.8	2.2	2.6	1.7	4.8	2.2	3.9	3.3	2.8	2.8
Ta	6.7	7.8	6.0	13.2	13.2	7.6	10.5	5.9	10.9	6.6	11.3	9.2	9.7	9.2
Nb	90	106	83	174	174	100	142	75	145	89	147	125	133	125
La	60	88	64	117	116	82	107	58	107	62	111	101	107	94
Ce	106	147	111	196	199	151	169	97	181	107	186	168	177	168
Pb	1.7	2.1	1.6	4.4	3.9	2.2	5.4	2.4	4.6	2.7	4.7	3.0	3.6	3.6
Pb (ID)		2.7												
Pr	13.6	18.1	14.1	20.0	21.1	17.3	19.1	10.3	19.0	11.6	19.2	18.0	19.0	18.4
Nd	58	74	58	73	80	71	72	40	73	46	73	71	75	72
Sr	996	1351	1236	1316	1378	939	1166	692	1126	802	1177	1087	1228	1407
Sm	12.5	14.9	12.0	13.0	14.7	14.1	14.0	8.0	13.7	9.0	14.0	13.9	14.4	13.0
Hf	6.3	9.8	8.1	11.9	12.3	10.0	9.0	5.3	9.3	6.0	9.5	7.4	7.7	10.1
Zr	278	440	376	637	633	440	443	230	488	281	477	352	346	470
Eu	3.7	4.4	3.7	4.1	4.5	4.2	4.0	2.5	4.1	2.8	4.2	4.1	4.2	4.0
Gd	12	14	11	12	14	13	14	8	13	9	13	13	13	12
Tb	1.6	1.8	1.5	1.5	1.7	1.5	1.8	1.0	1.6	1.1	1.7	1.6	1.6	1.4
Y	39	42	35	40	44	37	46	32	45	33	46	42	43	37
Dy	7.6	8.4	6.9	7.4	8.3	7.4	8.3	5.7	8.4	6.2	8.4	8.0	8.2	6.9
Ho	1.2	1.4	1.1	1.3	1.4	1.2	1.4	1.0	1.5	1.1	1.5	1.4	1.4	1.2
Er	3.3	3.6	3.0	3.5	3.9	3.0	4.0	2.8	4.0	3.0	4.0	3.7	3.7	3.2
Yb	3.1	3.4	2.8	-	-	-	4.1	-	-	-	-	-	-	-
Lu	0.4	0.5	0.4	0.5	0.5	0.4	0.6	0.4	0.6	0.4	0.6	0.5	0.5	0.5
Ni	547	287	330	-	-	-	646	-	-	-	-	-	-	-
Cu	272	177	219	-	-	-	248	-	-	-	-	-	-	-
Zn	97	103	94	-	-	-	98	-	-	-	-	-	-	-
V	205	148	162	32	46	143	133	152	131	157	137	136	145	139
Cr	11	53	127	7	7	429	338	288	276	244	293	113	134	45
$^{206}Pb/^{204}Pb$	-	19.87	19.80	19.99	19.96	-	-	19.63	-	-	-	19.46	19.47	19.64
$^{207}Pb/^{204}Pb$	-	15.56	15.62	15.63	15.61	-	-	15.56	-	-	-	15.55	15.57	15.60
$^{208}Pb/^{204}Pb$	-	39.12	39.38	39.44	39.36	-	-	39.01	-	-	-	38.90	39.30	39.12
$^{87}Sr/^{86}Sr$	-	0.70293	0.70296	0.70300	0.70303	-	-	0.70289	-	-	-	0.70344	0.70292	0.70317
$^{143}Nd/^{144}Nd$	-	0.51295	0.51292	0.51293	0.51295	-	-	0.51296	-	-	-	0.51300	0.51297	0.51288
$^{176}Hf/^{177}Hf$	-	0.28302	0.28301	0.28299	0.28299	-	-	0.28306	-	-	-	-	0.28304	0.28298

90

Table 3-2.

Sample	04DRE3-56	04DRE3-59	04DRE3-73	04DRE4-75	04DRE4-76	04DRE5-80	04DRE5-81	05DRE5-85	04DRE5-89	04DRE6-107
Location	Dredge 3 Seamount			Dredge 4 Seamount		Dredge 5 Seamount				Dredge 6 Seamount
Age (Ma) [a]	0.187 ± 0.176		0.089 ± 0.066	1.93 ± 0.04	1.92 ± 0.04	3.94 ± 0.08		3.73 ± 0.14		0.506 ± 0.024
SiO_2 (wt %)	39.45	41.14	40.41	41.11	43.66	42.19	41.56	42.57	41.73	40.24
TiO_2	2.56	2.44	2.63	3.22	2.58	4.00	4.05	3.34	3.62	3.39
Al_2O_3	11.84	12.33	12.01	12.47	12.07	13.17	11.95	11.54	12.19	13.09
Fe_2O_3	12.25	10.68	12.43	14.08	12.39	14.61	14.23	13.88	14.19	14.59
MnO	0.23	0.19	0.23	0.24	0.18	0.21	0.18	0.17	0.19	0.26
MgO	11.27	10.54	11.06	8.65	13.70	8.33	10.82	12.73	10.72	4.90
CaO	12.83	14.24	13.31	11.37	11.76	9.27	9.88	9.94	9.12	11.54
Na_2O	3.63	3.51	3.69	4.29	2.20	3.31	2.78	2.17	2.92	4.42
K_2O	1.77	1.22	1.69	0.97	0.88	1.73	1.48	1.29	1.39	2.71
P_2O_5	1.10	0.76	1.19	1.17	0.45	0.87	0.88	0.67	0.77	1.42
Rb (ppm)	62	33	50	15	24	45	37	29	32	78
Ba	870	657	869	664	326	479	415	363	457	1173
Th	15.2	11.0	13.7	13.2	4.1	7.8	7.0	5.2	7.1	15.2
U	3.6	2.3	2.9	2.9	1.0	1.9	1.5	1.2	1.6	3.6
Ta	9.3	7.0	8.4	9.4	3.5	6.8	5.9	4.4	5.8	10.9
Nb	104	92	116	123	47	87	75	59	77	152
La	89	65	91	96	33	63	54	44	56	118
Ce	152	111	152	169	64	119	102	82	106	198
Pb	3.1	2.5	3.4	3.2	1.4	2.0	1.9	1.5	1.9	4.5
Pb (ID)			4.9	3.5	-	-	3.0	-	-	-
Pr	17.5	12.4	16.3	18.4	7.5	14.1	12.1	9.7	12.2	21.6
Nd	71	50	64	73	32	59	52	40	51	86
Sr	1018	776	1005	1132	514	874	798	705	823	1264
Sm	13.8	9.8	12.4	14.0	6.6	12.7	11.2	8.3	10.5	16.9
Hf	6.9	5.2	6.1	9.1	4.4	10.2	8.4	5.9	7.6	8.5
Zr	264	225	273	396	185	442	364	267	336	380
Eu	4.1	3.0	3.7	4.1	2.1	3.9	3.4	2.6	3.2	5.0
Gd	12	9	12	13	6	12	10	8	10	15
Tb	1.5	1.1	1.4	1.6	0.9	1.5	1.3	1.0	1.2	1.8
Y	35	30	36	40	24	39	32	26	31	48
Dy	7.9	6.0	7.0	7.9	4.6	7.8	6.7	5.2	6.0	9.2
Ho	1.4	1.0	1.2	1.4	0.8	1.3	1.1	0.9	1.0	1.6
Er	3.6	2.7	3.2	3.5	2.2	3.3	2.7	2.3	2.6	4.0
Yb	-	-	-	-	-	-	-	-	-	-
Lu	0.5	0.3	0.4	0.5	0.3	0.4	0.3	0.3	0.3	0.6
Ni	-	-	-	-	-	-	-	-	-	-
Cu	-	-	-	-	-	-	-	-	-	-
Zn	-	-	-	-	-	-	-	-	-	-
V	204	251	210	208	232	196	205	194	196	183
Cr	342	413	348	276	614	96	284	405	292	18
$^{206}Pb/^{204}Pb$	-	-	19.53	19.75	19.40	19.82	19.71	-	-	19.28
$^{207}Pb/^{204}Pb$	-	-	15.60	15.59	15.59	15.59	15.60	-	-	15.48
$^{208}Pb/^{204}Pb$	-	-	39.06	39.24	39.06	39.26	39.21	-	-	38.50
$^{87}Sr/^{86}Sr$	-	-	0.70319	0.70338	0.70320	0.70313	0.70333	-	-	0.70352
$^{143}Nd/^{144}Nd$	-	-	0.51301	0.51294	0.51293	0.51292	0.51294	-	-	0.51300
$^{176}Hf/^{177}Hf$	-	-	0.28304	0.28307	0.28303	0.28301	0.28299	-	-	0.28306

REFERENCES

Ballentine, C. J., D. C. Lee, and A. N. Halliday (1997), Hafnium isotopic studies of the Cameroon line and new HIMU paradoxes, *Chemical Geology*, *139*, 111-124.

Behrendt, J. C. (1999), Crustal and lithospheric structure of the West Antarctic Rift System from geophysical investigations - a review, *Global And Planetary Change*, *23*, 25-44.

Behrendt, J. C., D. D. Blankenship, C. A. Finn, R. E. Bell, R. E. Sweeney, S. M. Hodge, and J. M. Brozena (1994), CASERTZ aeromagnetic data reveal late Cenozoic flood basalts in the West Antarctic rift system, *Geology*, *22*, 527-530.

Behrendt, J. C., R. Saltus, D. Damaske, A. McCafferty, C. A. Finn, D. Blankenship, and R. E. Bell (1996), Patterns of late Cenozoic volcanic and tectonic activity in the West Antarctic rift system revealed by aeromagnetic surveys, *Tectonics*, *15*, 660-676.

Berg, J. H., R. J. Moscati, and D. L. Herz (1989), A petrologic geotherm from a continental rift in Antarctica, *Earth and Planetary Science Letters*, *93*, 98-108.

Brown, B., C. Gaina, and R. D. Muller (2006), Circum-Antarctic palaeobathymetry: Illustrated examples from Cenozoic to recent times, *Palaeogeography, Palaeoclimatology, Palaeoecology*, *231*, 158-168.

Carmichael, I. S. E., R. A. Lange, and J. F. Luhr (1996), Quaternary minettes and associated volcanic rocks of Mascota, western Mexico: a consequence of plate extension above a subduction modified mante wedge, *Contributions to Mineralogy and Petrology*, *124*, 302-333.

Cherniak, D. J. (2001), Pb diffusion in Cr diopside, augite, and enstatite, and consideration of the dependence of cation diffusion in pyroxene on oxygen fugacity, *Chemical Geology*, *177*, 381-397.

Cherniak, D. J. (2003), REE diffusion in feldspar, *Chemical Geology*, *193*, 25-41.

Choi, S. H., S. B. Mukasa, A. V. Andronikov, Y. Osanai, S. L. Harley, and N. M. Kelly (2006), Lu-Hf systematics of the ultra-high temperature Napier Metamorphic Complex in Antarctica: Evidence for the early Archean differentiation of Earth's mantle, *Earth And Planetary Science Letters*, *246*, 305-316.

Coltorti, M., L. Beccaluva, C. Bonadiman, B. Faccini, T. Ntaflos, and F. Siena (2004), Amphibole genesis via metasomatic reaction with clinopyroxene in mantle xenoliths from Victoria Land, Antarctica, *Lithos*, *75*, 115-139.

Cooper, A. F., L. J. Adam, R. F. Coulter, G. N. Eby, and W. C. McIntosh (2007), Geology, geochronology and geochemistry of a basanitic volcano, White Island, Ross Sea, Antarctica, *Journal Of Volcanology And Geothermal Research*, *165*, 189-216.

Dixon, J., D. A. Clague, B. Cousens, M. L. Monsalve, and J. Uhl (2008), Carbonatite and silicate melt metasomatism of the mantle surrounding the Hawaiian plume: Evidence from volatiles, trace elements, and radiogenic isotopes in rejuvenated-stage lavas from Niihau, Hawaii, *Geochemistry Geophysics Geosystems*, *9*.

Dungan, M. A., M. M. Lindstrom, N. J. McMillan, S. Moorbath, H. J., and L. Haskin (1986), Open system magmatic evolution of the Taos Plateau volcanic field, northern New Mexico I: The petrology and geochemistry of the Servilleta Basalt, *Journal of Geophysical Research*, *91*, 5999–6028.

Eagles, G., K. Gohl, and R. D. Larter (2004), High-resolution animated tectonic reconstruction of the South Pacific and West Antarctic Margin, *Geochemistry Geophysics Geosystems*, *7*.

Esser, R. P., P. R. Kyle, and W. C. McIntosh (2004), Ar-40/Ar-39 dating of the eruptive history of Mount Erebus, Antarctica: volcano evolution, *Bulletin Of Volcanology*, *66*, 671-686.

Faccenna, C., F. Rossetti, T. W. Becker, S. Danesi, and A. Morelli (2008), Recent extension driven by mantle upwelling beneath the Admiralty Mountains (East Antarctica), *Tectonics*, *27*.

Finn, C. A., R. D. Muller, and K. S. Panter (2005), A Cenozoic diffuse alkaline magmatic province (DAMP) in the southwest Pacific without rift or plume origin, *Geochemistry Geophysics Geosystems*, *6*.

Futa, K., and W. E. LeMasurier (1983), Nd and Sr Isotopic Studies on Cenozoic Mafic Lavas from West Antarctica: Another Source for Continental Alkali Basalts, *Contributions to Mineralogy and Petrology*, *83*, 38-44.

Halliday, A. N., D.-C. Lee, S. Tommasini, G. R. Davies, C. R. Paslick, J. G. Fitton, and D. E. James (1995), Incompatible trace elements in OIB and MORB and source enrichment in the sub-oceanic mantle, *Earth and Planetary Science Letters*, *133*, 379-395.

Harrison, W. J., and B. J. Wood (1980), An Experimental Investigation Of The Partitioning Of Ree Between Garnet And Liquid With Reference To The Role Of Defect Equilibria, *Contributions To Mineralogy And Petrology*, *72*, 145-155.

Hart, S. R., J. Blusztajn, and C. Craddock (1995), Cenozoic volcanism in Antarctica: Jones Mountains and Peter I Island, *Geochimica e Cosmochimica Acta*, *9*, 3379-3388.

Hart, S. R., J. Blusztajn, W. E. LeMasurier, and D. C. Rex (1997), Hobbs Coast Cenozoic volcanism: Implications for the West Antarctic rift system, *Chemical Geology*, *139*, 223-248.

Hart, S. R., D. C. Gerlach, and W. M. White (1986), A Possible New Sr-Nd-Pb Mantle Array And Consequences For Mantle Mixing, *Geochimica Et Cosmochimica Acta*, *50*, 1551-1557.

Hirschmann, M. M., T. Kogiso, M. B. Baker, and E. M. Stolper (2003), Alkalic magmas generated by partial melting of garnet pyroxenite, *Geology*, *31(6)*, 481-484.

Hole, M. J., and W. E. LeMasurier (1994), Tectonic controls on the geochemical composition of Cenozoic, mafic alkaline volcanic rocks from West Antarctica, *Contributions to Mineralogy and Petrology*, *117*, 187-202.

Johnston, A. D., and B. E. Schwab (2004), Constaints on clinopyroxene/melt partitioning of REE, Rb, Sr, Ti, Cr, Zr, and Nb during mantle melting: First insights from direct peridotite melting experiments at 1.0 GPa, *Geochimica e Cosmochimica Acta*, *68*, 2929-2962.

Kelley, K. A., T. Plank, L. Farr, J. Ludden, and H. Staudigel (2005), Subduction cycling of U, Th, and Pb, *Earth And Planetary Science Letters*, *234*, 369-383.

Kempton, P. D., J. G. Fitton, C. J. Hawkesworth, and D. S. Ormbrod (1991), Isotopic and Trace Element Constraints on the Composition and Evolution of the Lithosphere Beneath the Southwestern United States, *Jounral of Geophysical Research*, *96*, 13,713-713,735.

Kogiso, T., M. B. Baker, and E. M. Stolper (2003), High-pressure partial melting of garnet pyroxenite:possible mafic lithologies in the source of ocean island basalts, *Earth and Planetary Science Letters*, *216*, 603-617.

Kogiso, T., K. Hirose, and E. Takahashi (1998), Melting experiments on homogeneous mixtures of peridotite and basalt: application to the genesis of ocean island basalts, *Earth And Planetary Science Letters*, *162*, 45-61.

Kyle, P., and P. C. Rankin (1976), Rare earth element geochemistry of Late Cenozoic alkaline lavas of the McMurdo Volcanic Group, Antarctica, *Geochimica e Cosmochimica Acta*, *40*, 1497-1507.

Kyle, P. R., J. A. Moore, and M. F. Thirlwall (1992), Petrologic Evolution Of Anorthoclase Phonolite Lavas At Mount Erebus, Ross Island, Antarctica, *Journal Of Petrology*, *33*, 849-875.

LeMasurier, W. E., K. Futa, M. Hole, and Y. Kawachi (2003), Polybaric Evolution of Phonolite, Trachyte, and Rhyolite Volcanoes in Eastern Marie Byrd Land, Antarctica: Controls on Peralkalinity and Silica Saturation, *International Geology Review*, *45*, 1055-1099.

LeMasurier, W. E., D. M. Harwood, and D. C. Rex (1994), Geology of Mount Murphy Volcano: An 8-m.y. history of interaction between a rift volcano and the West Antarctic ice sheet, *GSA Bulletin*, *106*, 265-280.

Mukasa, S. B., and I. W. D. Dalziel (2000), Marie Byrd Land, West Antarctica: Evolution of Gondwana's Pacific margin constrained by zircon U-Pb geochronology and feldspar common-Pb isotopic compositions, *Geological Society of America Bulletin*, *112*, 611-627.

Mukasa, S. B., R. McCabe, and J. B. Gill (1987), Pb-isotopic compositions of volcanic rocks in the West and East Philippine island arcs; presence of the Dupal isotopic anomaly, *Earth and Planetary Science Letters*, *84*, 152-164.

Mukasa, S. B., J. W. Shervais, H. G. Wilshire, and J. E. Nielson (1991), Intrinsic Nd, Pb, and Sr isotopic heterogeneities exhibited by the Lherz alpine peridotite massif, French Pyrenees, *Journal of Petrology*, *Special Lherzolite Volume*, 117-134.

Panter, K. S., J. Blusztajn, S. R. Hart, P. R. Kyle, R. Esser, and W. C. McIntosh (2006), The Origin of HIMU in the SW Pacific: Evidence from Intraplate Volcanism in Southern New Zealand and Subantarctic Islands, *Journal of Petrology*, *47(9)*, 1673-1704.

Panter, K. S., S. R. Hart, P. Kyle, J. Blusztanjn, and T. Wilch (2000), Geochemistry of Late Cenozoic basalts from the Crary Mountains: characterization of mantle sources in Marie Byrd Land, Antarctica, *Chemical Geology*, *165*, 215-241.

Paslick, C., A. Halliday, D. James, and J. B. Dawson (1995), Enrichment Of The Continental Lithosphere By Oib Melts - Isotopic Evidence From The Volcanic Province Of Northern Tanzania, *Earth And Planetary Science Letters*, *130*, 109-126.

Perinelli, C., P. Armienti, and L. Dallai (2006), Geochemical and O-isotope constraints on the evolution of lithospheric mantle in the Ross Sea rift area (Antarctica), *Contributions To Mineralogy And Petrology*, *151*, 245-266.

Pilet, S., M. B. Baker, and E. M. Stolper (2008), Metasomatized lithosphere and the origin of alkaline lavas, *Science*, *320*, 916-919.

Riley, T. R., P. T. Leat, S. P. Kelley, I. L. Millar, and M. F. Thirlwall (2003), Thinning of the Antarctic Peninsula lithosphere through the Mesozoic: evidence from Middle Jurassic basaltic lavas, *Lithos*, *67*, 163-179.

Rocchi, S., P. Armienti, M. D'Orazio, S. Tonarini, J. R. Wijbrans, and G. DiVincenzo (2002), Cenozoic magmatism in the western Ross Embayment: Role of mantle plume versus plate dynamics in the development of the West Antarctic Rift System, *Journal of Geophysical Research*, *107*.

Rocchi, S., S. Tonarini, P. Armienti, F. Innocenti, and P. Manetti (1998), Geochemical and isotopic structure of the early Palaeozoic active margin of Gondwana in northern Victoria Land, Antarctica, *Tectonophysics*, *284*, 261-281.

Rocholl, A., M. Stein, M. Molzahn, S. R. Hart, and G. Worner (1995), Geochimcal evolution of rift magmas by progressive tapping of a stratified mantle source beneath the Ross Sea Rift, Northern Victoria Land, Antarctica, *Earth and Planetary Science Letters*, *131*, 207-224.

Rossetti, F., F. Storti, M. Busetti, F. Lisker, G. Di Vincenzo, A. L. Laufer, S. Rocchi, and F. Salvini (2006), Eocene initiation of Ross Sea dextral faulting and implications for East Antarctic neotectonics, *Journal of the Geological Society of London*, *163*, 119-126.

Salvini, F., G. Brancolini, M. Busetti, F. Storti, F. Mazzarini, and F. Coren (1997), Cenozoic geodynamics of the Ross Sea region, Antarctica: Crustal extension, intraplate strike-slip faulting, and tectonic inheritance, *Journal of Geophysical Research*, *102(B11)*, 24,669-624,696.

Sieminski, A., E. Debayle, and J.-J. Leveque (2003), Seismic evidence for deep low-velocity anomalies in the transition zone beneath West Antarctica, *Earth and Planetary Science Letters*, *216*, 645-661.

Storey, B. C., P. T. Leat, and J. K. Ferris (2001), The location of mantle-plume centers during the initial stages of Gondwana breakup, *Mantle Plumes: Their Identification Through Time*, 71-80.

Trey, H., A. K. Cooper, G. Pellis, B. della Vedova, G. Cochrane, G. Brancolini, and J. Makris (1999), Transect across the West Antarctic rift system in the Ross Sea, Antarctica, *Tectonophysics*, *301*, 61-74.

Watson, T., A. A. Nyblade, D. A. Wiens, S. Anandakrishan, M. Benoit, P. J. Shore, D. Voigt, and J. VanDecar (2006), P and S velocity structure of the upper mantle beneath the Transantarctic Mountains, East Antarctic craton, and Ross Sea from travel time tomography, *Geochemistry Geophysics Geosystems*, *7(7)*.

Wilson, T. J., L. A. Lawver, S. A. Henrys, S. Mukasa, H. Horgan, M.Weiderspahn, M. Davis, J. Whittaker, A. Lowe, and M. Watson (2004), Cruise Report NBP0401 19 January to 18 February 2004 -
McMurdo Station to McMurdo Station, Ross Sea, Antarctica, *Institute of Geological and Nuclear Sciences Science Report*, *2004/03*, 85.

Worner, G. (1999), Lithospheric dynamics and mantle sources of alkaline magmatism of the Cenozoic West Antarctic Rift System, *Global and Planetary Change*, *23*, 61-77.

Zipfel, J., and G. Worner (1992), 4-Phase And 5-Phase Peridotites From A Continental Rift System - Evidence For Upper Mantle Uplift And Cooling At The Ross Sea Margin (Antarctica), *Contributions To Mineralogy And Petrology*, *111*, 24-36.

CHAPTER 4

PGE AND OS ISOTOPIC EVIDENCE FOR A LITHOSPHERIC CONTRIBUTION TO CENOZOIC MAGMAS IN THE WEST ANTARCTIC RIFT SYSTEM

ABSTRACT

This study provides the first combined platinum group element (PGE) distribution patterns and Os isotopic compositions for Cenozoic lavas from the West Antarctic Rift System (WARS). Ten and twelve samples from the Terror Rift were analyzed for PGEs and Os isotopic compositions, respectively. These lavas have lower PGE concentrations than other areas of intraplate volcanism, including Hawaii and the Kerguelen Islands, and for at least some of the lavas support a residual lithospheric magma source which has undergone previous melting and removal of host sulfide phases. The extremely unradiogenic $^{187}Os/^{188}Os$ signatures of as low as 0.1081 ± 0.0001 is best explained by melting of residual lithospheric mantle with a time-integrated record of low Re/Os values. Lavas with more radiogenic $^{187}Os/^{188}Os$ values may have originated in less depleted domains within the mantle lithosphere or are the products of asthenospheric melting. The WARS region has undergone a complex history of arc- and rift-related magmatism and may have led to slightly more heterogeneous PGE and Os isotopic signatures than would be expected for melting of typical continental lithosphere. These variations also prevent identification of a single dominant process, such as mantle metasomatism.

INTRODUCTION

The West Antarctic Rift System (WARS) has been identified as one of Earth's major rift zones based on its size [*Tessensohn and Worner*, 1991; *Worner*, 1999]; however, glacial cover and limited sampling have hampered studies of the causes and mechanisms of magmatism in the region. Volcanism of similar age and alkaline composition is found in all tectonic blocks that were once located in close proximity to each other along the paleo-Pacific Gondwanan margin but are now separated by entire ocean basins and distances upwards of 2000 km. Finn et al. [2005] termed this area of the Southern Ocean the Diffuse Alkaline Magmatic Province (or DAMP spot). Although early models attributed Cenozoic volcanism on the Antarctic continent to mantle plumes [*Behrendt, et al.*, 1994; *Behrendt, et al.*, 1996; *LeMasurier and Landis*, 1996; *Behrendt*, 1999], more recent studies have considered the presence of amphibole and phlogopite in mantle-derived xenoliths [*Coltorti, et al.*, 2004; *Perinelli, et al.*, 2006] and O-isotopic signatures [*Perinelli, et al.*, 2006; *Nardini, et al.*, 2009] to be evidence of a metasomatized subcontinental mantle lithosphere as the magma source. This study provides the first combined platinum group element (PGE) and Os-isotopic dataset for samples from within the WARS. A completely new dataset provides a fresh approach in attempts to understand the causes of Ross Sea magmatism and helps to evaluate the models aiming to explain the magmatism. An active mantle plume and decompression melting of the lithosphere are often the competing models for generation of alkaline magmatism in various areas of the world [*Halliday, et al.*, 1995; *Panter, et al.*, 2006; *Pilet, et al.*, 2008].

BACKGROUND

Regional geology

The WARS is recognized as one of the most extensive alkali volcanic provinces in the world (Fig.4-1). It is comprised of basaltic shield volcanoes and dominantly trachytic or phonolitic stratovolcanoes, commonly cut by widely scattered fields of basaltic cinder cones and lava flows, and/or domes of evolved lavas such as phonolite, trachyte and peralkaline rhyolite [*Kyle*, 1990]. In general,
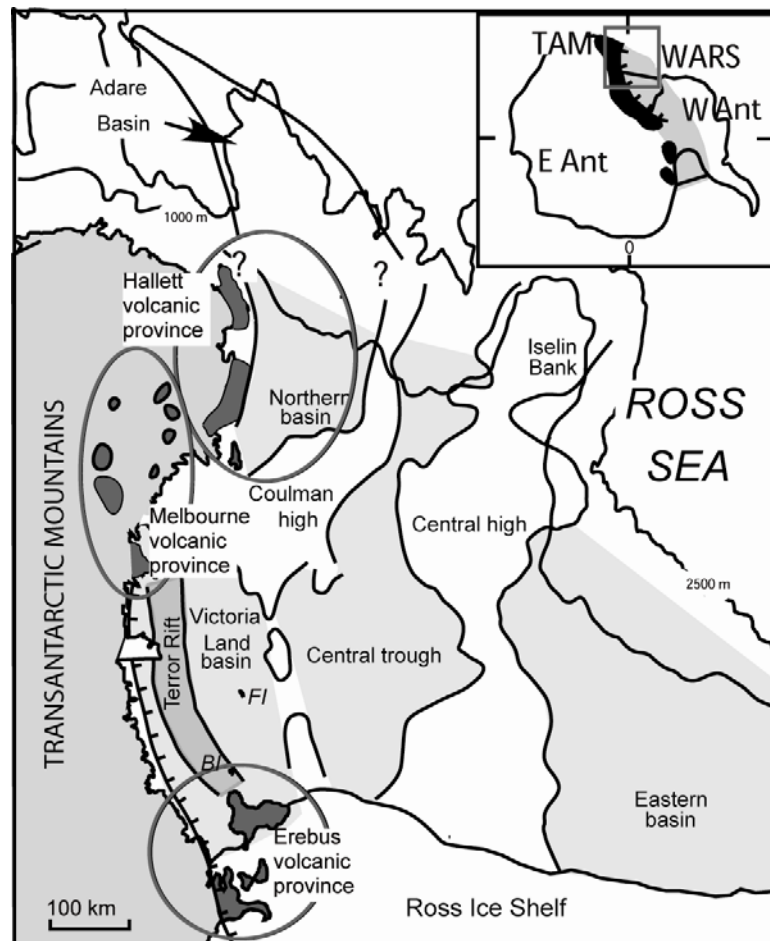

Figure 4-1. Simplified regional map of the study area. The Transantarctic Mountains represent the western rift shoulder of the West Antarctic Rift System (WARS) which extends across the Ross Sea into West Antarctica. The rift detachment runs along the eastern margin of the range. Black areas on the insert map and dark gray on the main map represent subaerial Cenozoic volcanism and the circles outline the division into three major volcanic provinces. Light grey shading indicates basin fill greater than 3000m. Figure modified from [*Hall, et al.*, 2007].

rocks in the Ross Island region (Erebus Volcanic Province) are more alkaline and more strongly undersaturated with respect to silica than those in the Hallett and Melbourne Volcanic Provinces farther to the north [*LeMasurier and Thomson*, 1990; *Armienti, et al.*, 1991; *Kyle, et al.*, 1992]. Further petrologic information about the Cenozoic volcanic activity in the Victoria Land region of the WARS is summarized in LeMasurier and Thomson [1990], and also Armienti et al. [1991], Kyle et al. [1992], Rocholl et al. [1995], Wörner et al. [1999], and Rocchi et al. [2002].

WARS magmatism has been explained by either a single plume model [*Behrendt, et al.*, 1994; *Hole and LeMasurier*, 1994; *Behrendt, et al.*, 1996; *Behrendt*, 1999], or by more passive, decompression melting models [*Rocholl, et al.*, 1995; *Panter, et al.*, 2000]. Hole and LeMasurier [1994] postulated that a mantle plume roughly 1500 km by 2500 km was responsible for volcanism in Marie Byrd Land (MBL) over the past 25-20 Ma, based on enrichments in incompatible trace element concentrations and the HIMU-like isotopic signature of analyzed lavas. Behrendt [1999] and Behrendt et al. [1994; 1996] also hypothesized the possible presence of a plume located beneath MBL in order to explain the large volumes of lava present under the West Antarctic Ice Sheet. Coeval alkaline volcanism in the Erebus Volcanic Province was interpreted by Kyle et al. [1992] and Esser et al. [2004] in terms of a mantle plume model on the NVL side of the WARS as well. This requires a second plume, at least 500 km in diameter and in close proximity to the MBL plume, to explain the young volcanism on both margins of the WARS.

A second generation of magma models focused on decompressional melting of potential mantle sources and may be related to a fossilized plume head underplating the Antarctic lithosphere. Rocholl et al. [1995] called for at least three mantle end-members (MORB-type or DMM-, EM-, and HIMU-like) in the source components of northern Victoria Land (NVL) magmatism, and suggested that the geochemical differences are the result of polybaric melting and variations in the degree of melting. Hart et al. [1997] also called for a stratified mantle source for volcanism in MBL. They noted that melts generated at the deepest levels yielded HIMU isotopic signatures while those generated at shallower depths yielded isotopic signatures more similar to FOZO, as defined by Hart et al. [1986]. As new locations are sampled, the debate over the WARS magma source continues to inspire new models.

The most recent models of magmatism in the WARS and Southern Ocean are based on the hypothesis that the local mantle source may be hydrated, potentially caused by ancient subduction history in the region[*Panter, et al.*, 2006]. West Antarctica is comprised of several tectonic blocks which were once amalgamated to form the long-lived subduction zone along the paleo-Pacific margin of the supercontinent Gondwana during much of the Paleozoic and Mesozoic [*Mukasa and Dalziel*, 2000]. Numerous tomographic studies of the upper mantle [*Sieminski, et al.*, 2003; *Finn, et al.*, 2005; *Watson, et al.*, 2006] have attributed slow seismic anomalies below the WARS to higher temperatures or abundance of volatiles in the mantle due to a long history of subduction. Small amounts of either water or carbon could account for larger amounts of melting during lithospheric thinning and decompression than would be possible in an anhydrous mantle setting. This metasomatized mantle hypothesis is supported by the presence of

hydrous phases, including amphibole and phlogopite, in mantle xenoliths from Victoria

Land [*Zipfel and Worner*, 1992; *Coltorti, et al.*, 2004; *Perinelli, et al.*, 2006; *Cooper, et al.*, 2007], and O-isotopic compositions of the Cenozoic WARS lavas [*Nardini, et al.*, 2009]. Pyroxenite veins, frozen in place after previous melting events, would also have a lower melting temperature and could be the source of WARS magmatism during a subsequent episode of melting, this time facilitated by decompression related to Cenozoic rifting. Abundances of platinum group elements (PGE) and Os-isotopic compositions of lavas from the Erebus Volcanic Province provide a new approach in attempts to provide a better understanding of whether a metasomatized or pyroxenite magma source existed beneath the WARS.

Platinum group elements

PGE abundances can be used to trace the source of magmas in a unique way for silicate systems. Because they are siderophile elements rather than lithophile, they are unaffected by the bulk silicate composition of the source like many other trace elements. Os, Ir, and Ru behave as compatible elements in the mantle, possibly ending up in Cr-spinel or some PGE alloys, while Pt, Pd, and Re behave incompatibly [*Barnes, et al.*, 1985]. Mid-ocean ridge basalts (MORB) tend to have a smooth positive slope for PGE distribution patterns when elements are plotted in order of compatibility [*Rehkamper, et al.*, 1997; *Bezos, et al.*, 2005]. Ocean island basalts (OIB) tend to have a step-like PGE profile with a sharp difference in the concentration of Os, Ir, and Ru compared to Pt, Pd, and Re [*Rehkamper, et al.*, 1997]. Rehkämper et al. [1999] initially found Pd/Ir of 30 – 100 and <5-10 for MORBs and alkali-rich OIB, respectively; however, more recent studies have shown that the slope of PGE abundance patterns are not directly related to

the degree of partial melting [*Agranier, et al.*, 2007; *Dale, et al.*, 2008]. Sulfide removal

during successive melting events more dominantly controls PGE concentrations,

potentially fractionating PGEs by transporting and precipitating Pt-Pd-enriched sulfides

over Ir-Ru-rich sulfides [*Lorand, et al.*, 2004].

Although the low-blank Carius tube method of PGE analysis was developed over

a decade ago [*Rehkamper, et al.*, 1997], poor understanding of PGE behavior both during

sample processing and in different natural environments continue to hamper

interpretations. PGEs tend to be clustered in small domains within lavas, referred to as

the "nugget effect," rather than being homogeneously scattered throughout the sample

[*Ely and Neal*, 2003]. This heterogeneity leads to difficulty in reproducing concentration

measurements as the variations could be analytical or natural. Ely and Neal [2003]

reported as much as 58% variability in replicate analyses from a single sample, and this

effect is more problematic in samples with low PGE concentrations. Although

determining the absolute PGE amounts in low-concentration samples can be difficult, the

relative abundances of PGEs should remain fairly consistent and generate parallel PGE

distribution patterns for replicates of a single sample. These new distribution patterns can

provide insights about a magma source that can not be obtained from examining

lithophile elements alone.

Re-Os isotopic system

^{187}Re decays to ^{187}Os by beta emission with a half-life of 42.3 Gy [*Faure and*

Mensing, 2005]. Because of the difference in compatibility between Re and Os, mantle-

derived basalts tend to have high Re/Os ratios and create radiogenic ^{187}Os/^{188}Os ratios

within only a million years despite the long half-life of ^{187}Re [*Shirey and Walker*, 1998].

The geologically rapid generation of radiogenic $^{187}Os/^{188}Os$ ratios can be used to trace recycling of subducted oceanic lithosphere and sediments in magmatic components [*Hauri and Hart*, 1993]. Meisel et al. [2001] determined a primitive upper mantle $^{187}Os/^{188}Os$ of ~ 0.130. Mid-ocean ridge basalts (MORBs) show similar isotopic compositions generally below 0.140 [*Schiano, et al.*, 1997; *Gannoun, et al.*, 2004; *Escrig, et al.*, 2005]. Melts derived from mafic materials in the crust or upper mantle also tend to have significantly lower concentrations and more radiogenic isotopic compositions of Os than direct melts of mantle peridotite sources [*Shirey and Walker*, 1998]. Pyroxenites -- comprising another potential mantle source – also possess a high Re/Os ratio due to their generation by earlier melting which elevated the Re/Os ratio, and in time the resulting radiogenic Os isotopic signatures [*Lassiter, et al.*, 2000]. Os isotopic compositions are therefore very sensitive to melting of a pyroxenite source. HIMU-type lavas, commonly interpreted as aged recycled oceanic lithosphere, typically yield $^{187}Os/^{188}Os$ ratios of ~0.145 – 0.155 [*Lassiter, et al.*, 2003].

In contrast, residual mantle materials tend to have lowered Re/Os ratios [*Hauri and Hart*, 1993] and produce melts with distinctively unradiogenic Os isotopic compositions. Abyssal peridotites have unradiogenic isotopic ratios of only 0.120-0.135 [*Gannoun, et al.*, 2004; *Escrig, et al.*, 2005]. Sub-continental lithospheric mantle xenoliths exhibit the least radiogenic $^{187}Os/^{188}Os$ ratios measured, 0.105-0.130, due to the preferential removal of Re relative to Os during repeated partial melting events through time leading to formation of continental crust [*Hassler and Shimizu*, 1998].

This paper reports the first combined Os-isotopic compositions and PGE abundance patterns for Cenozoic lavas from Antarctica. The data presented here will help

distinguish between the proposed models for magma generation in the WARS, which variously call for passive rifting and accompanying decompression of an asthenospheric or lithospheric mantle source, and a mantle plume comprised of ancient recycled oceanic lithosphere.

SAMPLES

Submarine samples were collected during a 2004 cruise of the *Nathaniel B. Palmer* (NBP-0401) that dredged seven volcanic edifices associated with seafloor structures identified by multibeam bathymetric mapping (Fig. 4-2). A variety of materials were collected, including basalts, hyaloclastites and peridotite xenoliths. Subaerial samples from Franklin and Beaufort Islands were collected by members of the research cruise and members of the TAMDEF research team, respectively. More detailed description of the sampled edifices and specific sample sites can be found in Rilling et al. [2009, *in press*]. Additional information on the volcanic stratigraphy of Franklin and Beaufort Islands can be found in LeMasurier and Thompson [1990]. The remaining samples from various localities in northern Victoria Land were collected during various field seasons by Prof Wesley LeMasurier.

The majority of the samples studied can be classified as basanites and primitive foidites on a total alkalis versus silica diagram (Fig. 4-3). Sample ANT1-6 from Franklin Island is slightly evolved and plots at the boundary between basalt and trachybasalt. MgO concentrations range from 13.70 wt% for sample DRE4-76 to only 6.72 wt% for sample DRE1-31. SiO_2, TiO_2, and Al_2O_3 plotted against MgO show evidence of olivine and Ti-rich clinopyroxene fractionation. All samples are enriched in incompatible elements. Nd
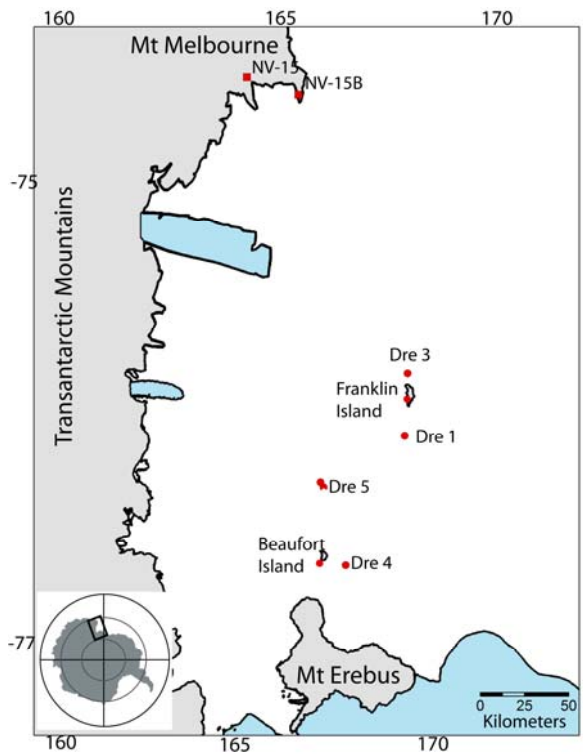
Figure 4-2. Locations of sampling sites from within the Ross Sea and near Mt Melbourne.
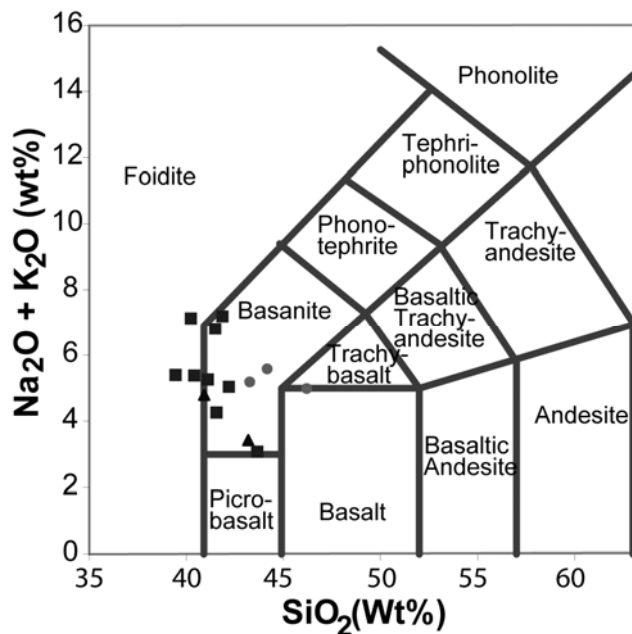

Figure 4-3. Total alkalis vs. SiO$_2$ wt% classification for analyzed samples. Circles represent samples from Beaufort and Franklin Islands. Triangles are samples from Mt Melbourne. Squares are dredged samples.

and Sr isotopic compositions plot in the previously defined field for HIMU-like lavas. Pb and Hf isotopic systems are decoupled from other isotopic systems, and their isotopic compositions plot between the fields define for HIMU and DMM.

METHODS

Borosilicate glass Carius tubes were soaked in *aqua regia* for 18 – 24 hours, rinsed with SDI, and dried before use. A minimum of 10 g of sample chips were crushed to < 150 μm grain size using a ceramic shatterbox. Two grams of sample powder were dissolved in each Carius tube, following the methods of [*Shirey and Walker*, 1995]. Carius tubes were cooled to -80ºC in a methanol-liquid nitrogen mixture before adding spikes and three mL of concentrated HCl. Once frozen, six mL of concentrated HNO_3 was added. The Carius tubes were sealed, placed in steel jackets, and allowed to thaw before heating for at least 36 hours at 220 ºC. Carius tubes were again frozen in the methanol-liquid nitrogen mixture before opening.

The aqua regia-rock sludge mixture was allowed to thaw, but not reach room temperature, before transferring to 50 mL centrifuge tubes for Os extraction. Nine mL of CCl_4 was added to the samples in 3 stages and then transferred to a beaker containing 4 mL of concentrated HBr. After several hours, the CCl_4 portion was removed as waste and the Os-bearing HBr fraction gently dried at temperatures below 80ºC. The Os fraction was picked up by CrO_3 and distilled to a bead of HBr in a conical Savillex beaker. The HBr was then dried down to 1 – 2 μL, loaded with a Ba(OH) emitter onto Pt filament, and analyzed by negative thermal ionization mass spectrometry (N-TIMS) as OsO_3^- at the Department of Terrestrial Magnetism, Carnegie Institution of Washington. All ratios

were corrected for instrument fractionation using a ^{192}Os/^{188}Os normalization value of 3.082614.

The remaining aqua regia-rock sludge mixture from the Carius tube was centrifuged and the aqua regia removed for PGE chemistry. After gently drying the aqua regia fraction, a few drops of concentrated HNO_3 and HF were added and then gently dried once more. The PGE fraction was loaded onto columns in 1N HCl following the procedure of Horan et al. [2003]. PGEs were analyzed by ICP-MS (ThermoFinnigan Element) at the University of Michigan, monitoring ^{89}Y, ^{90}Zr, ^{111}Cd, ^{175}Lu, and ^{177}Hf for potential oxide and isobaric interferences.

RESULTS

PGE concentrations

Rhenium and PGE concentrations are reported along with the Os isotopic compositions in Tables 4-1 and 4-2. Ir and Ru concentrations range from below detection limit (bdl) to 88 and from 11 to 44 parts per trillion (ppt), respectively. The average blank value for Ir is 6 picograms (pg), and the procedural detection limit is 19 pg. The average blank value for Ru is 12 pg, and the procedural detection limit is 16 pg. Pt concentrations are higher, ranging from bdl to 774 ppt. Pt blanks are considerably higher than those for other elements, 54 to 121 pg, due to leaching of the Carius tubes which are made of borosilicate glass [*Rehkamper and Halliday*, 1997]. This leads to a higher procedural detection limit of 167 pg. These concentrations overlap the upper range of MORB samples [*Rehkamper and Halliday*, 1997; *Schiano, et al.*, 1997; *Gannoun, et al.*, 2004; *Escrig, et al.*, 2005; *Dale, et al.*, 2008] and lower range of intraplate and OIB lavas

Table 4 - 1. Isotopic compositions, Re and Os concentrations for subaerial and submarine samples from the Ross Sea.

	$^{187}Os/^{188}Os_m$	ppt Os	ppt Re	Re/Os	$^{187}Re/^{188}Os$	Age (Ma)	$^{187}Os/^{188}Os_i$	$^{87}Sr/^{88}Sr_i$*	$^{143}Nd/^{144}Nd_i$*	MgO (wt%)
Subaerial										
ANT1-6	0.1862 ± 0.0004	59.7	235	3.9	16.5	3.28	0.1852	0.70289	0.51296	8.87
ANT1-9	0.1288 ± 0.0001	43.0	144	3.3	15.3	3.38	0.1280			9.28
BFT5	0.1253 ± 0.0001	113	157	1.4	6.8	6.7	0.1245	0.7030†	0.5129†	10.77
NV-13A	0.1848 ± 0.0002	44.6	318	7.1	52.0	1.00	0.1842	0.70338	0.51294	8.95
NV-13A(2)	0.1804 ± 0.0001	47.4	292	6.2	31.3	1.00	0.1799			8.95
NV-15	0.1290 ± 0.0001	72.9	351	4.8	22.4	1.53	0.1284	0.70340	0.51293	9.08
NV-15(2)	0.1266 ± 0.0022	62.4	273	4.4	20.2	1.53	0.1260			9.08
Submarine										
DRE1-31	0.1503 ± 0.0001	26.6	361	13.6	65.5	0.13	0.1502	0.70344	0.51300	6.72
DRE1-31(2)	0.1626 ± 0.0002	13.1	346	26.4	80.0	0.13	0.1624			6.72
DRE1-32	0.1647 ± 0.0003	18.8	364	19.4	93.8	0.12	0.1679	0.70292	0.51297	6.94
DRE3-56	0.1870 ± 0.0002	20.7	1182	57.1	41.2	0.00	0.1869			11.27
DRE3-73	0.1621 ± 0.0001	41.2	438	10.6	25.8	0.09	0.1621	0.70319	0.51301	11.06
DRE3-73(2)	0.1679 ± 0.0001	35.0	440	12.6	30.3	0.09	0.1679			11.06
DRE4-75	0.1959 ± 0.0002	8.0	182	22.8	111	1.93	0.1937	0.70338	0.51294	8.65
DRE4-76	0.1829 ± 0.0002	11.3	402	35.6	90.2	1.92	0.1787	0.70320	0.51293	13.70
DRE4-76(3)	0.1725 ± 0.0001	14.7	225	15.3	69.9	1.92	0.1702			13.70
DRE5-80	0.1113 ± 0.0002	34.1	339	9.9	46.0	3.94	0.1082	0.70313	0.51292	8.33
DRE5-80(2)	0.1092 ± 0.0001	90.8	301	3.3	15.3	3.94	0.1081			8.33
DRE5-81	0.1372 ± 0.0028	44.2	118	2.7	6.5	3.80	0.1368	0.70333	0.51294	10.82

*Sr and Nd isotopic compositions from Rilling et al. (in submission). †Sr and Nd isotopic ratios are averages of two different samples from the same site.

TABLE 4 - 2. PGE concentrations of Ross Sea lavas.

SAMPLE	Os (ppt)	Ir (ppt)	Ru (ppt)	Pt (ppt)	Re (ppt)
ANT1-9 (Franklin Island)	43	14	25	119	144
		23	36	322	122
		14	25	172	128
Ave		17	29	204	131
Variability (%)		35	24	58	10
BFT5 (Beaufort Island)	113	64	26	774	157
NV-15 (Mt Melbourne)	62.4	77	36	131	273
	72.9	68	17		351
Ave	67.7	73	27	131	312
NV-15B (Mt Melbourne)	34.8	33	28	281	90
	26.7	16	21	51	104
		38	28		99
Ave	30.8	29	26	166	98
Variability (%)		45	19		8
DRE1-31	26.6	23	18	151	361
	13.1	38	33	326	346
		33	33	180	340
		39	34	465	314
Ave	20	33	28	281	340
Variability (%)		30	31	65	6
DRE3-56	20.7	21	33	208	1182
DRE3-73	41.2	18	17	104	438
	35	BDL	28	175	440
Ave	38		30	140	439
Variability (%)			47		0
DRE4-76	14.7	60	36	186	225
	11.3	26	37	121	402
		39	16	199	334
					314
Ave	13	42	30	169	319
Variability (%)		43	47	28	29
DRE5-80	90.8	88	11	139	301
	34.1	BDL	34	81	210
		11	BDL	139	339
Ave	62.5	50	23	120	282
Variability (%)		151		32	26
DRE5-81	44.2	64	16	464	118
		31	20	141	99
		55	18	52	107
Ave		50	18	219	108
Variability (%)		38	11	112	9

[*Rehkamper, et al.*, 1999; *Chazey and Neal*, 2005; *Jamais, et al.*, 2008]. Average CI-chondrite normalized PGE distribution patterns for each of the samples are plotted in Figure 4-4.
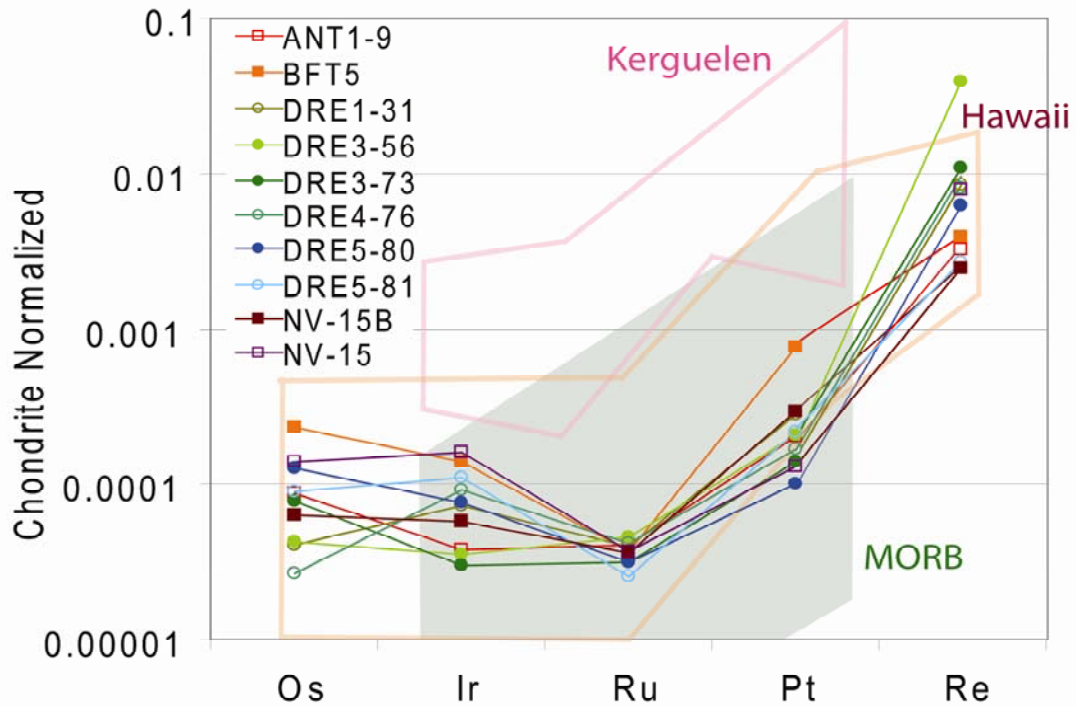

Figure 4-4. Average PGE distribution patterns for each set of sample replicates. The open boxes outline ranges of typical samples from Hawaii and the Kerguelan plateau [*Chazey and Neal*, 2005; *Jamais, et al.*, 2008]. Shaded area represents typical ranges for MORB samples [*Dale, et al.*, 2008].

Os isotopic compositions

Initial ^{187}Os/^{188}Os values range from 0.1081 ± 0.0001 to 0.1937 ± 0.0002 (Fig. 4-5). There are no differences in isotopic ranges between subaerial and submarine samples. Measured ^{187}Os/^{188}Os ratios were decay corrected based on the ^{40}Ar/^{39}Ar ages determined at the Argon Geochronology & Noble Gas Lab Department of Geological Sciences, University of Michigan, and reported in Rilling et al. [2009, *in press*]. Six of the thirteen

samples were run in duplicate. Isotopic compositions for samples DRE5-80, NV-13A, and NV-15 agree within 0.0045, but samples DRE1-31, DRE3-73, and DRE4-76 have poorer reproducibility. The latter samples have more radiogenic ^{187}Os/^{188}Os ratios and may have been more affected by secondary processes than the other set of samples. This interpretation is supported by the large differences in Re/Os for replicates of samples DRE1-31 and DRE4-76, which is not observed for other replicates. This will be further examined in the discussion section below.
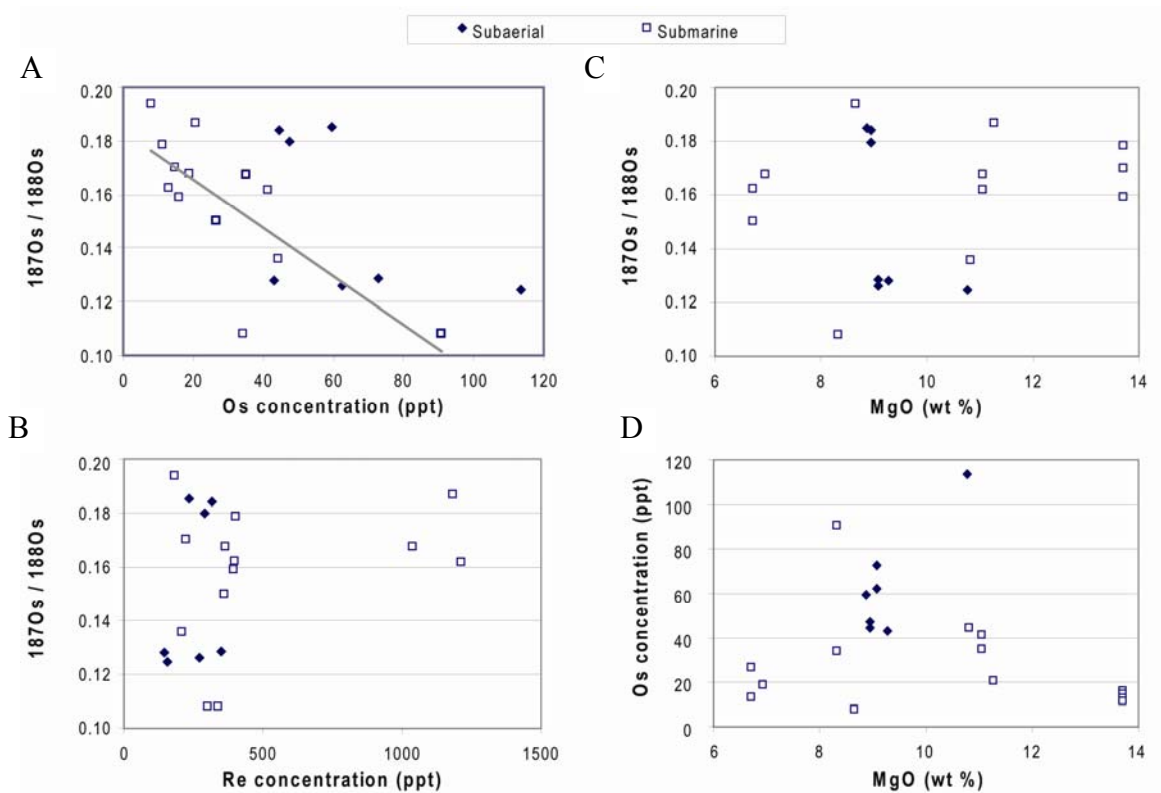

Figure 4-5. Age corrected Os isotopic compositions of samples from this study. A.) Note the trend of more radiogenic ^{187}Os/^{188}Os ratios with lower Os concentrations—likely the result of crustal contamination. The lowest ^{187}Os/^{188}Os ratios therefore are the most likely representation of the ^{187}Os/^{188}Os$_I$ of the magma source. Submarine, within rift, lavas show a larger range in Os concentrations than the subaerial lavas. Os isotopic compositions lack any trend with B.) Re concentrations or C.) MgO (wt%). D.) Os concentrations show similar ranges for all given MgO (wt%).

There is no apparent correlation between $^{187}Os/^{188}Os$ and MgO (wt%), but lower

Os concentrations do correlate with more radiogenic $^{187}Os/^{188}Os$ ratios. The correlation of

Os concentration and isotopic signatures has been discussed in numerous studies [*Shirey*

and Walker, 1998; *Widom, et al.*, 1999] and is thought to result from contamination

during magma ascent and evolution. Potential sources of the contamination and of the

evidence for source heterogeneity will be discussed further below.

Analytical details

Replicate analyses of the United States Geological Survey standard reference

material BHVO1 were run with the unknown samples to test for PGE yields and recovery.

Previous analyses of the standard have some variation which can be explained by the

"nugget effect" within the sample material and between fractions of the standard powder.

Meisel and Moser [2004] produced what is so far the most complete set of PGE data by

isotope dilution and ICP-MS methods for the BHVO1 standard. Their values are reported

along with ours in Table 4-3. Re concentrations yielded similar variability (up to 25%) as

our unknown samples but our average standard value is slightly below the certified value.

The average Re concentration of 244 ppt suggests only ~82% recovery of Re. Although

an HF dissolution step was included in the sample chemistry, previous studies have

suggested that full recovery of Re may not be possible using a Carius tube method

[*Uchida, et al.*, 2005]. Ir concentrations for replicates plot within range of certified

values, and all three replicates are within 10% variability. Ru concentrations showed 39%

variability and fell below the previously determined concentrations. The average Ru

concentration of BHVO1 in this study is only 68 ppt compared to 215-230 ppt from

Meisel and Moser [2004], suggesting only 30% recovery. The lack of full recovery may

Table 4 - 3. Procedural blanks, detection limits, and standard reproducibility.

	Os (ppt)	Ir (ppt)	Ru (ppt)	Pt (ppt)	Re (ppt)
Ave procedural blank	5.1	6	12	90	19
Range	2.8 - 9.4	1 - 12	10 - 13	54 - 121	10 - 28
Procedural det limit	12.9	19	16	167	39
BHVO1 (standard)		Ir (ppt)	Ru (ppt)	Pt (ppt)	Re (ppt)
Published range [a]	LOW	31	215	2420	298
	HIGH	96	230	4070	298
This work		69	67	2380	255
		61	25	2377	298
		75	111		180
Ave		68	68	2379	244
Variability (%)		10	39	0	26

[a] Reported range from Meisel and Moser (2004).

lead to slight differences in the element distribution patterns by generating a falsely concave upward pattern (Fig. 4-6). For this reason, we define our concave and convex distribution patterns based on the Os and Ir concentrations. For example, a negative slope between Os and Ir supports a concave shape, regardless of the apparent Ru concentration. The two Pt replicates were remarkably consistent with concentrations of 2377 ppt and 2380 ppt, but these concentrations fall slightly below the very large range in concentrations previously reported by Meisel and Moser [2004]. Because of uncertainties regarding within-sample heterogeneity, we are unable to provide a specific percentage of recovery. We can suggest that our Pt concentrations are likely minimum values. Examples of a sample with good and poor reproducibility are shown in Figure 4-7.

Several concentration calculations had complications due to some significant interferences by oxides. These interferences may lead to higher variability between replicates than those observed for the rest of the samples. DRE5-80 had particularly high amounts of HfO interference leading to 30-70% of the measured counts for masses 193, 194, and 195, which are used in the concentrations calculations for elements Ir and Pt.
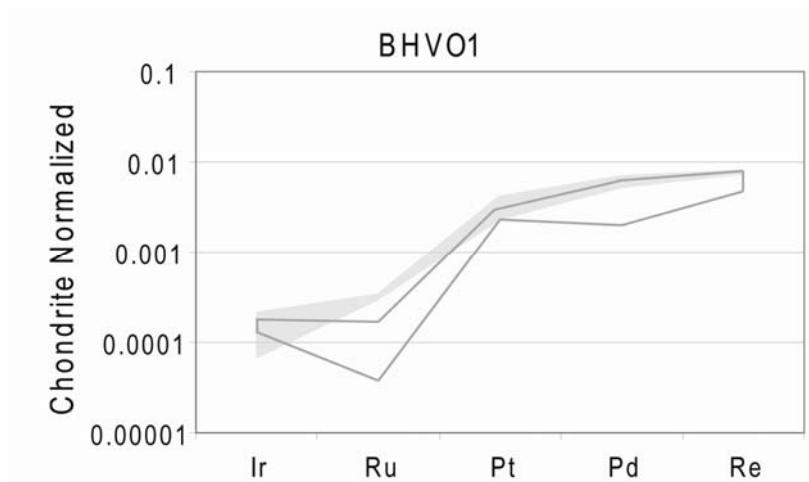
Figure 4-6. Range in chondrite-normalized PGE abundance patterns for the standard BHVO1, based on replicate analyses. Shaded area represents values reported in Meisel and Moser [2004]. Open area represents variations observed in our replicate analyses.
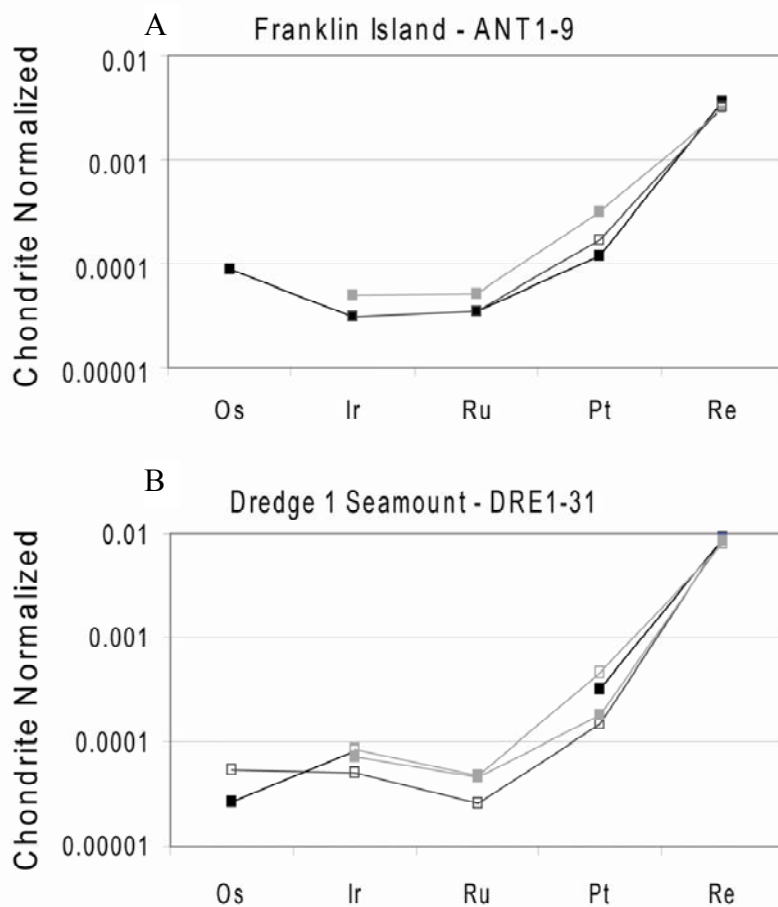

Figure 4-7. Example of sample replicates with A.) low variability and very reproducible distribution pattern and B.) high variability and variations in distribution patterns of sample replicates.

Replicate analyses of DRE1-31 and DRE3-56 also had interferences of ~15% on mass 193. The spiked isotope, ^{104}Ru, is unfortunately impacted by isobaric interferences from ^{104}Pd leading to larger uncertainties of these measurements than for other spiked masses. There is a large amount of variability in the proportion of measured counts on mass 104 that is Ru relative to Pd. Even after column chemistry, between 20 and 70% of the signal for mass 104 was Pd. For the majority of samples, greater than 95% of the signal measured for Ir masses, >93% of the signal for Pt masses, and >80% of the signal for Pd masses remained after isobaric and oxide interferences were removed.

DISCUSSION

PGE comparisons

PGE concentrations for samples from the Ross Sea region overlap with samples from Pacific MORB and OIB, but have a flat pattern for Os, Ir, and Ru and a much steeper slope for Pt and Re. The initial PGE distribution patterns for MORB and OIB were described in Rehkämper et al. [1997] and Rehkämper et al. [1999]. They found that MORB distribution patterns tend to have smooth, positive slopes (Fig. 4-4) with Ir concentrations between 2 and 93 ppt. Bezos et al. [2005] completed a more detailed study of the Pacific, Indian, and Atlantic Ocean MORB samples and found similar distribution patterns. The Indian and Atlantic Ocean samples were similar with PGE concentrations varying over three orders of magnitude, but the Pacific samples have PGE distribution patterns with a shallower slope and in all cases have concentrations <200 ppt [*Bezos, et al.*, 2005]. The Os, Ir and Ru distribution patterns for the Ross Sea samples are similar to

those of Pacific MORB, except for the more sharply concave upward pattern for the Ross Sea samples. The Pt, Pd, and Re distributions fall between the smooth positive slope of the MORB samples, with concentrations of 1 – 2 ppb [*Rehkamper, et al.*, 1999; *Ely and Neal*, 2003; *Chazey and Neal*, 2005], and the split, step-shaped pattern typical of OIB distribution patterns, with concentrations of 10s of ppb [*Rehkamper, et al.*, 1999; *Ely and Neal*, 2003; *Chazey and Neal*, 2005; *Jamais, et al.*, 2008].

The smooth, positive slope observed from MORB samples can be explained simply as a result of the varying degrees of incompatibility between the different elements [*Bezos, et al.*, 2005]. The step-shaped pattern observed from OIB requires a more complex explanation. Recent experiments [*Bockrath, et al.*, 2004] have shown that PGE concentrations are predominantly controlled by the presence of two separate phases in magmatic sources; Os, Ir, and Ru are present in crystalline monosulfides while Pt and Pd remain in immiscible sulfide droplets. These immiscible droplets may be segregated more easily during melting and metasomatism, leading to Pt and Pd enrichments or depletions relative to the other PGEs [*Lorand, et al.*, 2003; *Lorand, et al.*, 2004].

Potential effects of magma contamination on Os isotopic compositions

Os isotopic compositions in a single study area tend to display large ranges (Fig. 4-8) and are partially the result of multiple processes, i.e., contamination and/or assimilation during magma transport, rather than reflecting heterogeneity in the magma source [*Reisberg, et al.*, 1993; *Shirey and Walker*, 1998; *Escrig, et al.*, 2005; *Dale, et al.*, 2008; *Jamais, et al.*, 2008]. This study provides a unique perspective on potential sources of contamination due to the analysis of both submarine and subaerial samples as well as
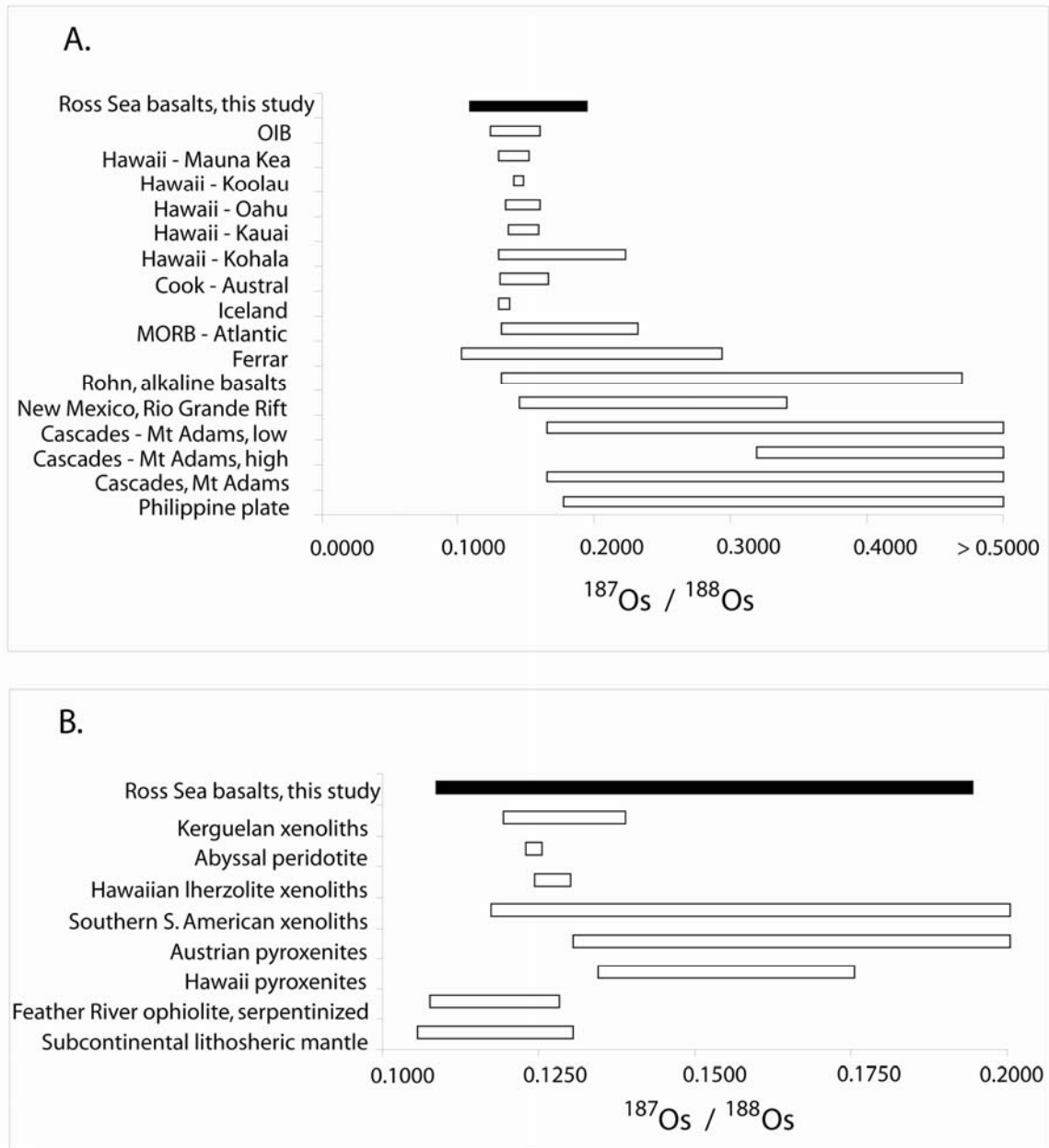
Figure 4-8. Comparisons of Ross Sea samples to other values reported in the literature. A.) Comparison of basalts from other settings. Ross Sea lavas range to unradiogenic Os isotopic ratios not observed elsewhere in the world. The Jurassic-age Ferrar flood basalts along the TAM have the only other similarly low reported values. B.) Comparison to analyses of potential mantle source materials. Best match at the minimum $^{187}Os/^{188}Os$ end is the metasomatized Feather River ophiolite and subcontinental lithospheric mantle xenoliths. Data from [*Molzahn, et al.*, 1996; *Hassler and Shimizu*, 1998; *Lassiter and Hauri*, 1998; *Hassler, et al.*, 2000; *Lassiter, et al.*, 2000; *Hart, et al.*, 2003; *Lassiter, et al.*, 2003; *Becker, et al.*, 2004; *Escrig, et al.*, 2005; *Jung, et al.*, 2005; *Thompson, et al.*, 2005; *Agranier, et al.*, 2007; *Brandon, et al.*, 2007; *Dale, et al.*, 2008; *Jamais, et al.*, 2008; *Schilling, et al.*, 2008; *Jicha, et al.*, 2009].

the analysis of both lavas from within the rift, on crust only ~15 km thick [*Trey, et al.*, 1999], and lavas erupted on the rift shoulder through thicker, up to 40 km, crust [*Sieminski, et al.*, 2003].

Assimilation and contamination by very young lower crust or lithospheric mantle could potentially contaminate transiting magmas and lead to unradiogenic $^{187}Os/^{188}Os$ ratios [*Reisberg, et al.*, 1993]. This would also create a trend of more unradiogenic $^{187}Os/^{188}Os$ ratios with lower (more easily contaminated) Os concentrations, which is not often observed. More commonly, the contamination results in more radiogenic $^{187}Os/^{188}Os$ ratios for the erupted lavas. This is because both mafic lower crust and more evolved upper continental crust have high Re/Os ratios which rapidly generate radiogenic $^{187}Os/^{188}Os$ ratios and can easily contaminate magmas with low Os concentrations, even when other isotopic systems show no evidence of crustal contamination [*Esser and Turekian*, 1993]. A general correlation between low Os concentrations and more radiogenic $^{187}Os/^{188}Os$ ratios is commonly observed in continental arc settings where lavas transit through thick continental crust [*Shirey and Walker*, 1998; *Dale, et al.*, 2008]. Ross Sea lavas also exhibit a rough correlation between radiogenic $^{187}Os/^{188}Os$ ratios and low Os concentrations. The origin of this trend is best explained by contamination during magma ascent, though heterogeneity in the source may also contribute to some of the variation observed in the isotopic signatures. Greater than 50% contamination by continental crust to the most unradiogenic signature is required to generate the most radiogenic $^{187}Os/^{188}Os$ ratios measured in the Ross Sea lavas, which would have compositional consequences to the bulk rock compositions unless Os becomes decoupled from the other elements. Although this is possible for samples with the lowest Os

concentrations (< 10 ppt), massive crustal contamination is less likely to explain the Os isotopic compositions of samples with $\geq$ 50 ppt Os concentrations. Samples ANT1-6, NV-15, and DRE5-80 all have > 50 ppt Os concentrations and exhibit average $^{187}Os/^{188}Os$ ratios of 0.1852, 0.1272, and 0.1082, respectively. These values outline the potential variation in the magma source.

Submarine samples are not without their own sources of contamination. Seawater has a $^{187}Os/^{188}Os$ ratio of ~1, but has very low Os concentrations of ~0.01 ppt [*Levasseur, et al.*, 1998, 1999]. Thus large amounts of seawater interaction would be required to dramatically increase the $^{187}Os/^{188}Os$ ratio of submarine lavas. This extreme amount of contamination would also be apparent in the corresponding Sr isotopic compositions of the lavas [*Escrig, et al.*, 2005]. The Ross Sea samples have HIMU-like $^{87}Sr/^{88}Sr$ values of 0.702869-0.703442 and show no evidence of seawater contamination. Mn-oxides have also been hypothesized as a potential source of contamination for submarine samples due to their prevalence near submarine volcanic edifices and their radiogenic $^{187}Os/^{188}Os$. However, Mn-oxides typically have high Pt/Pd ratios, which should also be observed in the contaminated lavas [*Dale, et al.*, 2008]. There is no correlation between concentrations of Pt or average Pt/Pd ratios and the Os isotopic composition for the Ross Sea samples.

The correlation of more radiogenic $^{187}Os/^{188}Os$ ratios with lower Os concentrations leads us to conclude that the lowest $^{187}Os/^{188}Os$ ratios, 0.1081 – 0.1284, represent the primary Os isotopic composition of the magma source beneath the Ross Sea. Some scatter off of this contamination trend may be related to minor contributions by pyroxenite melts or to metasomatic contamination of the source as described below. The

correlation of Os isotopic ratios with concentration appears more pronounced in the submarine samples, but lack of a strong correlation for the subaerial samples may be related to the small sample set or to contamination by older crustal materials which may have drastically different Os isotopic signatures. The high $^{187}Os/^{188}Os$ values in some of the lavas make it permissible for a fraction of the magmas to have originated in the asthenosphere. However, it would be a only coincidence that all lavas with high $^{187}Os/^{188}Os$ values have correspondingly low Os concentrations. The negative slope illustrated by the diagram in Fig. 4-5a therefore underscores the vulnerability of magmas with low Os concentrations to contamination, which is our preferred model.

Although the submarine samples from within the Terror Rift travelled through thinner continental crust than samples along the TAM, there is a thick section, potentially >5 km [*Trey, et al.*, 1999], of mafic material intruded into the crust. This mafic material would have higher Os concentrations than the more evolved crust along the rift shoulder and therefore have greater potential for contamination. This finding suggests that the contamination observed in many arcs may be related more to the thickness of and interaction with mafic lower crust rather than to the overall thickness of continental crust.

Comparison of mantle source compositions

Although the Ross Sea samples show a variety of $^{187}Os/^{188}Os$ ratios due to secondary processes during magma transport and eruption, the least contaminated ratios of 0.1081-0.1284 can be used for comparison with the mantle endmembers defined previously using other radiogenic isotopes. Both Sr and Nd isotopic compositions for WARS-related lavas have been shown to consistently plot within the range defined by a HIMU-like mantle source [*Hart, et al.*, 1995; *Rocholl, et al.*, 1995; *Hart, et al.*, 1997;

122

Panter, et al., 2000]; however, the Os isotopic compositions determined in this study are much less radiogenic than the HIMU mantle endmember (Fig. 4-9). The $^{187}Os/^{188}Os$ ratios are closer to or are even less radiogenic than those typically observed in MORB samples. This suggests that even when the effects of crustal contamination are removed, the Ross Sea lavas do not exhibit the expected chemical signatures of magmas from a HIMU endmember source. These extremely unradiogenic Os isotopic ratios are unusual and cannot be explained by a pure, single source corresponding to a previously defined mantle endmember.

The Os isotopic compositions of the Ross Sea lavas are also not easily produced by typical mantle source materials. For example, primitive mantle and abyssal peridotites have $^{187}Os/^{188}Os$ of ~0.120 – 0.130 [*Hassler and Shimizu*, 1998; *Meisel, et al.*, 2001]. Lherzolite xenoliths from both the Kerguelen and Hawaiian hotspots are similarly radiogenic with $^{187}Os/^{188}Os$ ratios >0.120 [*Hassler and Shimizu*, 1998; *Lassiter, et al.*, 2000]. The $^{187}Os/^{188}Os$ compositions of the Ross Sea samples overlap these ratios, but range to more unradiogenic values not previously observed in primitive mantle xenoliths. Pyroxenite xenoliths have $^{187}Os/^{188}Os$ ratios greater than 0.130 [*Lassiter, et al.*, 2000; *Becker, et al.*, 2004], related to their generation by melting in a source with a time-integrated record of high Re/Os ratios. Minor involvement of pyroxenite veins in the mantle source could also play a role in the large range of Os compositions observed in the Ross Sea magmas, but can not be the dominant component generating the lowest $^{187}Os/^{188}Os$ ratios of the Ross Sea lavas.
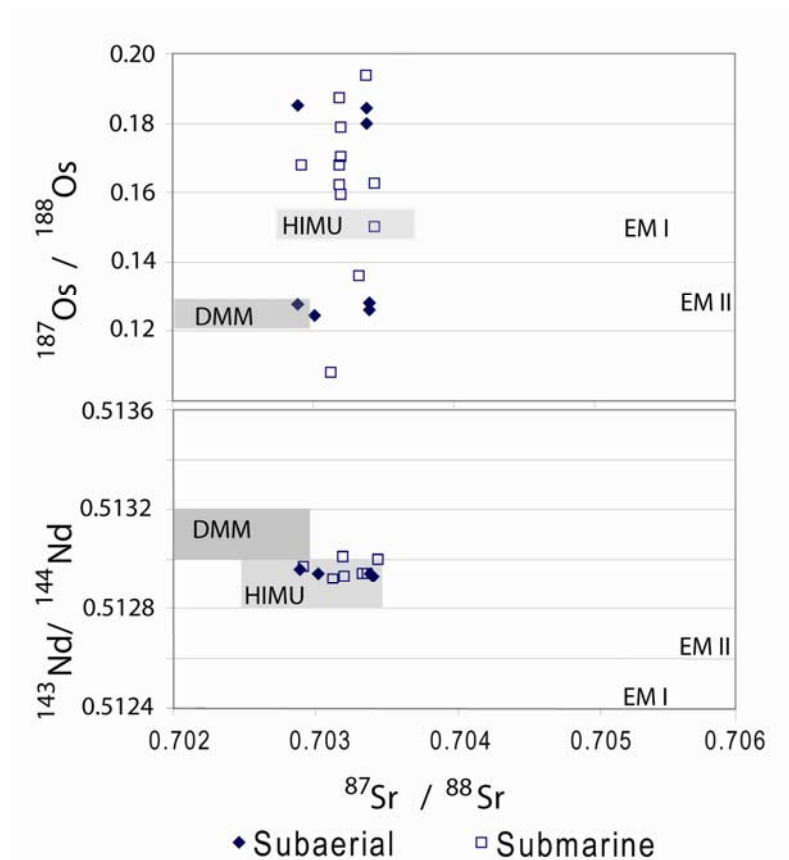
Figure 4-9. Comparison of Os isotopic compositions to traditional isotopes and predetermined mantle endmembers.

The unradiogenic Os isotopic compositions measured from xenoliths of

subcontinental lithospheric mantle [*Reisberg and Lorand*, 1995; *Hassler and Shimizu*,

1998; *Reisberg, et al.*, 2004] are the best match for the most unradiogenic source of the

Ross Sea magmatism. This residual mantle material was probably generated during

repeated partial melting events leading to formation of continental crust, and has had

preferential removal of Re relative to Os for an extended period of geologic time,

probably measured in billions of years. Reisberg and Lorand [1995] found that

$^{187}Os/^{188}Os$ ratios of both Archean- and post-Archean-age subcontinental lithospheric

xenoliths ranged between 0.1142 and 0.1288. Hassler and Shimizu [1998] reported

similar Os isotopic ratios for subcontinental xenoliths from the Kerguelen Islands,

between 0.1189 and 0.1383. More recent analyses of metasomatized subcontinental

lithosphere from the East Africa Rift show that these unradiogenic ratios are preserved

through metasomatism [*Reisberg, et al.*, 2004]. They found $^{187}Os/^{188}Os$ ratios of 0.11453

– 0.12916. Although none of these studies reported Os isotopic compositions quite as low

as measured in sample DRE5-80, subcontinental lithospheric mantle xenoliths from

Antarctica have not yet been analyzed, but will probably yield such low ratios.

The Jurassic Ferrar flood basalts, erupted along the TAM, are also thought to have

been generated by partial melting of a lithospheric mantle source and have similarly low

$^{187}Os/^{188}Os_i$ ratios of 0.102 – 0.293 [*Molzahn, et al.*, 1996]. An alternative argument to

the lithospheric mantle source is that the Ross Sea samples were contaminated during

ascent through buried Ferrar lavas. However, the Ferrar flood basalts are not known to

exist beneath the Terror Rift region, and there is no correlation of lower Os isotopic ratios

for samples located along the TAM compared to within rift samples in the Terror Rift.

The unradiogenic $^{187}Os/^{188}Os$ ratios are best explained by a lithospheric mantle source for

Ross Sea magmatism. The chemical similarity of these samples to samples located

through Victoria Land suggests that much of the WARS may be sourced by lithospheric

melting.

The absolute contribution of lithospheric melting relative to asthenospheric

melting is difficult to determine due to the variety of potential source materials (i.e.,

pyroxenite, peridotite, basalt, etc.) and range of different Os isotopic values within each

potential source. For example, melts of pyroxenite veins from within the lithosphere

beneath the Ross Sea may have $^{187}Os/^{188}Os$ ratios of > 0.130, but asthenospheric

peridotite melts with minor crustal contamination may generate the same Os isotopic

signatures. The effect of crustal contamination has been noted in numerous previous studies [*Esser and Turekian*, 1993; *Reisberg, et al.*, 1993; *Shirey and Walker*, 1998; *Dale, et al.*, 2008; *Jicha, et al.*, 2009]. These studies demonstrated the importance of crustal contamination in magmas with the lowest Os concentration to yield the highest $^{187}Os/^{188}Os$ ratios. This model is supported further by examining the average values for only the submarine subset of data from this study. These samples represent a much smaller geographic area, minimizing the potential heterogeneity of contaminating materials. These eight samples show a significantly cleaner correlation than when all replicates are plotted (Fig. 4-10), supporting an originally unradiogenic magma source similar to the Os isotopic signature of samples from the dredge 5 seamount.
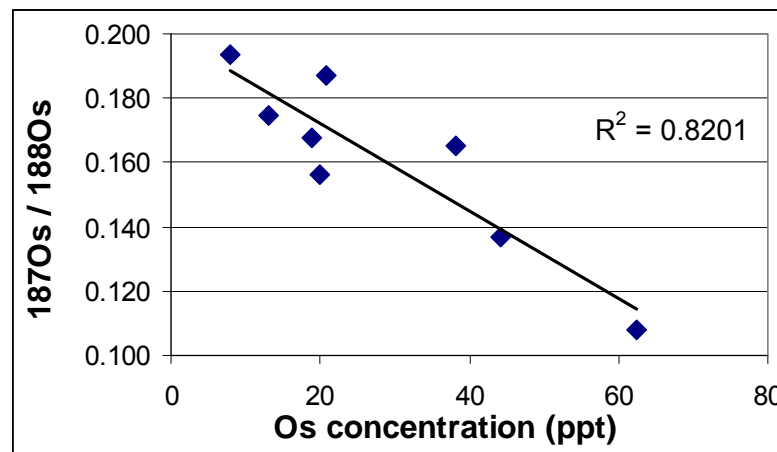

Figure 4-10. Average values for samples from seamounts in the Ross Sea.

Evidence of metasomatism?

The effects of metasomatism are still heavily debated in the literature [*Widom, et al.*, 2003; *Reisberg, et al.*, 2004; *Jung, et al.*, 2005; *Reisberg, et al.*, 2005]. Experimental studies are beginning to provide a clearer understanding of the behavior of certain elements at mantle conditions, though as Lorand et al. [2004] explained, the result of

metasomatism is highly dependant on the composition of the metasomatizing agent (i.e., carbonatitic alkaline melts, H_2O-CO_2-rich fluids, Si-rich melts with high melt/rock proportions, etc.). Several authors have suggested that metasomatism leads to enrichment or depletion of PGEs by mobilization of sulfides in the mantle source. Widom et al. [2003] analyzed xenoliths from the Kamchatka margin and found that the radiogenic Os isotopic ratio of metasomatized portions did not match their low $^{187}Re/^{188}Os$ ratio. They determined that the ages required to generate the observed Os isotopic signatures were significantly longer than the ages of the terranes from which the xenoliths were taken, and that Re and Os may have been scavenged from source and deposited during subduction-related metasomatism. Lorand and Alard [2001] came to a similar conclusion in their study of ultramafic xenoliths from Massif Central, France, stating that metasomatism may lead to removal of up to 90% of PGE abundances if there is a high melt/rock ratio, but has lesser effects with lower melt/rock ratios. Chazey and Neal [2005] argued that if excess Pt and Pd is the result of a S-saturated melt being emplaced into the magma source, these elements should be enriched relative to Y (which has a similar melt incompatibility, but behaves as a lithophile element). The low concentrations of PGEs in the Ross Sea samples, the high CI-chondrite normalized Y/Pt of 15 to 27, and the preservation of extremely unradiogenic $^{187}Os/^{188}Os$ ratios suggest that these models of PGE precipitation are not applicable in the Ross Sea lithospheric source.

Metasomatism unrelated to subduction margins may have little effect on PGE abundances and Os isotopic compositions. Numerous Os isotopic studies have noted that metasomatized xenoliths tend to preserve the same $^{187}Os/^{188}Os$ as unmetasomatized xenoliths in the same region [*Reisberg, et al.*, 2004; *Jung, et al.*, 2005; *Reisberg, et al.*,

2005], even in areas which have undergone large amounts of modification by a plume and/or lithospheric removal. These findings imply that the Re/Os of these xenoliths could not have been significantly altered by melt percolation or metasomatism. Both Jung et al. [2005] and Reisberg et al. [2005] observed that originally unradiogenic Os isotopic signatures had been preserved through metasomatic events in the lithosphere within rift systems. Furthermore, PGE concentrations from a serpentinized section of the Feather River Ophiolite in California overlap those measured in fresh peridotites, and showed no evidence of enrichment in Pd and Pt relative to Ir and Ru [*Agranier, et al.*, 2007]. Metasomatism by SiO_2-deficient alkaline melts may lead to precipitation of Pt-Re-Os rich sulfides in the mantle source, although the behavior of PGEs in melts of these compositions are not well understood [*Handler, et al.*, 1997]. The solubility of S, PGEs by proxy, in carbonatitic fluids are also poorly understood but may lead to stripping of PGEs from the magma source as well [*Lorand, et al.*, 2004].

The complex history of the Ross Sea lithosphere offers the possibility of multiple-stage metasomatism leading to a variety of effects; however, the lower abundances of PGEs and shallower slope of PGE distribution in the Ross Sea lavas relative to hotpot lavas with similar lithophile element compositions support a model of PGE removal from the lithosphere. The more step-shaped pattern clearly displayed by samples DRE1-31, DRE4-76, and DRE5-81 may be related to the presence of melt veins, enriched in the more incompatible PGEs, that has been emplaced into the magma source. The concave distribution pattern displayed by samples ANT1-9, DRE3-56, DRE3-73, DRE5-80 may be the result of a more depleted original source undergoing secondary Pt and Re enrichment. A recent study by Luguet et al. [2007] supported a sulfide and Pt-alloy

control of the PGE budget, even in what had previously been described as sulfide-free refractory harzburgite residue. These sulfides and alloys are present along grain boundaries of olivine and spinel and are particularly resistant to alteration due to high closure temperatures. This is a plausible model for the Ross Sea lithosphere which had seen extensive melting related to both arc magmatism during the Paleozoic and Mesozoic [*Mukasa and Dalziel*, 2000] and the eruption of the Jurrasic age Ferrar flood basalts [*Molzahn, et al.*, 1996]. These earlier events, involving more SiO_2-rich melts with high melt/rock ratios, would have removed significant proportions of the original PGE budget from the lithospheric mantle. Younger, Cenozoic melting and metasomatism by carbonatitic alkaline magmas may precipitate minor amounts of Cu-rich sulfides and Pt-alloys in the lithosphere. Although this is thought to be a minor effect, the low Os concentrations of the lithospheric mantle source are easily contaminated by this new more radiogenic source of Os and leads to an isotopically heterogeneous source.

CONCLUSION

This paper has presented the first combined PGE distribution patterns and Os isotopic compositions for Cenozoic lavas from the West Antarctic Rift System or WARS. Ross Sea lavas have lower PGE concentrations than most other examples of intraplate volcanism all over the globe. The low PGE concentrations support a residual lithospheric magma source, which has undergone previous melting and removal of host sulfide phases. Subsequent alkaline melt percolation and metasomatism may have enriched Pt and Re concentrations relative to Os, Ir, and Ru. A wide range of $^{187}Os/^{188}Os$ ratios were measured including values as unradiogenic as 0.1081. The more abundant radiogenic

isotopic compositions could be the result of several source materials. They may be due to some asthenospheric component, gt-pyroxenite veins in the mantle lithosphere, or originally unradiogenic lithosphere which has been contaminated by more radiogenic sources during magma transit. The more unradiogenic Os isotopic compositions strongly support the involvement of a lithospheric mantle source component. An additional complication may be related to minor metasomatic contamination which precipitated new sulfides and metal alloys, creating a slightly heterogeneous Os isotopic signature of the source. The complex melt history of the region and poor understanding of PGE behavior in these conditions prevents us from finding conclusive evidence of metasomatism in the PGE distribution patterns or Os isotopic compositions.

REFERENCES

Agranier, A., C. T. A. Lee, Z. X. A. Li, and W. P. Leeman (2007), Fluid-mobile element budgets in serpentinized oceanic lithospheric mantle: Insights from B, As, Li, Pb, PGEs and os isotopes in the feather river Ophiolite, California, *Chemical Geology*, *245*, 230-241.

Armienti, P., L. Civetta, F. Innocenti, P. Manetti, A. Tripodo, L. Villari, and G. Vita (1991), New petrological and geochemical data on Mt. Melbourne volcanic field, northern Victoria Land, Antarctica, *Memorie della Societa Geologica Italiana*, *46*, 397-424.

Barnes, S. J., A. J. Naldrett, and M. P. Gorton (1985), The Origin Of The Fractionation Of Platinum-Group Elements In Terrestrial Magmas, *Chemical Geology*, *53*, 303-323.

Becker, H., R. W. Carlson, and S. B. Shirey (2004), Slab-derived osmium and isotopic disequilibrium in garnet pyroxenites from a Paleozoic convergent plate margin (lower Austria), *Chemical Geology*, *208*, 141-156.

Behrendt, J. C. (1999), Crustal and lithospheric structure of the West Antarctic Rift System from geophysical investigations - a review, *Global And Planetary Change*, *23*, 25-44.

Behrendt, J. C., D. D. Blankenship, C. A. Finn, R. E. Bell, R. E. Sweeney, S. M. Hodge, and J. M. Brozena (1994), CASERTZ aeromagnetic data reveal late Cenozoic flood basalts in the West Antarctic rift system, *Geology*, *22*, 527-530.

Behrendt, J. C., R. Saltus, D. Damaske, A. McCafferty, C. A. Finn, D. Blankenship, and R. E. Bell (1996), Patterns of late Cenozoic volcanic and tectonic activity in the West Antarctic rift system revealed by aeromagnetic surveys, *Tectonics*, *15*, 660-676.

Bezos, A., J. P. Lorand, E. Humler, and M. Gros (2005), Platinum-group element systematics in Mid-Oceanic Ridge basaltic glasses from the Pacific, Atlantic, and Indian Oceans, *Geochimica Et Cosmochimica Acta*, *69*, 2613-2627.

Bockrath, C., C. Ballhaus, and A. Holzheid (2004), Fractionation of the platinum-group elements during mantle melting, *Science*, *305*, 1951-1953.

Brandon, A. D., D. W. Graham, T. Waight, and B. Gautason (2007), 186Os and 187Os enrichments and high-3He/4He sources in the Earth s mantle: Evidence from Icelandic picrites, *Geochimica Et Cosmochimica Acta*, *71*, 4570–4591.

Chazey, W. J., and C. R. Neal (2005), Platinum-group element constraints on source composition and magma evolution of the Kerguelen Plateau using basalts from ODP Leg 183, *Geochimica Et Cosmochimica Acta*, *69*, 4685-4701.

Coltorti, M., L. Beccaluva, C. Bonadiman, B. Faccini, T. Ntaflos, and F. Siena (2004), Amphibole genesis via metasomatic reaction with clinopyroxene in mantle xenoliths from Victoria Land, Antarctica, *Lithos*, *75*, 115-139.

Cooper, A. F., L. J. Adam, R. F. Coulter, G. N. Eby, and W. C. McIntosh (2007), Geology, geochronology and geochemistry of a basanitic volcano, White Island, Ross Sea, Antarctica, *Journal Of Volcanology And Geothermal Research*, *165*, 189-216.

Dale, C. W., A. Luguet, C. G. Macpherson, D. G. Pearson, and R. Hickey-Vargas (2008), Extreme platinum-group element fractionation and variable Os isotope compositions in Philippine Sea Plate basalts: Tracing mantle source heterogeneity, *Chemical Geology*, *248*, 213-238.

Ely, J. C., and C. R. Neal (2003), Using platinum-group elements to investigate the origin of the Ontong Java Plateau, SW Pacific, *Chemical Geology*, *196*, 235-257.

Escrig, S., P. Schiano, J.-G. Schilling, and C. Allegre (2005), Rhenium-osmium isotope systematics in MORB from the Southern Mid-Atlantic Ridge (40degrees - 50degrees S), *Earth And Planetary Science Letters*, *235*, 528-548.

Esser, B. K., and K. K. Turekian (1993), The Osmium Isotopic Composition Of The Continental-Crust, *Geochimica Et Cosmochimica Acta*, *57*, 3093-3104.

Esser, R. P., P. R. Kyle, and W. C. McIntosh (2004), Ar-40/Ar-39 dating of the eruptive history of Mount Erebus, Antarctica: volcano evolution, *Bulletin Of Volcanology*, *66*, 671-686.

Faure, G., and T. Mensing (2005), *Isotopes: Principles and Applications*, Third Edition ed., John Wiley and Soncs, Inc., Hoboken, New Jersey.

Finn, C. A., R. D. Muller, and K. S. Panter (2005), A Cenozoic diffuse alkaline magmatic province (DAMP) in the southwest Pacific without rift or plume origin, *Geochemistry Geophysics Geosystems*, *6*.

Gannoun, A., K. W. Burton, L. E. Thomas, I. J. Parkinson, P. van Calsteren, and P. Schiano (2004), Osmium Isotope Heterogeneity in the Constituent Phases of Mid-Ocean Ridge Basalts, *Science*, *303*, 70-72.

Hall, J. M., T. J. Wilson, and S. Henrys (2007), Structure of the central Terror Rift, western Ross Sea, Antarctica, paper presented at Tenth International Symposium on Antarctic Earth Sciences, United States Geological Society and The National Academies, Santa Barbara, CA.

Halliday, A. N., D. C. Lee, S. Tommasini, G. R. Davies, C. R. Paslick, J. G. Fitton, and D. E. James (1995), Incompatible Trace-Elements In Oib And Morb And Source Enrichment In The Sub-Oceanic Mantle, *Earth And Planetary Science Letters*, *133*, 379-395.

Handler, M. R., V. C. Bennett, and T. M. Esat (1997), The persistence of off-cratonic lithospheric mantle: Os isotopic systematics of variably metasomatised southeast Australian xenoliths, *Earth And Planetary Science Letters*, *151*, 61-75.

Hart, G. L., C. M. Johnson, W. Hildreth, and S. B. Shirey (2003), New osmium isotope evidence for intracrustal recycling of crustal domains with discrete ages, *Geology*, *31*, 427-430.

Hart, S. R., J. Blusztajn, and C. Craddock (1995), Cenozoic volcanism in Antarctica: Jones Mountains and Peter I Island, *Geochimica e Cosmochimica Acta*, *9*, 3379-3388.

Hart, S. R., J. Blusztajn, W. E. LeMasurier, and D. C. Rex (1997), Hobbs Coast Cenozoic volcanism: Implications for the West Antarctic rift system, *Chemical Geology*, *139*, 223-248.

Hart, S. R., D. C. Gerlach, and W. M. White (1986), A Possible New Sr-Nd-Pb Mantle Array And Consequences For Mantle Mixing, *Geochimica Et Cosmochimica Acta*, *50*, 1551-1557.

Hassler, D. R., B. Peucker-Ehrenbrink, and G. A. Ravizza (2000), Rapid determination of Os isotopic composition by sparging OsO4 into a magnetic-sector ICP-MS, *Chemical Geology*, *166*, 1-14.

Hassler, D. R., and N. Shimizu (1998), Osmium Isotopic Evidence for Ancient Subcontinental Lithospheric Mantle Beneath the Kerguelen Islands, Southern Indian Ocean, *Science*, *280*, 418-421.

Hauri, E. H., and S. R. Hart (1993), Re-Os isotope systematics of HIMU and EMII oceanic island basalts from the south Pacific Ocean, *Earth And Planetary Science Letters*, *114*, 353-371.

Hole, M. J., and W. E. LeMasurier (1994), Tectonic controls on the geochemical composition of Cenozoic, mafic alkaline volcanic rocks from West Antarctica, *Contributions to Mineralogy and Petrology*, *117*, 187-202.

Horan, M. F., R. J. Walker, J. W. Morgan, J. N. Grossman, and A. E. Rubie (2003), Highly siderophile element in chondrites, *Chemical Geology*, *196*, 5-20.

Jamais, M., J. C. Lassiter, and G. E. Brugmann (2008), PGE and Os-isotopic variations in lavas from Kohala Volcano, Hawaii: Constraints on PGE behavior and melt/crust interaction, *Chemical Geology*, *250*, 16-28.

Jicha, B. R., C. M. Johnson, W. Hildreth, B. L. Beard, G. L. Hart, S. B. Shirey, and B. S. Singer (2009), Discriminating assimilants and decoupling deep- vs. shallow-level crystal records at Mount Adams using U-238-Th-230 disequilibria and Os isotopes, *Earth And Planetary Science Letters*, *277*, 38-49.

Jung, S., J. A. Pfander, G. Brugmann, and A. Stracke (2005), Sources of primitive alkaline volcanic rocks from the central European volcanic province (Rhon, Germany) inferred from Hf, Os and Pb isotopes, *Contributions To Mineralogy And Petrology*, *150*, 546-559.

Kyle, P. R. (1990), Erebus Volcanic Province, in *Volcanoes of the Antarctic Plate and the Southern Oceans*, edited by W. E. LeMasurier and J. W. Thompson, pp. 81-88, American Geophysical Uniion, Washington, D.C.

Kyle, P. R., J. A. Moore, and M. F. Thirlwall (1992), Petrologic Evolution Of Anorthoclase Phonolite Lavas At Mount Erebus, Ross Island, Antarctica, *Journal Of Petrology*, *33*, 849-875.

Lassiter, J. C., J. Blichert-Toft, E. H. Hauri, and H. G. Barsczus (2003), Isotope and trace element variations in lavas from Raivavae and Rapa, Cook-Austral islands: constraints on

the nature of HIMU- and EM-mantle and the origin of mid-plate volcanism in French Polynesia, *Chemical Geology*, *202*, 115-138.

Lassiter, J. C., J. Blichert-Toft, E. H. Hauri, and H. G. Barsczus (2003), Isotope and trace element variations in lavas from Raivavae and Rapa, Cook-Austral islands: constraints on the nature of HIMU- and EM-mantle and the origin of mid-plate volcanism in French Polynesia, *Chemical Geology*, *202*, 115-138.

Lassiter, J. C., and E. H. Hauri (1998), Osmium-isotope variations in Hawaiian lavas: evidence for recycled oceanic lithosphere in the Hawaiian plume, *Earth And Planetary Science Letters*, *164*, 483-496.

Lassiter, J. C., E. H. Hauri, P. W. Reiners, and M. O. Garcia (2000), Generation of Hawaiian post-erosional lavas by melting of a mixed lherzolite/pyroxenite source, *Earth And Planetary Science Letters*, *178*, 269-284.

LeMasurier, W. E., and C. A. Landis (1996), Mantle-plume activity recorded by low-relief erosion surfaces in West Antarctica and New Zealand, *GSA Bulletin*, *108*, 1450-1466.

LeMasurier, W. E., and J. W. Thomson (Eds.) (1990), *Volcanoes of the Antarctic Plate and Southern Oceans*, 487 pp., American Geophysical Union, Washington, D.C.

Levasseur, S., J. L. Birck, and C. J. Allegre (1998), Direct measurement of femtomoles of osmium and the Os-187/Os-186 ratio in seawater, *Science*, *282*, 272-274.

Levasseur, S., J. L. Birck, and C. J. Allegre (1999), The osmium riverine flux and the oceanic mass balance of osmium, *Earth And Planetary Science Letters*, *174*, 7-23.

Lorand, J. P., and O. Alard (2001), Platinum-group element abundances in the upper mantle: New constraints from in situ and whole-rock analyses of Massif Central xenoliths (France), *Geochimica Et Cosmochimica Acta*, *65*, 2789-2806.

Lorand, J. P., G. Delpech, M. Gregoire, B. Moine, S. Y. O'Reilly, and J. Y. Cottin (2004), Platinum-group elements and the multistage metasomatic history of Kerguelen lithospheric mantle (South Indian Ocean), *Chemical Geology*, *208*, 195-215.

Lorand, J. P., L. Reisberg, and R. M. Bedini (2003), Platinum-group elements and melt percolation processes in Sidamo spinel peridotite xenoliths, Ethiopia, East African Rift, *Chemical Geology*, *196*, 57-75.

Luguet, A., S. B. Shirey, J. P. Lorand, M. F. Horan, and R. W. Carlson (2007), Residual platinum-group minerals from highly depleted harzburgites of the Lherz massif (France) and their role in HSE fractionation of the mantle, *Geochimica Et Cosmochimica Acta*, *71*, 3082-3097.

Meisel, T., and J. Moser (2004), Reference materials for geochemical PGE analysis: new analytical data for Ru, Rh, Pd, Os, Ir, Pt and Re by isotope dilution ICP-MS in 11 geological reference materials, *Chemical Geology*, *208*, 319-338.

Meisel, T., R. J. Walker, A. J. Irving, and J. P. Lorand (2001), Osmium isotopic compositions of mantle xenoliths: A global perspective, *Geochimica Et Cosmochimica Acta*, *65*, 1311-1323.

Molzahn, M., L. Reisberg, and G. Worner (1996), Os, Sr, Nd, Pb, O isotope and trace element data from the Ferrar flood basalts, Antarctica: evidence for an enriched subcontinental lithospheric source, *Earth and Planetary Science Letters*, *144*, 529-546.

Mukasa, S. B., and I. W. D. Dalziel (2000), Marie Byrd Land, West Antarctica: Evolution of Gondwana's Pacific margin constrained by zircon U-Pb geochronology and feldspar common-Pb isotopic compositions, *Geological Society of America Bulletin*, *112*, 611-627.

Nardini, I., P. Armienti, S. Rocchi, L. Dallai, and D. Harrison (2009), Sr-Nd-Pb-He-O Isotope and Geochemical Constraints on the Genesis of Cenozoic Magmas from theWest Antarctic Rift, *Journal of Petrology*.

Panter, K. S., J. Blusztajn, S. R. Hart, P. R. Kyle, R. Esser, and W. C. McIntosh (2006), The Origin of HIMU in the SW Pacific: Evidence from Intraplate Volcanism in Southern New Zealand and Subantarctic Islands, *Journal of Petrology*, *47(9)*, 1673-1704.

Panter, K. S., S. R. Hart, P. Kyle, J. Blusztanjn, and T. Wilch (2000), Geochemistry of Late Cenozoic basalts from the Crary Mountains: characterization of mantle sources in Marie Byrd Land, Antarctica, *Chemical Geology*, *165*, 215-241.

Perinelli, C., P. Armienti, and L. Dallai (2006), Geochemical and O-isotope constraints on the evolution of lithospheric mantle in the Ross Sea rift area (Antarctica), *Contributions To Mineralogy And Petrology*, *151*, 245-266.

Pilet, S., M. B. Baker, and E. M. Stolper (2008), Metasomatized lithosphere and the origin of alkaline lavas, *Science*, *320*, 916-919.

Rehkamper, M., and A. N. Halliday (1997), Development and application of new ion-exchange techniques for the separation of the platinum group and other siderophile elements from geological samples, *Talanta*, *44*, 663-672.

Rehkamper, M., A. N. Halliday, D. Barfod, J. G. Fitton, and J. B. Dawson (1997), Platinum-Group Element Abundance Patterns in Different Mantle Environments, *Science*, *278*, 1595-1598.

Rehkamper, M., A. N. Halliday, J. G. Fitton, D. C. Lee, M. Wieneke, and N. T. Arndt (1999), Ir, Ru, Pt, and Pd in basalts and komatiites: New constraints for the geochemical behavior of the platinum-group elements in the mantle, *Geochimica Et Cosmochimica Acta*, *63*, 3915-3934.

Reisberg, L., and J. P. Lorand (1995), Longevity Of Sub-Continental Mantle Lithosphere From Osmium Isotope Systematics In Orogenic Peridotite Massifs, *Nature*, *376*, 159-162.

Reisberg, L., J. P. Lorand, and R. M. Bedini (2004), Reliability of Os model ages in pervasively metasomatized continental mantle lithosphere: a case study of Sidamo spinel peridotite xenoliths (East African Rift, Ethiopia), *Chemical Geology*, *208*, 119-140.

Reisberg, L., X. C. Zhi, J. P. Lorand, C. Wagner, Z. C. Peng, and C. Zimmermann (2005), Re-Os and S systematics of spinel peridotite xenoliths from east central China: Evidence for contrasting effects of melt percolation, *Earth And Planetary Science Letters*, *239*, 286-308.

Reisberg, L., A. Zindler, F. Marcantonio, W. White, D. Wyman, and B. Weaver (1993), Os Isotope Systematics In Ocean Island Basalts, *Earth And Planetary Science Letters*, *120*, 149-167.

Rilling, S. E., S. B. Mukasa, T. J. Wilson, L. A. Lawver, and C. M. Hall (2009, *in press*), New Determinations of 40Ar/39Ar Isotopic Ages and Flow Volumes for Cenozoic Volcanism in the Terror Rift, Ross Sea, Antarctica, *Journal of Geophysical Research*.

Rocchi, S., P. Armienti, M. D'Orazio, S. Tonarini, J. R. Wijbrans, and G. DiVincenzo (2002), Cenozoic magmatism in the western Ross Embayment: Role of mantle plume versus plate dynamics in the development of the West Antarctic Rift System, *Journal of Geophysical Research*, *107*.

Rocholl, A., M. Stein, M. Molzahn, S. R. Hart, and G. Worner (1995), Geochimcal evolution of rift magmas by progressive tapping of a stratified mantle source beneath the Ross Sea Rift, Northern Victoria Land, Antarctica, *Earth and Planetary Science Letters*, *131*, 207-224.

Schiano, P., J. L. Birck, and C. J. Allegre (1997), Osmium-strontium-neodymium-lead isotopic covariations in mid-ocean ridge basalt glasses and the heterogeneity of the upper mantle, *Earth And Planetary Science Letters*, *150*, 363-379.

Schilling, M. E., R. W. Carlson, R. V. Conceicao, C. Dantas, G. W. Bertotto, and E. Koester (2008), Re-Os isotope constraints on subcontinental lithospheric mantle evolution of southern South America, *Earth And Planetary Science Letters*, *268*, 89-101.

Shirey, S., and R. J. Walker (1995), Carius Tube Digestion for Low-Blank Rhenium-Osmium Analysis, *Analytical Chemistry*, *67*, 2136-2141.

Shirey, S., and R. J. Walker (1998), The Re-Os isotope system in cosmochemistry and high-temperature geochemistry, *Annual Review of Earth and Planetary Science Letters*, *26*, 423-500.

Sieminski, A., E. Debayle, and J.-J. Leveque (2003), Seismic evidence for deep low-velocity anomalies in the transition zone beneath West Antarctica, *Earth and Planetary Science Letters*, *216*, 645-661.

Tessensohn, F., and G. Worner (1991), The Ross Sea rift system, Antarctica; structure, evolution and analogues, paper presented at International Symposium on Antarctic Earth Sciences, Cambridge, United Kingdom.

Thompson, R. N., C. J. Ottley, P. M. Smith, D. G. Pearson, A. P. Dickin, M. A. Morrison, P. T. Leat, and S. A. Gibson (2005), Source of the Quaternary Alkalic Basalts, Picrites and Basanites of the Potrillo Volcanic Field, New Mexico, USA: Lithosphere or Convecting Mantle? *Journal of Petrology*, *46*, 1603-1643.

Trey, H., A. K. Cooper, G. Pellis, B. della Vedova, G. Cochrane, G. Brancolini, and J. Makris (1999), Transect across the West Antarctic rift system in the Ross Sea, Antarctica, *Tectonophysics*, *301*, 61-74.

Uchida, S., K. Tagami, and K. Tabei (2005), Comparison of alkaline fusion and acid digestion methods for the determination of rhenium in rock and soil samples by ICP-MS, *Analytica Chimica Acta*, *535*, 317-323.

Watson, T., A. A. Nyblade, D. A. Wiens, S. Anandakrishan, M. Benoit, P. J. Shore, D. Voigt, and J. VanDecar (2006), P and S velocity structure of the upper mantle beneath the Transantarctic Mountains, East Antarctic craton, and Ross Sea from travel time tomography, *Geochemistry Geophysics Geosystems*, *7(7)*.

Widom, E., K. A. Hoernle, S. B. Shirey, and H. U. Schmincke (1999), Os isotope systematics in the Canary Islands and Madeira: Lithospheric contamination and mantle plume signatures, *Journal Of Petrology*, *40*, 279-296.

Widom, E., P. Kepezhinskas, and M. Defant (2003), The nature of metasomatism in the sub-arc mantle wedge: evidence from Re-Os isotopes in Kamchatka peridotite xenoliths, *Chemical Geology*, *196*, 283-306.

Worner, G. (1999), Lithospheric dynamics and mantle sources of alkaline magmatism of the Cenozoic West Antarctic Rift System, *Global and Planetary Change*, *23*, 61-77.

Zipfel, J., and G. Worner (1992), 4-Phase And 5-Phase Peridotites From A Continental Rift System - Evidence For Upper Mantle Uplift And Cooling At The Ross Sea Margin (Antarctica), *Contributions To Mineralogy And Petrology*, *111*, 24-36.

CHAPTER 5

CONCLUSIONS

The work presented in this dissertation provided three different methods to determine the relation between tectonism and rift-related volcanism in the West Antarctic Rift System (WARS). The primary goal of this work was to address the relatively new model of magmatism generated by melting of metasomatized mantle sources rather than the previously proposed model of active melting due to interactions between mantle plumes and the continental lithosphere. The resulting explanation for WARS magmatism is not only important for understanding the world's largest alkaline province but also for providing analogues to other rift systems and areas of alkaline volcanism which have also been under question.

Chapter 2 provided the framework for the samples analyzed in all three studies. The lavas sampled from Franklin Island, Beaufort Island, and the seven seamounts along the Terror Rift range in age from 6.7 Ma to 89 ka. These ages are similar to the terrestrial lavas dated in both the Melbourne and Erebus Volcanic Provinces (to the north and south of the study area, respectively), and are consistent with decompressional melting models, because they post-date the main phase of extension along the Terror Rift. The change in pressure resultant from the proposed degrees of Miocene rifting is insufficient for an unmetasomatized mantle peridotite source rock along the regional geotherm to cross the solidus and generate the observed volumes of magma. A modified mantle source must be

invoked in order for melting to be solely the result of extensional deformation, consistent with the metasomatism hypothesis.

Chapter 3 illustrates the similarity of these alkaline basalts to other volcanic rocks throughout the WARS. These compositions are best matched to experimental melts of carbonated peridotite which have undergone crystal fractionation, although some involvement of gt-pyroxenite could also be invoked. The long-lived Paleozoic and Mesozoic subduction history along the paleo-Pacific margin of Gondwana could have led to the formation of these compositions within the mantle lithosphere beneath the WARS. The Ross Sea lavas possess an overall enrichment of incompatible elements; however, the large negative Pb anomaly and the concave shape of LILE on element distribution diagrams support the hypothesis of removal of the fluid-mobile elements from the residual mantle lithosphere source during generation of the subduction-related volcanism. The slight heterogeneity in patterns on element distribution diagrams (EDD) is likely the result of differing proportions of asthenospheric and lithospheric sources in the generated melts. The decoupling of the Pb- and Nd-isotopic systems agrees with this model of lithospheric contributions.

Chapter 4 presents the first determinations of Os isotopic compositions and platinum group element (PGE) distribution patterns for Cenozoic WARS lavas. These data provide the strongest support for involvement of a subcontinental lithospheric mantle source for WARS magmatism. Ross Sea lavas have lower PGE concentrations than most other reported values for intraplate volcanism from around the globe and have extremely unradiogenic $^{187}Os/^{188}Os$ ranging to as low as 0.1081 ± 0.0001. The low PGE concentrations are best explained by previous fractional melting and removal of host

sulfide phases from the residual lithospheric mantle. Pt and Re concentrations relative to Os, Ir, and Ru have been heterogeneously enriched during subsequent alkaline melt percolation and metasomatism; although the behavior of PGEs during metasomatism is not yet well constrained. Precipitation of new sulfides and metal alloys during metasomatic contamination may also create a slightly heterogeneous Os isotopic signature in the source. Unradiogenic Os isotopic compositions have not been observed in mantle xenoliths other than a few examples of residual lithospheric materials. Recycled oceanic lithosphere, a potential composition in mantle plumes, would have radiogenic Os isotopic signatures due to their high Re/Os ratios. The unradiogenic Os signature of the WARS lavas is again best explained by a proportion of melting in the lithospheric mantle source, typified by low Re/Os due to earlier melting episodes, although the degree of lithospheric versus asthenospheric source can not be determined. More radiogenic Os ratios may be caused by contamination during magma evolution or may actual represent contributions from asthenospheric melts or gt-pyroxenite in the mantle lithosphere. Additional studies will improve on the available dataset and may allow for more clarity in this area.

The results presented in these three studies provide consistent support of contributions of lithospheric mantle source for Cenozoic WARS lavas. The younger ages of these lavas relative to the ages of extension along the Terror Rift, along with their chemical signatures, agree with the originally proposed hypothesis that melting is the result of passive, decompressional melting of the asthenosphere as well as the resulting thermal erosion of the subcontinental lithosphere. The chemical signatures are also best explained by a magma source that has undergone previous episodes of melting and

metasomatism. These conclusions agree with the original hypothesis of this dissertation and lead to acceptance of the passive melting model. Cenozoic alkaline lavas in the WARS are produced by extension and decompressional melting of the lithospheric mantle which has an anomalously low melting temperature due to metasomatism.